1996

Torque on the cylinder block of an axial-piston swash-plate type hydrostatic pump

Noah Denver Manring
Iowa State University

INFORMATION TO USERS

This manuscript has been reproduced from the microfilm master. UMI films the text directly from the original or copy submitted. Thus, some thesis and dissertation copies are in typewriter face, while others may be from any type of computer printer.

The quality of this reproduction is dependent upon the quality of the copy submitted. Broken or indistinct print, colored or poor quality illustrations and photographs, print bleedthrough, substandard margins, and improper alignment can adversely affect reproduction.

In the unlikely event that the author did not send UMI a complete manuscript and there are missing pages, these will be noted. Also, if unauthorized copyright material had to be removed, a note will indicate the deletion.

Oversize materials (e.g., maps, drawings, charts) are reproduced by sectioning the original, beginning at the upper left-hand corner and continuing from left to right in equal sections with small overlaps. Each original is also photographed in one exposure and is included in reduced form at the back of the book.

Photographs included in the original manuscript have been reproduced xerographically in this copy. Higher quality 6" x 9" black and white photographic prints are available for any photographs or illustrations appearing in this copy for an additional charge. Contact UMI directly to order.

UMI

A Bell & Howell Information Company
300 North Zeeb Road, Ann Arbor MI 48106-1346 USA
313/761-4700 800/521-0600

Torque on the cylinder block of an axial-piston swash-plate type hydrostatic pump

by

Noah Denver Manring

A Dissertation Submitted to the

Graduate Faculty in Partial Fulfillment of the

Requirements for the Degree of

DOCTOR OF PHILOSOPHY

Department: Mechanical Engineering
Major: Mechanical Engineering

Approved:

Signature was redacted for privacy.

Signature was redacted for privacy.

In Charge of Major Work

Signature was redacted for privacy.

For the Major Department

Signature was redacted for privacy.

For the Graduate College

Iowa State University
Ames, Iowa

1996

From God:

the giver of all things, including knowledge.

To my wife:

who loves me regardlessly.

For my children:

who make it all worthwhile.

TABLE OF CONTENTS

LIST OF SYMBOLS

A	"decay constant" for the decay of the coefficient-of-friction for mixed lubrication
A_b	effective pressurized-area on the cylinder block within a single piston bore
A_o	varying discharge-area of the control volume for the piston bore
A_p	pressurized area on the face of a single piston
$A_{p_n}^y$	radial effective pressurized-area on the cylinder block within the nth piston bore in the y-direction
$A_{p_n}^z$	radial effective pressurized-area on the cylinder block within the nth piston bore in the z-direction
A_s	effective pressurized-area on the face of a single slipper
a	offset dimension describing the cocked orientation of the piston; generic constant
b	offset dimension describing the cocked orientation of the piston; generic constant
C_d	orifice discharge-coefficient for the control volume of a single piston-bore
D_p	piston diameter
D_s	outside diameter of the slipper land
D_v	width of the diametrical land on the cylinder block
d_n	distance of the nth piston away from the z-axis
E_1	geometric location in the y-direction of the force exerted on the cylinder block from the valve plate
E_2	geometric location in the negative z-direction of the force exerted on the cylinder block from the valve plate

F_{bal_n} vector force exerted on the slipper from the effective pressurized-area on the face of the *n*th slipper

F_{c_n} vector force exerted on the cylinder block from the pressure within the *n*th piston bore (also called the "clamping force")

F_{hd} vector force exerted on a single slipper from the slipper hold-down mechanism

F_{hd} force exerted on a single slipper from the slipper hold-down mechanism in the direction normal to the swash plate

F_{l_n} vector force exerted on the cylinder block at the inner edge of the *n*th bushing from the *n*th piston

$F_{l_n}^{y}$ force exerted on the cylinder block at the inner edge of the *n*th bushing from the *n*th piston in the *y*-direction

$F_{l_n}^{z}$ force exerted on the cylinder block at the inner edge of the *n*th bushing from the *n*th piston in the *z*-direction

F_n idealized force exerted on the cylinder block by the *n*th piston

F_{o_n} vector force exerted on the cylinder block at the outer edge of the *n*th bushing from the *n*th piston

$F_{o_n}^{y}$ force exerted on the cylinder block at the outer edge of the *n*th bushing from the *n*th piston in the *y*-direction

$F_{o_n}^{z}$ force exerted on the cylinder block at the outer edge of the *n*th bushing from the *n*th piston in the *z*-direction

F_{p_n} vector force exerted on the cylinder block from the *n*th piston

$F_{p_n}^{y}$ force exerted on the cylinder block from the *n*th piston in the *y*-direction

$F_{p_n}^{z}$ force exerted on the cylinder block from the *n*th piston in the *z*-direction

F_{pr_n} vector force exerted on the face of the *n*th piston by the axial pressure within the *n*th piston bore

$\boldsymbol{F}_{r_n}$ vector force exerted on the on the cylinder block by the radial pressure within the nth piston bore

$\boldsymbol{F}_{s_n}$ vector force exerted on the nth piston from the nth slipper

$F_{s_n}^x$ force exerted on the nth piston from the nth slipper in the x-direction

$F_{s_n}^y$ force exerted on the nth piston from the nth slipper in the y-direction

$F_{s_n}^z$ force exerted on the nth piston from the nth slipper in the z-direction

$\boldsymbol{F}_{sh}$ vector force exerted on the cylinder block from the shaft

F_{sh}^y force exerted on the cylinder block from the shaft in the y-direction

F_{sh}^z force exerted on the cylinder block from the shaft in the z-direction

$\boldsymbol{F}_{sp}$ vector force exerted on the cylinder block from the cylinder-block spring

F_{sp} force exerted on the cylinder block from the cylinder-block spring in the x-direction

F_{sp_1} first assembled spring-load used in the reduced spring-load tests

F_{sp_2} second assembled spring-load used in the reduced spring-load tests

$\boldsymbol{F}_{sw_n}$ vector force exerted on the nth slipper from the swash plate

F_{sw_n} force exerted on the nth slipper from the swash plate in the direction normal to the swash plate

$\boldsymbol{F}_v$ vector force exerted on the cylinder block from the valve plate

F_v force exerted on the cylinder block from the valve plate in the negative x-direction

f_{i_n} friction force exerted on the cylinder block at the inner edge of the nth bushing from the nth piston in the x-direction

f_{o_n} friction force exerted on the cylinder block at the outer edge of the nth bushing from the nth piston in the x-direction

f_{p_n} net friction-force exerted on the cylinder block from the nth piston in the x-direction

f_{s_n} friction force exerted on the slipper from the swash plate

f_v friction moment exerted on the cylinder block from the valve plate in the negative x-direction

H_{1_n} primary geometric-location of the force exerted on the nth slipper from the swash plate

H_{2_n} secondary geometric-location of the force exerted on the nth slipper from the swash plate

h generic fluid-film thickness

h^* critical fluid film thickness describing the transition between mixed-lubrication and fully hydrodynamic-lubrication

h_{max} generic maximum fluid-film thickness

h_{min} generic minimum fluid-film thickness

I_b matrix representation of the cylinder block's mass moment of inertia about the location of the shaft reaction against the cylinder block

I_p matrix representation of the piston's mass moment of inertia about the location of the shaft reaction against the cylinder block

I_s matrix representation of the slipper's mass moment of inertia about the location of the shaft reaction against the cylinder block

I_λ influence on torque loss when a parameter, λ, is perturbed $\pm 1\%$ from a nominal value

$\hat{i}$ unit vector in the x-direction of the Cartesian coordinate-system

$\hat{j}$ unit vector in the y-direction of the Cartesian coordinate-system

K_p fluid-film factor for the skewed radial pressure-profile between the piston and the cylinder block

K_μ hydrodynamic fluid-film constant

$\hat{k}$ unit vector in the z-direction of the Cartesian coordinate-system

L_{p_n} distance from the location of the shaft reaction to the location of the nth piston reaction in the x-direction

L_1 distance from the location of the shaft reaction to the face of the valve plate in the x-direction

L_2 distance from the location of the slipper reaction to the face of the piston in the x-direction

l generic length of hydrodynamic lubrication

l_p bushing length also the length of hydrodynamic lubrication between the piston and the cylinder block

l_s length of hydrodynamic lubrication between the slipper and the swashplate

l_v length of hydrodynamic lubrication between the valve plate and the cylinder block

M fluid mass

M_b mass of the cylinder block

M_{bal_n} vector moment exerted on the slipper from the effective-pressurized area on the face of the nth slipper

M_{c_n} vector moment exerted on the cylinder block from the axial pressure within the nth piston bore

M_{hd} vector moment exerted on a single slipper from the slipper hold-down mechanism

M_{l_n} vector moment exerted on the cylinder block at the inner edge of the nth bushing from the nth piston

M_{o_n} vector moment exerted on the cylinder block at the outer edge of the nth bushing from the nth piston

M_{p_n} vector moment exerted on the piston from the nth piston reaction

M_p mass of a single piston

M_{pr_n} vector moment exerted on the nth piston from the axial pressure within the nth piston bore

M_{r_n} vector moment exerted on the cylinder block from the radial pressure within the nth piston bore

M_{s_n} vector moment exerted on the nth piston from the nth slipper

M_s mass of a single slipper

M_{sh} vector moment exerted on the cylinder block from the shaft

M_{sp} vector moment exerted on the cylinder block from the cylinder-block spring

M_{sw_n} vector moment exerted on the nth slipper from the swash plate

M_v vector moment exerted on the cylinder block from the valve plate

m linearized transition-slope for the pressure carry-over on the valve plate

m_n instantaneous overhang-length of the nth piston

m_o nominal overhang-length of the piston

N total number of pistons

n slipper and / or piston counter (i.e., the nth slipper or the nth piston)

P fluid pressure

P_b boundary pressure outside the control volume of the nth piston-bore

P_d discharge pressure of the pump

P_i intake pressure of the pump

P_n pressure within the nth piston-bore

P_p skewed radial pressure-profile between the piston and the cylinder block

P_s pressure profile across the outside land of the slipper

P_{b_i} pressure profile across the inside region of the diametrical land on the cylinder block

P_{b_o} pressure profile across the outside region of the diametrical land on the cylinder block

Q volumetric flow-rate into the control volume of a single piston-bore

R_a RMS surface roughness of surface "a"

R_b RMS surface roughness of surface "b"

R_{b_i} outside radius of the inner region of the diametrical land on the cylinder block

R_{b_o} outside radius of the outer region of the diametrical land on the cylinder block

R_p radius of a piston bore

R_s outside radius of the slipper land

r piston pitch-radius; generic radial polar-coordinate

r_{b_i} inside radius of the inner region of the diametrical land on the cylinder block

r_{b_o} inside radius of the outer region of the diametrical land on the cylinder block

r_p radius of a piston

r_s inside radius of the slipper land

T instantaneous torque exerted on the cylinder block in the x-direction by the shaft

$\bar{T}$ average torque exerted on the cylinder block in the x-direction by the shaft

T_a torque value resulting from a 1% decrease in the nominal value of a design parameter

T_b torque value resulting from a 1% increase in the nominal value of a design parameter

T_I instantaneous idealized-torque exerted on the cylinder block in the x-direction by the shaft

$\bar{T}_I$ average idealized-torque exerted on the cylinder block in the x-direction by the shaft

T_L instantaneous torque-loss on the cylinder block in the x-direction

$\bar{T}_L$ average torque-loss on the cylinder block in the x-direction

T_n idealized torque exerted on the cylinder block by the nth piston

T_o nominal torque-value

T_{TH} theoretical torque exerted on the cylinder block in the x-direction by the shaft

T_γ torque difference between the idealized and the theoretical torque exerted on the cylinder block in the x-direction also called the "gamma effect"

ΔT_m average differential measured-torque for the reduced spring-load tests

ΔT_t differential theoretical-torque for the reduced spring-load tests

t time

U generic description of relative velocity

U_{p_n} relative axial-velocity between the nth piston and the cylinder block

U_{s_n} relative velocity between the nth slipper and the swash plate

U_v linearized relative-velocity between the cylinder block and the valve plate

u fluid velocity-profile

V instantaneous volume of the control volume of the piston bore

V_o reference volume of fluid within a single piston-bore

W generic load per unit width

W_{l_n} load per unit width between the *n*th piston and the cylinder block at the inner edge of the *n*th bushing

W_{o_n} load per unit width between the *n*th piston and the cylinder block at the outer edge of the *n*th bushing

W_{s_n} load per unit width between the *n*th slipper and the swash plate

W_v load per unit width between the cylinder block and the valve plate

w distance from the slipper reaction against the piston to the swash plate

$\ddot{X}_b$ vector translational-acceleration of the cylinder block

X_{p_n} vector translational-position of the *n*th piston

$\dot{X}_{p_n}$ vector translational-velocity of the *n*th piston

$\ddot{X}_{p_n}$ vector translational-acceleration of the *n*th piston

$\ddot{X}_{s_n}$ vector translational-acceleration of the *n*th slipper

x primary Cartesian-coordinate

y secondary Cartesian-coordinate

z tertiary Cartesian-coordinate

α swash-plate angle

β fluid bulk-modulus

γ pressure carry-over angle on the valve plate

ζ fluid-film dimensionless variable

η fluid viscosity

η_{oa} overall efficiency of the pump

η_t torque efficiency of the pump

η_v volumetric efficiency of the pump

$\dot{\Theta}_b$ vector angular-velocity of the cylinder block

$\ddot{\Theta}_b$ vector angular-acceleration of the cylinder block

$\dot{\Theta}_{p_n}$ vector angular-velocity of the *n*th piston

$\ddot{\Theta}_{p_n}$ vector angular-acceleration of the *n*th piston

$\dot{\Theta}_{s_n}$ vector angular-velocity of the *n*th slipper

$\ddot{\Theta}_{s_n}$ vector angular-acceleration of the *n*th slipper

θ angular polar-coordinate

θ_n angular polar-coordinate of the *n*th piston

λ generic design-parameter

λ_a 99% of the nominal value of a generic design-parameter

λ_b 101% of the nominal value of a generic design-parameter

λ_o nominal value of a generic design-parameter

μ generic variable coefficient-of-friction

$\hat{\mu}$ generic maximum-boundary coefficient-of-friction

μ_{hyd} coefficient-of-friction for hydrodynamic lubrication

μ_{l_n} coefficient-of-friction between the *n*th piston and the cylinder block at the inside edge of the *n*th bushing

μ_{mix} coefficient-of-friction for mixed lubrication conditions

μ_{o_n} coefficient-of-friction between the *n*th piston and the cylinder block at the outside edge of the *n*th bushing

$\hat{\mu}_p$ maximum boundary coefficient-of-friction between the piston and the cylinder block

$\hat{\mu}_s$ maximum boundary coefficient-of-friction between the slipper and the swash plate

μ_{s_n} coefficient-of-friction between the *n*th slipper and the swash plate

μ_v coefficient-of-friction between the cylinder block and the valve plate

$\hat{\mu}_v$ maximum boundary coefficient-of-friction between the cylinder block and the valve plate

ξ even integers

ρ fluid mass-density

ρ_p offset circular-relationship between the piston bore and the cocked piston

τ fluid shear

ϕ generic angular polar-coordinate

ψ_n angular position describing the cocked orientation on the *n*th piston

ω rotational speed of the pump shaft and cylinder block

ACKNOWLEDGEMENTS

I would like to thank my committee: Richard J. Smith, Greg R. Luecke, Judy M. Vance, Donald R. Flugrad and Ambar Mitra, for their advisement and support of my graduate program at Iowa State University. The technical input and the continual encouragement received from this group of scholars has been greatly valued.

I would also like to thank my colleagues at Sauer-Sundstrand. Without the patient teaching of these men, especially John Pinkerton, Kerry Geringer, and Jim Bolinger, the making of this dissertation would not have been possible.

CHAPTER 1. INTRODUCTION

1.1 Background

Axial-piston swash-plate type hydrostatic pumps are used within hydraulic circuitry for transmitting power. The history and use of these machines begins as far back as the late 1800's; however, the extensive use of axial-piston pumps in many applications did not flourish until the middle part of this century. (See Pippenger's *Fluid Power — The Hidden Giant* (1992) for a thorough history of the use and development of axial-piston pumps.) In the marketplace, the highest selling point of the hydrostatic pump has been its unique ability to transmit very large amounts of power using a very compact system (an attribute often referred to as "power density"). Though these machines boast significant power-to-size ratios, a price is paid for using them to transmit energy; namely, axial-piston hydrostatic pumps exhibit less efficient operation than most power transmission devices. This is especially true in the low power ranges of operation.

Power is lost in a hydrostatic pump in two ways: 1) high-pressure fluid leaks away from the path of power transmission, or 2) machinery components create friction that causes energy to dissipate away from the machine in the form of heat. The leakage losses contribute to a decrease in the pump's *volumetric* efficiency, η_v, while the frictional loss contribute to a decrease in the pump's *torque* efficiency, η_t. The overall efficiency of the pump is given mathematically as $\eta_{oa} = \eta_v \eta_t$ (Merritt 1967, 71). In the past, the inefficiency of axial-piston

swash-plate type hydrostatic pumps has simply been accepted as an unavoidable penalty of using hydraulic circuitry for transmitting power. As long as fuel has been reasonably cheap, many industrial applications have opted to take advantage of the power-to-size ratio offered by hydrostatics while tolerating the higher operating cost associated with them. Though by-and-large this fact remains true, a growing number of users are beginning to voice an objection to the needless waste of hydraulic power. In response to these objections, manufacturers of hydraulic equipment are trying to find ways to reduce the energy that is lost when transmitting power hydraulically.

1.2 Research Survey

With the increased use of hydrostatic pumps, published research associated with these same machines has slowly emerged. Particular areas of emphasis have been placed on the control and dynamic behavior of *variable-displacement* pumps, the performance and efficiency of hydrostatic pumps in general, and the tribological characteristics of the pump components themselves. The reader is encouraged to peruse the References of this dissertation; however, a summary of these publications will be made in the following subsections.

1.2.1 Control Research

The control of a variable-displacement pump is accomplished by intelligently varying the angle of the machine's swash plate. (See Section 2.2 of Chapter 2 for a diagram of the

pump's general configuration.) In the past, the greatest difficulty of modeling this component has been determining the naturally-induced torque exerted on the swash plate from the pumping action of the pump itself. Because the general model for this torque has been unknown, most control research has been done using either oversimplified assumptions or experimental procedures (Schoenau, Burton, and Kavanagh 1990; Kim, Cho, and Lee 1987; Thoma 1979; Merritt 1967). In 1985, Zeiger and Akers published a ninth-order numerical model for the torque on the swash plate that correlated well with experimental results. This work was foundational in that it paved the way for a-priori investigations that could be carried out numerically rather than experimentally (Inoue and Nakazato 1993). Further advancements of the model presented by Zeiger and Akers were made in 1994 when Manring and Johnson published an empirically verified closed-form result of the same torque on the swash plate which allows for reasonable models of the pump to be built without the expensive computational overhead of a ninth-order model.

1.2.2 Performance Research

Past research conducted on the overall performance of axial-piston swash-plate type hydrostatic pumps has taken a definite path of empirical study (Puormovahed 1992; McCandlish and Dorey 1981; Browns, Rolfe, and Chapple 1978; Wilson and Lemme 1968; Peterson 1966; Taylor 1958; Wilson 1948). Some of this research has been guised within titles that make the research appear analytical in nature (McCAndlish and Dorey 1984; Zarotti

and Nervegna 1981; Schlosser 1961); however, the heavy dependance of these studies on empirical test-data quickly shows a dominate emphasis within the test lab and not the office. While these studies have revealed the *actual* characteristics of the hydrostatic pump's performance and provided typical "efficiency maps" to be expected from such machines (Merritt 1967, 71), they have not provided a means for correcting the performance when it appears undesirable. The reason for this is that typical performance research has been conducted on a *macro* scale rather than a *micro* scale and has not provided enough detail for understanding what actually occurs *within* the pump itself. In this regard, a tremendous void exists within the research for creating a-priori models that describe the physical phenomenon of leakage and frictional losses as they occur locally within an entirely assembled machine working throughout its typical range of operation.

1.2.3 Component Research

While it has been recognized that a need exists for understanding the physical behavior of the components within the pump (i.e., a *micro* scale understanding versus and *macro* scale understanding), it has also been observed that the problem is complex. The complexity of this work has forced researchers to remove the components from within the pump itself and to study the problem by emphasizing idealized situations that don't actually exist during normal operation. (While some of this work has been conducted on pistons, far and above the majority of this work has been placed on slippers, while none of it has emphasized the valve

plate. Again, see Section 2.2 of Chapter 2 for a diagram of the pump's general configuration showing these components.) An exception to this rule would be the work done by Hooke and Kakoullis (1983) which studied the influence of "non-flat" slippers on fluid film-thicknesses between the slipper and the swash plate. This work is excellent and was conducted within an assembled machine as it worked under normal operating conditions. Still, much of the research done at the component level lacks theoretical explanation and simply emphasizes the *results* of studies that were conducted on specialized test stands (Tanaka, Nakahara, and Kyogoku 1993; Ezato and Ikeya 1986). In opposition to this last statement stands a singular purely-theoretical paper written by Kazama and Yamaguchi (1993) presenting a complex numerical analysis for the lubrication of the slipper. Though much has been learned from the research that has been conducted on individual components within the pump, the task of assembling this information into a single comprehensive model describing the performance characteristic of an entire pump has yet to be done. Studies in this direction would prove to be unique and tremendously useful for the advancement of hydrostatic-pump research, design, and development.

1.3 Dissertation Objectives

The research of this dissertation concerns itself with the performance of an entirely assembled pump working under normal operating conditions. Specifically, this research emphasizes the torque characteristics of the machine including both the idealized torque and

the torque that is lost due to friction. The reader should note that the topics within this study do *not* address the energy losses within the pump as they relate to leakage. The itemized objectives of this dissertation are as follows:

1. To evaluate the theoretical torque on the cylinder block and to suggest an improved model for the well-known mathematical expression describing this quantity.

2. To develop a comprehensive model for the actual torque on the cylinder block and to verify this model using acquired test data.

3. To determine the percent of the overall torque-loss within the pump that is generated by the pistons, the slippers, and the valve plate respectively.

4. To identify the design parameters of the pump that have the most significant impact on the overall torque-loss when they are perturbed a small amount from nominal conditions.

By accomplishing these tasks, this study will have advanced the current understanding of the phenomenal characteristics within axial-piston hydrostatic pumps and provided insight regarding parametric design changes that can be made to favorably alter the overall performance of the machine itself.

1.4 Dissertation Outline

This dissertation begins in Chapter 2 by familiarizing the reader with the basic geometry of the pump and the nomenclature used throughout the research. Upon defining terms and describing the basic components of the pump, a comprehensive mechanical analysis

of the machine is conducted in Chapter 3 using the basic principles of Mechanics. The results of this analysis are dependent upon several quantities; specifically, they depend upon the quantity that describes the pressure within each piston bore, the effective pressurized-areas on the piston, the cylinder block, and the slipper, and the models that describe the friction acting on each component within the pump. Chapter 4 is used to derive a numerical and a closed-form approximation for the pressure within a single piston bore while Chapter 5 derives the expressions for the effective pressurized-areas throughout the pump. In this dissertation, the basic theories of tribology as they relate to journal bearings are applied to the pump components for determining coefficients of friction and these theories are presented in Chapter 6. Chapter 7 uses the results of Chapter 6 to model the friction for each component within the pump and individual attempts are made to verify these models empirically. Finally, in Chapter 8, the results of Chapters 3 through 7 are assembled to describe the net torque on the cylinder block including both the idealized torque and the cylinder-block torque loss. This chapter discusses the theoretical torque on the cylinder block using closed-form results and presents the numerical program used in the research for determining characteristics of torque loss. (A copy of this program is included in the Appendix.) In this chapter an improved expression for the idealized torque on the cylinder block is presented and the numerical model for determining torque loss is verified using laboratory data. With the aid of the verified computer model, the torque loss is numerically separated into losses that result from individual components within the machine and a graph is presented that shows what percent of the torque

loss results from the operation of each component. Again, using the verified model of Chapter 8, Chapter 9 examines the torque sensitivity to the variation of several key parameters within the pump and identifies the most significant design parameters that may be adjusted to influence the torque loss characteristics. Lastly, the conclusions of this work are assembled and discussed in Chapter 10.

CHAPTER 2. GENERAL DESCRIPTIONS

2.1 Introduction

This chapter is written to familiarize the reader with the basic function and components of an axial-piston swash-plate type hydrostatic pump and to define the terminology used in this dissertation. In the following sections, the assembled design of the pump and its overall operation are described followed by a brief description of each major component within the system.

2.2 Overall Pump-Configuration

This section describes the overall function and appearance of the axial-piston swash-plate type hydrostatic pump. The characteristics of this pump are chosen in such a way as to represent *typical* pump designs. Figure 2-1 shows the pump's general configuration.

The pump consists of several pistons within a common cylindrical block. The pistons are nested in a circular array within the block at equal intervals about the x-axis. As shown in Figure 2-1, the cylinder block is held tightly against a valve plate using the force of the compressed cylinder-block spring. A thin film of oil separates the valve plate from the cylinder block which, under normal operating conditions, forms a hydrodynamic bearing between the two parts. A ball-and-socket joint connects the base of each piston to a slipper. The slippers themselves are kept in reasonable contact with the swash plate by a retainer (not

shown in Figure 2-1) where a hydrostatic and hydrodynamic bearing surface separates the slippers from the swash plate. The swash plate is held at a fixed angle.

While the valve plate is held in a fixed position, the cylinder block is driven about the x-axis at a constant angular speed, ω. During this motion, each piston periodically passes over the discharge and intake ports on the valve plate. Furthermore, because the slippers are

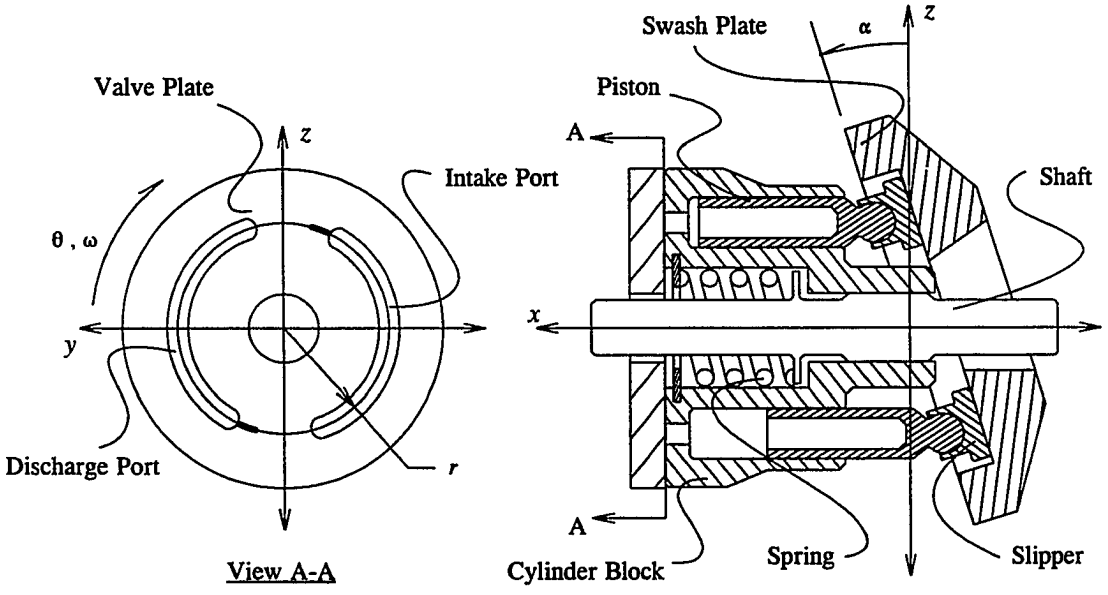

Figure 2-1. General pump configuration.

held against the inclined plane of the swash plate, the pistons undergo an oscillatory displacement in and out of the cylinder block. As the pistons pass over the intake port, the piston withdraws from the cylinder block and fluid is drawn into the piston bore. As the pistons pass over the discharge port, the piston advances into the cylinder block and fluid is pushed out of the piston bore. This motion repeats itself for each pump revolution and the

basic task of pumping fluid is then accomplished.

2.3 Valve-Plate Geometry

Figure 2-2 shows the geometry of the valve plate used for this study. Note: the intake port and the discharge port are shown to be geometrically identical; in general, this does not have to be the case.

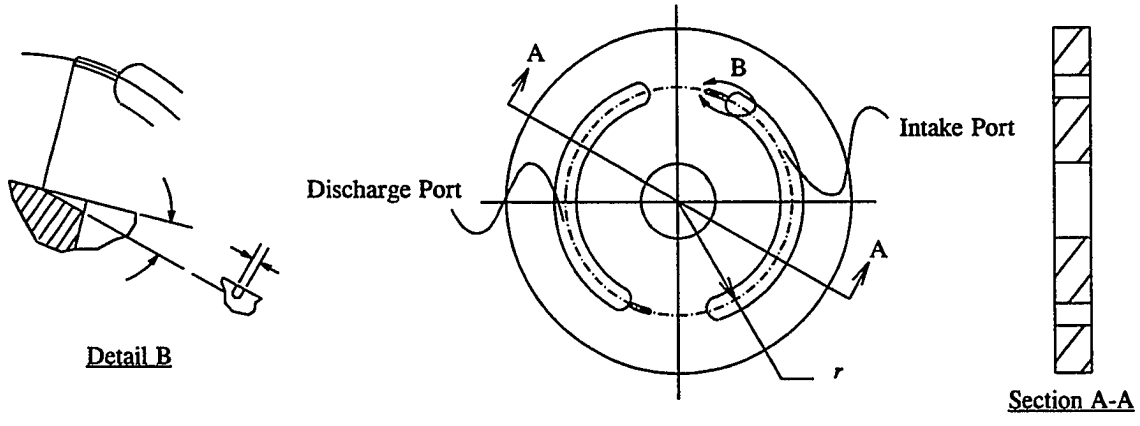

Figure 2-2. Valve-plate geometry.

The valve plate is designed to allow for a smooth pressure transition as the pistons pass from the discharge port to the intake port and vice-versa. This is accomplished by cutting slots in the valve plate at the entry of each port. Detail B of Figure 2-2 shows the basic geometry of these slots; however, in general, these slots may be quite intricate and often exhibit unique geometric features that may vary depending upon the manufacturer of the pump.

2.4 Cylinder-Block Geometry

Figure 2-3 shows a cylinder block that is designed to accommodate 9 pistons. In general, 9 is the most common number of pistons used in hydrostatic-pump designs; however, manufacturers will occasionally design a pump with only 7 pistons. Note: the number of pistons within the pump is usually odd since this tends to reduce the discharge flow-ripple of the machine (Thoma 1979, 44). For the theoretical development of this study, the number of pistons is incidental.

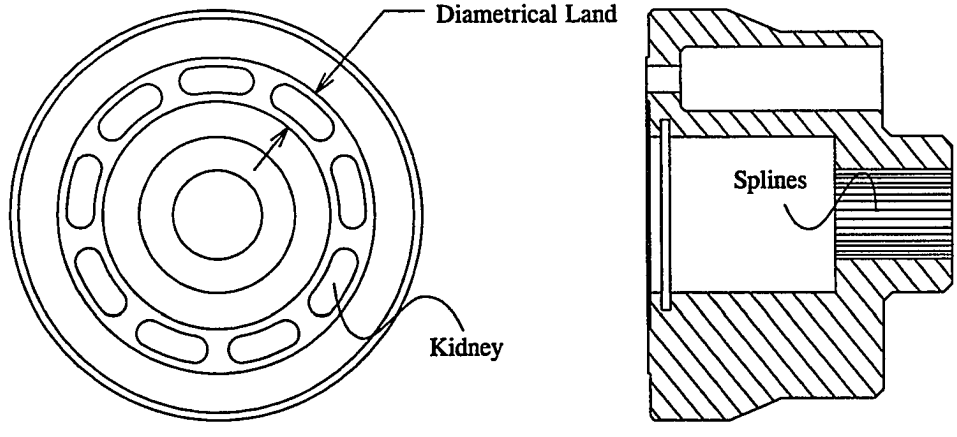

Figure 2-3. Cylinder-block geometry.

The opening of each piston chamber is designed to match the shape of the valve-plate ports. Due to the inherent shape of these openings, they are often referred to as "kidneys". The kidneys are contained within an elevated diametrical-land which is machined onto the face of the cylinder block. It is this diametrical land that provides sealing and a running surface between the valve plate and the cylinder block. Note: the diametrical land is very short and

can hardly be seen in the sectioned view of Figure 2-3.

2.5 Piston / Slipper Geometry

Figure 2-4 shows a sectioned view of a piston-slipper assembly. The piston itself is shown to be hollow because a lightweight piston is desirable. The ball-and-socket joint and the swash-plate riding surface are both in constant need of oil; therefore, the piston and the

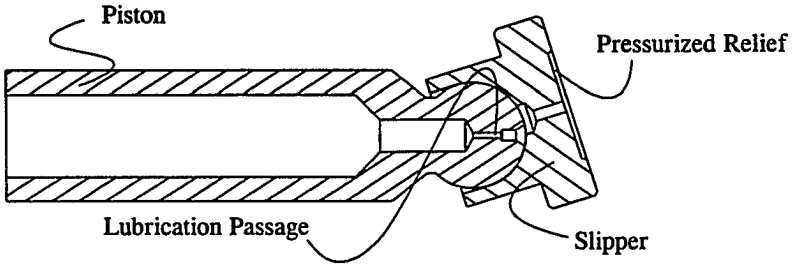

Figure 2-4. Piston / slipper geometry.

slipper are designed with lubrication passages. Figure 2-4 shows a shallow relief that is cut into the running face of the slipper. This relief is pressurized, through the lubrication passage, to provide a lifting force between the slipper and the swash plate. This pressurized fluid between the swash plate and the slipper provides the hydrostatic bearing that was mentioned in Section 2.2 of this chapter.

2.6 Shaft Geometry

The shaft is shown in Figure 2-5. It should be assumed by the reader that this shaft is supported at both ends by a robust frictionless bearing-system. Typically, the types of bearings that support this shaft vary widely and are therefore not shown in the drawings.

The shaft performs three functions: 1) it transmits torque to the cylinder-block via a spline connection (see Figures 2-3 and 2-5), 2) it maintains the alignment of the cylinder block with the valve plate, and 3) it provides a constant compressed length of the cylinder-block spring using the machined ledge shown in Figures 2-1 and 2-5.

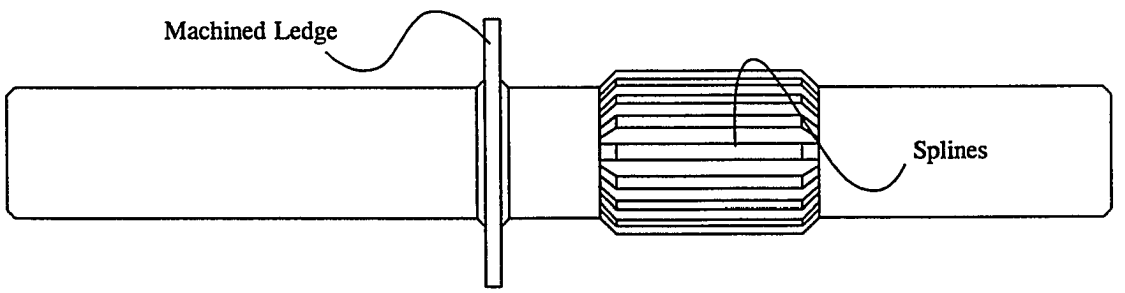

Figure 2-5. Shaft geometry.

2.7 Conclusion

The previous descriptions have included the major, and most generic, components of the axial-piston pump. Other components in the system, such as the slipper retaining-mechanism and the shaft bearing-system, have been omitted from this discussion because of their lack of generality. As the need arises, these omitted components will be described.

CHAPTER 3. MECHANICAL ANALYSIS

3.1 Introduction

In this chapter, the equations that govern the behavior of the cylinder block, the pistons, and the slippers of an axial-piston swash-plate type hydrostatic pump are derived by relating the kinematics of each component to the forces that act upon them using the standard

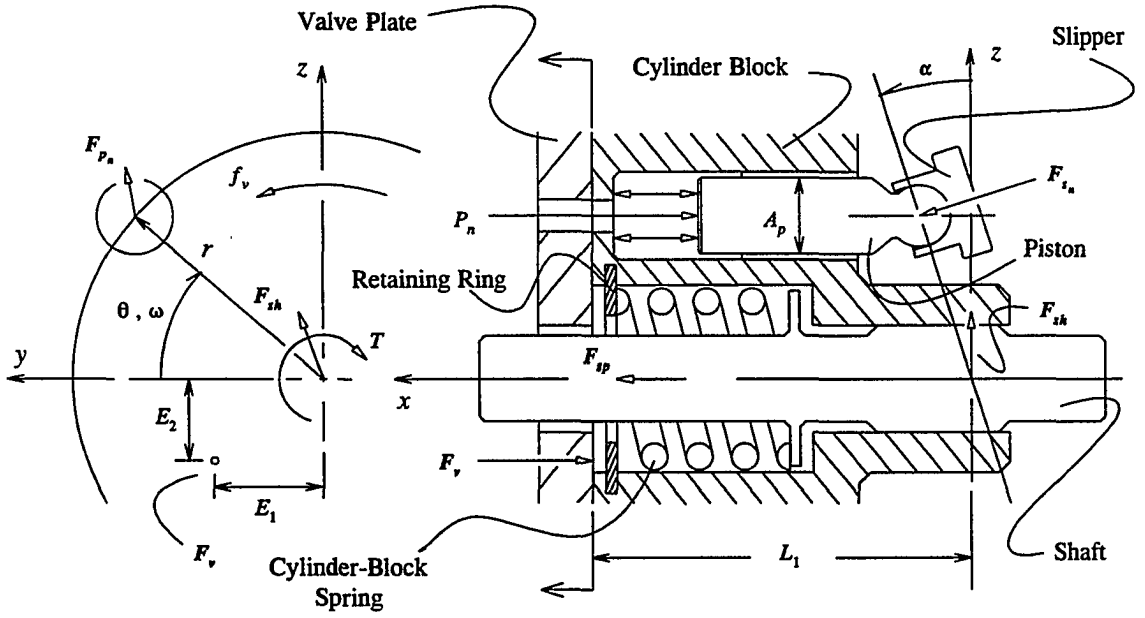

Figure 3-1. A sparse schematic-of-forces that coexist within the axial-piston pump.

practices of Mechanics (Newton's Second Law). In the concluding section of this chapter, the equations that describe significant physical-quantities are written in their most primitive forms for the cylinder block, the pistons, and the slippers. Any simplifications to these quantities based upon symmetry are also performed.

Before beginning this chapter, it may be helpful for the reader to study Figure 3-1. This figure introduces the reader to several forces that coexist within the axial-piston pump under normal operating-conditions. The reader should keep in mind that Figure 3-1 is only a sparse schematic and that not all of the forces within the machine are presented here. More detail will be added to this figure as the analysis in this chapter progresses.

3.2 Cylinder Block Free-Body Diagram

Figure 3-2 shows the free-body diagram of the cylinder block. The forces acting on the cylinder block come from the block spring (F_{sp}), the reaction of the shaft (F_{sh}), the reaction of the valve plate (F_v), the clamping force from the pressure within each piston bore (F_{c_n}), the radial pressure force within each piston bore (F_{r_n}), and the reaction of the piston against the side-wall of each piston bore (F_{p_n}). Using standard mechanical analysis, these forces are summed and set equal to the translational inertia of the cylinder block, $M_b \ddot{X}_b$, to derive the following equation-of-motion:

$$M_b \ddot{X}_b = F_{sp} + F_{sh} + F_v + \sum_{n=1}^{N} F_{c_n} + \sum_{n=1}^{N} F_{r_n} + \sum_{n=1}^{N} F_{p_n} \quad . \tag{3.1}$$

In general, each force on the cylinder block generates a corresponding moment about the location of the shaft reaction. Summing these moments, and setting them equal to the angular inertia of the cylinder block, $I_b \ddot{\Theta}_b + \dot{\Theta}_b \times I_b \dot{\Theta}_b$, it can be shown that

$$I_b \ddot{\Theta}_b + \dot{\Theta}_b \times I_b \dot{\Theta}_b = M_{sp} + M_{sh} + M_v + \sum_{n=1}^{N} M_{c_n} + \sum_{n=1}^{N} M_{r_n} + \sum_{n=1}^{N} M_{p_n} \quad . \tag{3.2}$$

Equations (3.1) and (3.2) provide the basis for determining the equations of motion for the cylinder block. The following subsections will examine the components of equations (3.1) and (3.2) in closer detail.

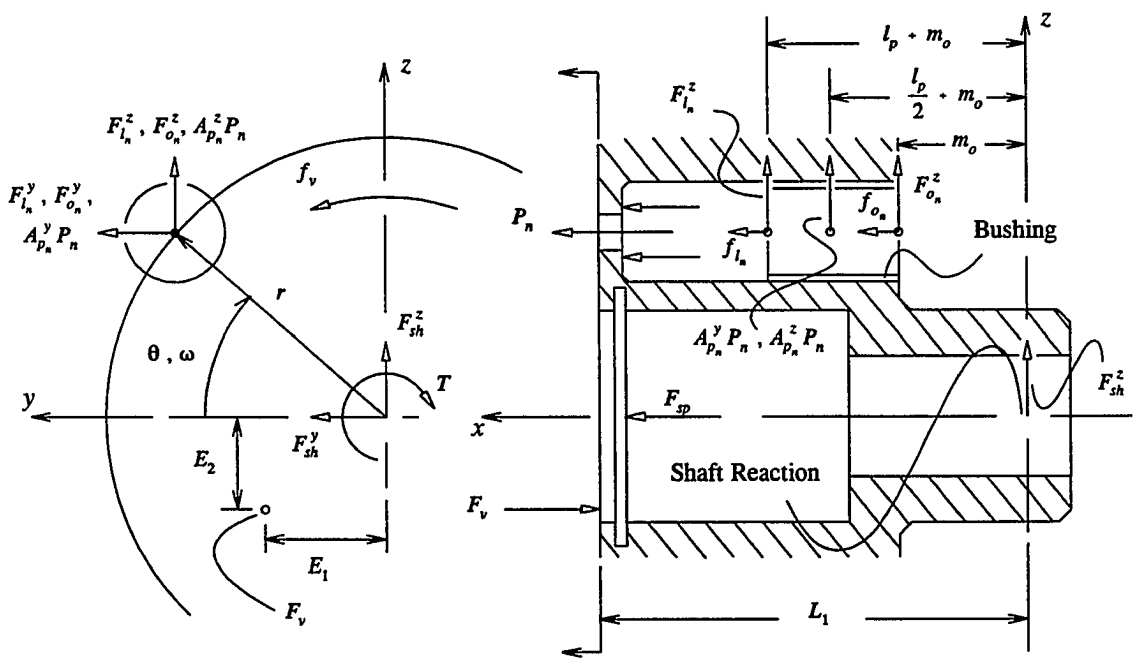

Figure 3-2. A free-body diagram of the cylinder block.

3.2.1 Cylinder-Block Kinematics and Inertia

Figure 3-1 shows the cylinder block forced against the valve plate by the cylinder-block spring. The cylinder-block spring is compressed between the retaining ring mounted within the cylinder block and the machined ledge on the shaft. Furthermore, a pressure force

(which will be discussed later) exists within each piston bore that "clamps" the cylinder block against the valve plate. Due to these constraints, under normal operating conditions, the cylinder block is not able to move in the x-direction. Furthermore, the shaft passing through the center of the cylinder block keeps the cylinder block from moving in either the y or z-directions; therefore, the translational inertia of the cylinder block is given by

$$M_b \ddot{X}_b = 0 \quad . \tag{3.3}$$

In this analysis, it is assumed that the cylinder block rotates about the x-axis at a *constant* angular speed, ω (i.e., there is no angular acceleration in the x-direction). Since, under normal operating conditions, the face of the cylinder block remains reasonably parallel with the face of the valve plate, there is no angular acceleration in either the y or z-directions either. Due to symmetry there are no products-of-inertia for the cylinder block and therefore the total angular inertia of the cylinder block is written

$$I_b \ddot{\Theta}_b + \dot{\Theta}_b \times I_b \dot{\Theta}_b = 0 \quad . \tag{3.4}$$

3.2.2 Cylinder-Block Spring Force

As previously mentioned, the cylinder-block spring is compressively assembled between a retaining ring, mounted within the cylinder block, and a machined ledge on the shaft. (Again, see Figure 3-1.) The cylinder-block spring is used to hold the cylinder block

against the valve plate and acts only in the x-direction. Hence, this force is written

$$\boldsymbol{F}_{sp} = F_{sp}\,\hat{\boldsymbol{i}} + 0\,\hat{\boldsymbol{j}} + 0\,\hat{\boldsymbol{k}} \quad , \tag{3.5}$$

where F_{sp} is the assembled load of the cylinder-block spring. The distance of this force away from the shaft reaction is given by $L_1\,\hat{\boldsymbol{i}} + 0\hat{\boldsymbol{j}} + 0\,\hat{\boldsymbol{k}}$. Taking the cross product of this distance with equation (3.5) it can be seen that the net moment generated about the shaft reaction from the block spring is

$$\boldsymbol{M}_{sp} = \boldsymbol{0} \quad . \tag{3.6}$$

3.2.3 Shaft Reaction

The shaft is used to drive the cylinder block about the x-axis and to maintain the alignment of the cylinder block with the valve plate. The connection between the cylinder block and the shaft is accomplished through a set of splines that run parallel to the shaft; as such, the spline interaction allows for no resultant force along the x-axis. In general, the forces from the shaft acting on the cylinder block may be written as

$$\boldsymbol{F}_{sh} = 0\,\hat{\boldsymbol{i}} + F_{sh}^{y}\,\hat{\boldsymbol{j}} + F_{sh}^{z}\,\hat{\boldsymbol{k}} \quad . \tag{3.7}$$

Since moments are conventionally being summed about the shaft reaction for this research, it is clear that $\boldsymbol{F}_{sh}$ exerts no moment about itself; however, the torque on the cylinder block,

T, is present at this location and therefore the net moment on the cylinder block, generated by the shaft, is given by

$$M_{sh} = T\,\hat{i} + 0\,\hat{j} + 0\,\hat{k} \quad . \tag{3.8}$$

It should be noted that the driving torque on the cylinder block, T, is the primary quantity of interest in this dissertation.

3.2.4 Valve-Plate Reaction

The valve plate is set rigidly within the pump and exerts a keeping force on the cylinder block in the negative x-direction. In general, this force is distributed over the contact area between the valve plate and the cylinder block; however, for the purposes of this analysis, this force will be treated as a point-load located at the centroid of the actual distributed-load. This force is then written

$$F_v = -F_v\,\hat{i} + 0\,\hat{j} + 0\,\hat{k} \quad . \tag{3.9}$$

From Figure 3-2 it can be seen that the distance of this force away from the shaft reaction is given by $L_1\,\hat{i} + E_1\hat{j} - E_2\,\hat{k}$, where E_1 and E_2 locate the centroid of the distributed load between the cylinder block and the valve plate. Taking the cross product of this distance with equation (3.9), and recognizing that the friction on the valve plate, f_v, imposes a moment on the cylinder block in the negative x-direction, the net moment generated on the cylinder block by

the valve plate may be expressed

$$M_v = -f_v \hat{i} - F_v E_2 \hat{j} + F_v E_1 \hat{k} \quad . \tag{3.10}$$

3.2.5 Pressure-Clamping Force

The cylinder block is designed so that the pressure within the *n*th piston bore forces the block in the positive *x*-direction. This effect is often called pressure-clamping because it "clamps" the block onto the valve plate. See Figure 3-2. Because each piston bore contains fluid under different pressures, each piston bore exerts a different pressure-clamping force on the cylinder block. For the *n*th piston bore the pressure-clamping force may be written as

$$F_{c_n} = A_b P_n \hat{i} + 0 \hat{j} + 0 \hat{k} \quad , \tag{3.11}$$

where A_b is the effective pressurized-area within a single piston bore and P_n is the instantaneous pressure within the *n*th piston bore. The distance of the *n*th clamping force away from the shaft reaction is given by $L_1 \hat{i} + r\cos(\theta_n)\hat{j} + r\sin(\theta_n)\hat{k}$. Taking the cross product of this distance with equation (3.11), it may be shown that the moment acting on the cylinder block from the pressure-clamping force within the *n*th piston bore is given by

$$M_{c_n} = 0 \hat{i} + A_b P_n r\sin(\theta_n) \hat{j} - A_b P_n r\cos(\theta_n) \hat{k} \quad . \tag{3.12}$$

3.2.6 Radial Pressure-Force

Within the nth piston bore, the pressure drops across the bushing from the existing bore pressure, P_n, to a nominally low pressure outside the cylinder block. Although it is not intuitive, this pressure drop does not occur symmetrically about the centerline of the piston bore. It is slightly skewed. The skewedness of this pressure drop results in a net radial-force that acts against the side of the piston bore. In general, this force is expressed as

$$\boldsymbol{F}_{r_n} = 0\,\hat{\boldsymbol{i}} + A_{p_n}^{y} P_n \hat{\boldsymbol{j}} + A_{p_n}^{z} P_n \hat{\boldsymbol{k}} \quad , \tag{3.13}$$

where $A_{p_n}^{y}$ and $A_{p_n}^{z}$ are the effective pressurized-areas within the nth piston bore in the y and z-directions respectively. As shown in Figure 3-2, the distance of this force away from the shaft reaction is give by $(l_p/2 + m_o)\,\hat{\boldsymbol{i}} + r\cos(\theta_n)\,\hat{\boldsymbol{j}} + r\sin(\theta_n)\,\hat{\boldsymbol{k}}$. Taking the cross product of this distance with equation (3.13) the moment acting on the cylinder block from the radial pressure-force within the nth piston bore is given by

$$\boldsymbol{M}_{r_n} = \left(A_{p_n}^{z} P_n r\cos(\theta_n) - A_{p_n}^{y} P_n r\sin(\theta_n)\right)\hat{\boldsymbol{i}} - A_{p_n}^{z} P_n (l_p/2 + m_o)\,\hat{\boldsymbol{j}} + A_{p_n}^{y} P_n (l_p/2 + m_o)\,\hat{\boldsymbol{k}} \quad . \tag{3.14}$$

3.2.7 Piston Reaction

The piston bore of the cylinder block is lined with a metal bushing. See Figure 3-2. The bushing and the piston are designed so that the piston can never withdraw past the inner edge of the bushing during the operation of the machine. The length of the bushing is

commonly referred to as the engaged piston-bore length because it is assumed that the piston remains engaged at all points along the bushing during the operation of the hydrostatic machine. This assumption, however, is false. By examining worn cylinder blocks, it is consistently clear that the piston reaction within the piston bore is located at the inner and outer edges of the bushing. This situation is verified by the locations of polishing and wear within the piston bore; and, in fact, after examining a worn cylinder-block, one questions whether or not the piston *ever* touches the piston bore near the center of the bushing during normal operation. For this reason, in this analysis, the reaction forces of the piston within the piston bore are placed along the centerline of the piston bore at both the inner and outer ends of the bushing. See Figure 3-2.

The net reaction of the *n*th piston against the *n*th piston-bore is given by the summation of the forces acting at the inner edge of the *n*th bushing (F_{l_n}) and the forces acting at the outer edge of the *n*th bushing (F_{o_n}). This quantity is expressed vectorially as

$$F_{p_n} = F_{l_n} + F_{o_n} \quad . \tag{3.15}$$

Correspondingly, the net moment exerted about the location of the shaft reaction by the *n*th piston-reaction within the *n*th piston-bore is given by

$$M_{p_n} = M_{l_n} + M_{o_n} \quad , \tag{3.16}$$

where M_{l_n} and M_{o_n} are the moments resulting from the forces F_{l_n} and F_{o_n} respectively.

3.2.7.1 Reactions at the Inner Edge of the Bushing

From Figure 3-2, it can be seen that the forces exerted on the inner edge of the *n*th bushing by the *n*th piston may be expressed as

$$\boldsymbol{F}_{l_n} = f_{l_n}\hat{i} + F_{l_n}^{y}\hat{j} + F_{l_n}^{z}\hat{k} \quad , \tag{3.17}$$

where f_{l_n} is the friction generated at the inner edge of the bushing by the reaction of the *n*th piston at the same edge. The distance of the force $\boldsymbol{F}_{l_n}$ from the location of the shaft reaction is given by $(l_p + m_o)\hat{i} + r\cos(\theta_n)\hat{j} + r\sin(\theta_n)\hat{k}$. Taking the cross product of this distance with equation (3.17), the moment exerted about the location of the shaft reaction by the force $\boldsymbol{F}_{l_n}$ within the *n*th piston-bore is given by

$$\boldsymbol{M}_{l_n} = \left(F_{l_n}^{z} r\cos(\theta_n) - F_{l_n}^{y} r\sin(\theta_n)\right)\hat{i} + \left(f_{l_n} r\sin(\theta_n) - F_{l_n}^{z}(l_p + m_o)\right)\hat{j} + \left(F_{l_n}^{y}(l_p + m_o) - f_{l_n} r\cos(\theta_n)\right)\hat{k} \quad . \tag{3.18}$$

3.2.7.2 Reactions at the Outer Edge of the Bushing

Similar to the reaction at the inner edge of the bushing, from Figure 3-2, it can be seen that the forces exerted on the outer edge of the *n*th bushing by the *n*th piston may be expressed as

$$\boldsymbol{F}_{o_n} = f_{o_n}\hat{i} + F_{o_n}^{y}\hat{j} + F_{o_n}^{z}\hat{k} \quad , \tag{3.19}$$

where f_{o_n} is the friction generated at the outer edge of the bushing by the reaction of the *n*th

piston. The distance of this force away from the location of the shaft reaction is given by $m_o \hat{i} + r\cos(\theta_n)\hat{j} + r\sin(\theta_n)\hat{k}$. Taking the cross product of this distance with equation (3.19), the moment exerted about the location of the shaft reaction by the force F_{o_n} within the nth piston-bore is given by

$$M_{o_n} = \left(F_{o_n}^z r\cos(\theta_n) - F_{o_n}^y r\sin(\theta_n)\right)\hat{i} + \left(f_{o_n} r\sin(\theta_n) - F_{o_n}^z m_o\right)\hat{j} + \left(F_{o_n}^y m_o - f_{o_n} r\cos(\theta_n)\right)\hat{k} \quad . \quad (3.20)$$

3.2.7.3 Summary

By substituting the results of equations (3.17) and (3.19) into equation (3.15), the net load exerted by the nth piston against the inside wall of the nth piston-bore may generally be expressed as

$$F_{p_n} = f_{p_n}\hat{i} + \left(F_{l_n}^y + F_{o_n}^y\right)\hat{j} + \left(F_{l_n}^z + F_{o_n}^z\right)\hat{k} \quad , \quad (3.21)$$

where the net friction within the nth piston-bore is given by $f_{p_n} = f_{l_n} + f_{o_n}$. Similarly, by substituting the results of equations (3.18) and (3.20) into equation (3.16), the net moment generated by the nth piston within the nth piston-bore about the shaft reaction is given by

$$\begin{aligned} M_{p_n} = {} & \left(\left(F_{l_n}^z + F_{o_n}^z\right)r\cos(\theta_n) - \left(F_{l_n}^y + F_{o_n}^y\right)r\sin(\theta_n)\right)\hat{i} + \left(f_{p_n} r\sin(\theta_n) - F_{l_n}^z (l_p + m_o) - F_{o_n}^z m_o\right)\hat{j} \\ & + \left(F_{l_n}^y (l_p + m_o) + F_{o_n}^y m_o - f_{p_n} r\cos(\theta_n)\right)\hat{k} \quad . \end{aligned} \quad (3.22)$$

3.2.8 Summary

Collecting the forces acting on the cylinder block by substituting equations (3.3), (3.5), (3.7), (3.9), (3.11), (3.13) and (3.21) into equation (3.1), the forces exerted on the cylinder block are summarized by

$$\mathbf{0} = \begin{cases} \left(F_{sp} - F_v + \sum_{n=1}^{N} (A_b P_n + f_{p_n}) \right) \hat{i} + \left(F_{sh}^y + \sum_{n=1}^{N} \left(F_{l_n}^y + F_{o_n}^y + A_{p_n}^y P_n \right) \right) \hat{j} \\ + \left(F_{sh}^z + \sum_{n=1}^{N} \left(F_{l_n}^z + F_{o_n}^z + A_{p_n}^z P_n \right) \right) \hat{k} \quad . \end{cases} \tag{3.23}$$

Similarly, by substituting equations (3.4), (3.6), (3.8), (3.10), (3.12), (3.14) and (3.22) into equation (3.2) the moments exerted on the cylinder block are summarized as

$$\mathbf{0} = \begin{cases} \left(T - f_v + \sum_{n=1}^{N} \left(\left(F_{l_n}^z + F_{o_n}^z + A_{p_n}^z P_n \right) r \cos(\theta_n) - \left(F_{l_n}^y + F_{o_n}^y + A_{p_n}^y P_n \right) r \sin(\theta_n) \right) \right) \hat{i} \\ + \left(\sum_{n=1}^{N} \left((A_b P_n + f_{p_n}) r \sin(\theta_n) - F_{l_n}^z (l_p + m_o) - F_{o_n}^z m_o - A_{p_n}^z P_n (l_p/2 + m_o) \right) - F_v E_2 \right) \hat{j} \\ - \left(\sum_{n=1}^{N} \left((A_b P_n + f_{p_n}) r \cos(\theta_n) - F_{l_n}^y (l_p + m_o) - F_{o_n}^y m_o - A_{p_n}^y P_n (l_p/2 + m_o) \right) - F_v E_1 \right) \hat{k} \; . \end{cases} \tag{3.24}$$

Equations (3.23) and (3.24) contain quantities that depend upon the behavior of the pistons. In the following section, the influence of the pistons will be analyzed in closer detail.

3.3 Piston Free-Body Diagram

Figure 3-3 shows the free-body diagram of a single piston. The forces acting on the *n*th piston come from the reaction of the *n*th slipper at the piston / slipper ball-joint (F_{s_n}), the equal and opposite radial pressure-force acting within each piston bore ($-F_{r_n}$), the equal and

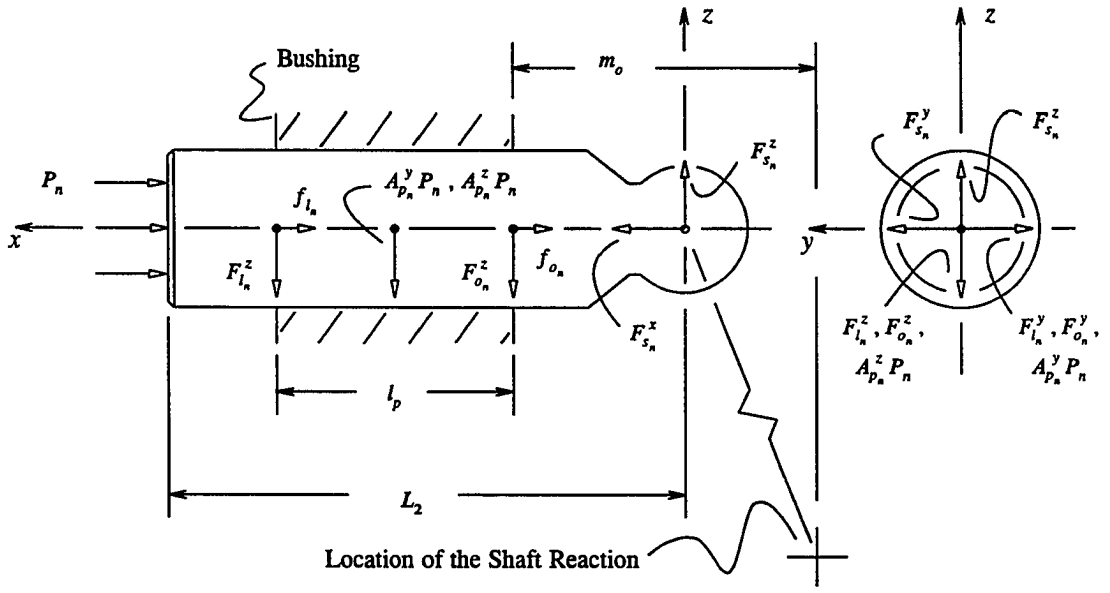

Figure 3-3. A free-body diagram of a single piston.

opposite reaction of the piston against the cylinder block ($-F_{p_n}$), and the pressure within the *n*th piston-bore acting on the face of the piston (F_{pr_n}). Summing these forces and setting them equal to the inertia of the piston, $M_p \ddot{X}_{p_n}$, gives

$$M_p \ddot{X}_{p_n} = F_{s_n} - F_{r_n} - F_{p_n} + F_{pr_n} \quad . \tag{3.25}$$

In general, each force on the piston generates a corresponding moment about the location of the shaft reaction. Summing these moments and setting them equal to the angular inertia of the piston, $I_p \ddot{\Theta}_{p_n} + \dot{\Theta}_{p_n} \times I_p \dot{\Theta}_{p_n}$, yields

$$I_p \ddot{\Theta}_{p_n} + \dot{\Theta}_{p_n} \times I_p \dot{\Theta}_{p_n} = M_{s_n} - M_{r_n} - M_{p_n} + M_{pr_n} \quad . \tag{3.26}$$

Equations (3.25) and (3.26) provide a basis for fully determining the equations that describe the behavior of a single piston.

3.3.1 Piston Kinematics and Inertia

From geometry, it can be shown that the position of the *n*th piston is given by

$$X_{p_n} = r \tan(\alpha) \sin(\theta_n)\, \hat{i} + r \cos(\theta_n)\, \hat{j} + r \sin(\theta_n)\, \hat{k} \quad . \tag{3.27}$$

Differentiating equation (3.27) once, with respect to time, yields the following result for the piston's translational velocity:

$$\dot{X}_{p_n} = r\,\omega \tan(\alpha) \cos(\theta_n)\, \hat{i} - r\,\omega \sin(\theta_n)\, \hat{j} + r\,\omega \cos(\theta_n)\, \hat{k} \quad , \tag{3.28}$$

where ω is the constant angular velocity of the shaft. Differentiating equation (3.28) with respect to time, and multiplying this result by the mass of a single piston, the final translational-inertia of the piston is given as

$$M_p \ddot{X}_{p_n} = - M_p r\,\omega^2 \tan(\alpha) \sin(\theta_n)\, \hat{i} - M_p r\,\omega^2 \cos(\theta_n)\, \hat{j} - M_p r\,\omega^2 \sin(\theta_n)\, \hat{k} \quad . \tag{3.29}$$

Due to the constraining nature between the piston and the piston bore, and due to the symmetry of the piston, the piston's net angular-inertia is written

$$I_p \ddot{\Theta}_{p_n} + \dot{\Theta}_{p_n} \times I_p \dot{\Theta}_{p_n} = 0 \quad . \tag{3.30}$$

3.3.2 Slipper Reaction

The slipper is connected to the spherical end of the piston using a forming process called swaging. The final result of this process is a connection that allows for three degrees of rotational freedom and zero degrees of translational freedom within the ball-joint. In general, the forces exerted on the piston by the slipper may be expressed as

$$F_{s_n} = F_{s_n}^x \hat{i} + F_{s_n}^y \hat{j} + F_{s_n}^z \hat{k} \quad . \tag{3.31}$$

From geometry, it can be shown that the distance of this force away from the shaft reaction is given by $r\tan(\alpha)\sin(\theta_n)\hat{i} + r\cos(\theta_n)\hat{j} + r\sin(\theta_n)\hat{k}$. Taking the cross product of this distance with equation (3.31), the moment generated about the shaft reaction by the slipper reaction at the ball of the piston is given by

$$\begin{aligned} M_{s_n} = &\left(F_{s_n}^z r\cos(\theta_n) - F_{s_n}^y r\sin(\theta_n)\right)\hat{i} + \left(F_{s_n}^x r\sin(\theta_n) - F_{s_n}^z r\tan(\alpha)\sin(\theta_n)\right)\hat{j} \\ &+ \left(F_{s_n}^y r\tan(\alpha)\sin(\theta_n) - F_{s_n}^x r\cos(\theta_n)\right)\hat{k} \quad . \end{aligned} \tag{3.32}$$

3.3.3 Radial Pressure-Force

The force and moment generated on the cylinder block by the skewed pressure drop within each bore exerts an equal and opposite force and moment against the piston. These quantities are described in Subsection 3.2.6 and are rewritten here for convenience. They are

$$\boldsymbol{F}_{r_n} = 0\,\hat{\imath} + A_{p_n}^{y} P_n \hat{\jmath} + A_{p_n}^{z} P_n \hat{k} \tag{3.33}$$

and

$$\boldsymbol{M}_{r_n} = \left(A_{p_n}^{z} P_n r\cos(\theta_n) - A_{p_n}^{y} P_n r\sin(\theta_n)\right)\hat{\imath} - A_{p_n}^{z} P_n (l_p/2 + m_o)\hat{\jmath} + A_{p_n}^{y} P_n (l_p/2 + m_o)\hat{k} \quad . \tag{3.34}$$

3.3.4 Piston Reaction

The force and moment generated on the cylinder block by the piston also exerts an equal and opposite force and moment against the piston itself. This force and moment is described in Subsection 3.2.7 and is rewritten here for convenience. These quantities are

$$\boldsymbol{F}_{p_n} = f_{p_n}\,\hat{\imath} + \left(F_{l_n}^{y} + F_{o_n}^{y}\right)\hat{\jmath} + \left(F_{l_n}^{z} + F_{o_n}^{z}\right)\hat{k} \tag{3.35}$$

and

$$\begin{aligned}\boldsymbol{M}_{p_n} = {} & \left(\left(F_{l_n}^{z} + F_{o_n}^{z}\right) r\cos(\theta_n) - \left(F_{l_n}^{y} + F_{o_n}^{y}\right) r\sin(\theta_n)\right)\hat{\imath} + \left(f_{p_n} r\sin(\theta_n) - F_{l_n}^{z}(l_p + m_o) - F_{o_n}^{z} m_o\right)\hat{\jmath} \\ & + \left(F_{l_n}^{y}(l_p + m_o) + F_{o_n}^{y} m_o - f_{p_n} r\cos(\theta_n)\right)\hat{k} \quad .\end{aligned} \tag{3.36}$$

3.3.5 Piston-Bore Pressure Force

The pressure acting on the face of the piston within the bore tends to drive the piston in the negative x-direction. This force is simply given as

$$F_{pr_n} = -A_p P_n \hat{i} + 0\,\hat{j} + 0\,\hat{k} \quad . \tag{3.37}$$

Again, from geometry, it can be seen that the distance of this force away from the shaft reaction is given by $\left(L_2 + r\tan(\alpha)\sin(\theta_n)\right)\hat{i} + r\cos(\theta_n)\hat{j} + r\sin(\theta_n)\hat{k}$. Taking the cross product of this distance with equation (3.37) shows that the moment exerted about the location of the shaft reaction due to the piston-bore pressure on the face of the nth piston is given by

$$M_{pr_n} = 0\,\hat{i} - A_p P_n r\sin(\theta_n)\hat{j} + A_p P_n r\cos(\theta_n)\hat{k} \quad . \tag{3.38}$$

3.3.6 Summary

By substituting the results of equations (3.29), (3.31), (3.33), (3.35), and (3.37) into equation (3.25) the net force acting on the nth piston may be rewritten as

(3.39)

$$-M_p r\tan(\alpha)\,\omega^2\sin(\theta_n)\hat{i} - M_p r\,\omega^2\cos(\theta_n)\hat{j} - M_p r\,\omega^2\sin(\theta_n)\hat{k} =$$
$$(F_{s_n}^x - f_{p_n} - A_p P_n)\hat{i} + (F_{s_n}^y - F_{l_n}^y - F_{o_n}^y - A_{p_n}^y P_n)\hat{j} + (F_{s_n}^z - F_{l_n}^z - F_{o_n}^z - A_{p_n}^z P_n)\hat{k} \quad .$$

Similarly, by substituting equations (3.30), (3.32), (3.34), (3.36), and (3.38) into equation (3.26) the net moment about the location of the shaft reaction due to the forces acting on the

*n*th piston may be summarized as

$$0 = \begin{cases} \left((F_{s_n}^z - F_{l_n}^z - F_{o_n}^z - A_{p_n}^z P_n)\, r\cos(\theta_n) - (F_{s_n}^y - F_{l_n}^y - F_{o_n}^y - A_{p_n}^y P_n)\, r\sin(\theta_n) \right) \hat{i} \\ + \left((F_{s_n}^x - F_{s_n}^z \tan(\alpha) - A_p P_n - f_{p_n})\, r\sin(\theta_n) + F_{l_n}^z (l_p + m_o) + F_{o_n}^z m_o + A_{p_n}^z P_n (l_p/2 + m_o) \right) \hat{j} \\ - \left((F_{s_n}^x - A_p P_n - f_{p_n})\, r\cos(\theta_n) - F_{s_n}^y r\tan(\alpha)\sin(\theta_n) + F_{l_n}^y (l_p + m_o) + F_{o_n}^y m_o + A_{p_n}^y P_n (l_p/2 + m_o) \right) \hat{k} \end{cases} . \tag{3.40}$$

Equations (3.39) and (3.40) are dependent upon forces that are exerted, by the slipper, on the *n*th piston. The following section investigates these forces in detail.

3.4 Slipper Free-Body Diagram

The free-body diagram of a single slipper is shown in Figure 3-4. The forces acting on the slipper come from the mechanical hold-down force exerted on the slipper (F_{hd}), the equal and opposite reaction of the slipper against the piston ($-F_{s_n}$), the reaction of the swash plate against the slipper (F_{sw_n}) and the pressure balance acting between the slipper and the swash plate (F_{bal_n}). Summing these forces and setting them equal to the translational inertia of the slipper, $M_s \ddot{X}_{s_n}$, it can be seen that

$$M_s \ddot{X}_{s_n} = F_{hd} - F_{s_n} + F_{sw_n} + F_{bal_n} . \tag{3.41}$$

In general, each force on the slipper generates a corresponding moment about the location of the shaft reaction. Summing these moments and setting them equal to the angular inertia of the piston, $I_s \ddot{\Theta}_{s_n} + \dot{\Theta}_{s_n} \times I_s \dot{\Theta}_{s_n}$, yields

$$I_s \ddot{\Theta}_{s_n} + \dot{\Theta}_{s_n} \times I_s \dot{\Theta}_{s_n} = M_{hd} - M_{s_n} + M_{sw_n} + M_{bal_n} \quad . \tag{3.42}$$

Equations (3.41) and (3.42) provide the basis for describing the behavior of the slipper. The following subsections examines the components of these equations in more detail.

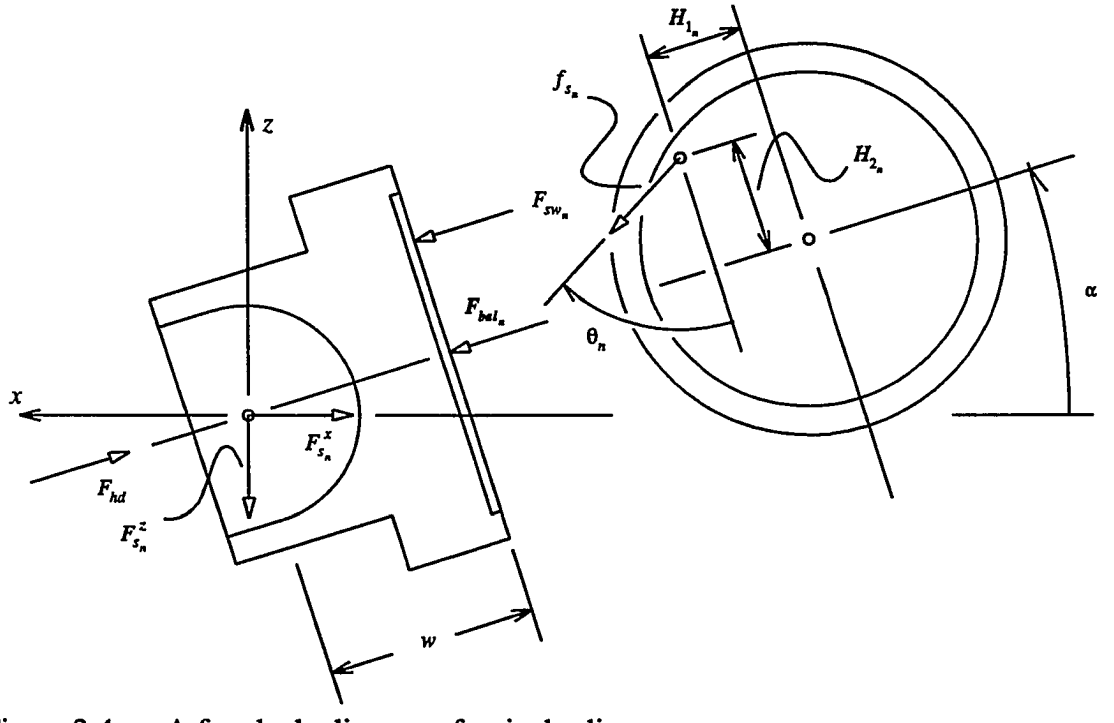

Figure 3-4. A free-body diagram of a single slipper.

3.4.1 Slipper Kinematics and Inertia

Because the *n*th slipper is connected to the *n*th piston, the *n*th slipper's translational position, velocity and acceleration are identical to that of the *n*th piston's. This means that the *n*th slipper's translational inertia is given by

$$M_s \ddot{X}_{s_n} = - M_s r \omega^2 \tan(\alpha) \sin(\theta_n) \hat{i} - M_s r \omega^2 \cos(\theta_n) \hat{j} - M_s r \omega^2 \sin(\theta_n) \hat{k} \quad , \qquad (3.43)$$

which is a result similar to the one presented in equation (3.29) for the inertia of the *n*th piston. During normal operation, the angular acceleration of the *n*th slipper is zero in all directions. Due to the angular rotation of the slipper about the *y*-axis a product-of-inertia is induced. Because of this, the angular inertia of the slipper is strictly *not* zero; however, since the angle α is small this contribution is considered negligible and the angular inertia of the *n*th slipper is written

$$I_s \ddot{\Theta}_{s_n} + \dot{\Theta}_{s_n} \times I_s \dot{\Theta}_{s_n} = 0 \quad . \qquad (3.44)$$

3.4.2 Slipper Hold-Down Force

The design of an axial-piston hydrostatic pump always includes a mechanism to insure that the slippers remain in reasonable contact with the swash plate. In general, this mechanism takes on many different forms and is therefore not included in the general drawings of this study; however, it is usually classified as one of two types: 1) a fixed clearance hold-down or 2) a positive force hold-down. See Figure 3-5. A fixed clearance hold-down allows for a controlled gap or clearance between the slipper and the swash plate. Note, this clearance is *allowed*, not required. It is expected that applied loads will force the slipper against the swash plate during normal operating-conditions. A positive force hold-down exerts a separate

force on the slipper that insures the slipper's contact with the swash plate. Usually this force is generated by a compressed spring and remains constant throughout the cycle of operation. In this analysis, the more general case is assumed where the slipper is in constant contact with the swash plate and is held down by a positive force hold-down mechanism.

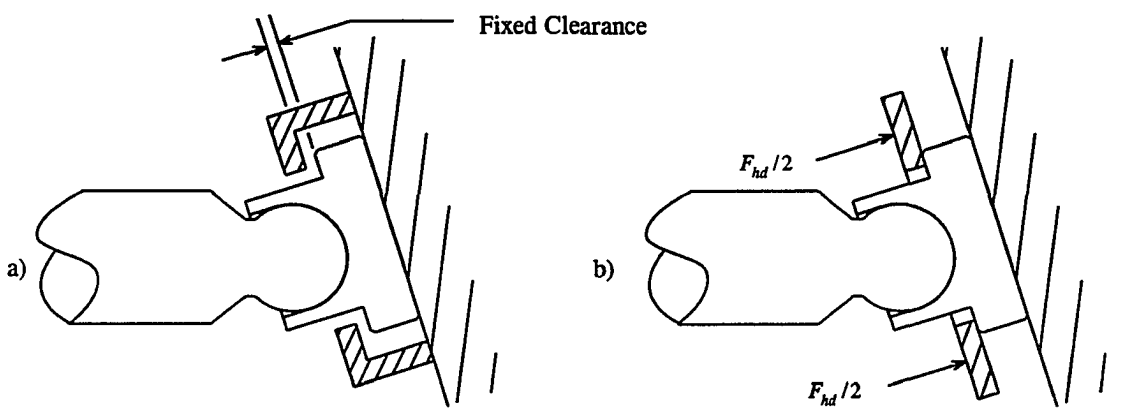

Figure 3-5. A schematic of two types of slipper hold-down mechanisms: a) fixed clearance, and b) positive force.

The force from the slipper hold-down mechanism acts on the slipper normal to the swash plate and is expressed by

$$\boldsymbol{F}_{hd} = -F_{hd}\cos(\alpha)\,\hat{\boldsymbol{i}} + 0\,\hat{\boldsymbol{j}} + F_{hd}\sin(\alpha)\,\hat{\boldsymbol{k}} \quad . \tag{3.45}$$

Since this force is applied symmetrically about the slipper, its centroid passes through the reaction point of the slipper against the piston. The distance of this point away from the location of the shaft reaction is $r\tan(\alpha)\sin(\theta_n)\,\hat{\boldsymbol{i}} + r\cos(\theta_n)\,\hat{\boldsymbol{j}} + r\sin(\theta_n)\,\hat{\boldsymbol{k}}$. Taking the cross

product of this distance with equation (3.45) yields the following moment generated about the location of the shaft reaction by the hold-down force acting on the *n*th slipper:

$$M_{hd} = F_{hd} r \sin(\alpha) \cos(\theta_n) \hat{i} - F_{hd} r (\sin(\alpha) + \cos(\alpha)) \sin(\theta_n) \hat{j} + F_{hd} r \cos(\alpha) \cos(\theta_n) \hat{k} \quad . \quad (3.46)$$

3.4.3 Slipper Reaction

The force and moment of the slipper acting on the piston is applied equally and oppositely against the slipper. This force and moment is described in Subsection 3.3.2 and is rewritten here for convenience. These quantities are expressed as

$$F_{s_n} = F_{s_n}^x \hat{i} + F_{s_n}^y \hat{j} + F_{s_n}^z \hat{k} \quad (3.47)$$

and

$$\begin{aligned} M_{s_n} = & \left(F_{s_n}^z r \cos(\theta_n) - F_{s_n}^y r \sin(\theta_n) \right) \hat{i} + \left(F_{s_n}^x r \sin(\theta_n) - F_{s_n}^z r \tan(\alpha) \sin(\theta_n) \right) \hat{j} \\ & + \left(F_{s_n}^y r \tan(\alpha) \sin(\theta_n) - F_{s_n}^x r \cos(\theta_n) \right) \hat{k} \quad . \end{aligned} \quad (3.48)$$

3.4.4 Swash-Plate Reaction

The reaction of the swash plate against the slipper is described with two forces: 1) the centroid of the load distributed across the area of contact between the slipper and the swash plate, F_{sw_n}, and 2) the friction force that results from the relative sliding between the swash

plate and the slipper, f_{s_n}. After a careful look at Figure 3-4, it can be seen that the combination of these two forces may be expressed as

$$F_{sw_n} = (F_{sw_n}\cos(\alpha) - f_{s_n}\sin(\alpha)\cos(\theta_n))\,\hat{i} + f_{s_n}\sin(\theta_n)\,\hat{j} - (F_{sw_n}\sin(\alpha) + f_{s_n}\cos(\alpha)\cos(\theta_n))\,\hat{k} \quad . \tag{3.49}$$

Using geometry, the distance of this force away from the shaft reaction is shown to be $(r\tan(\alpha)\sin(\theta_n) + H_{2_n}\sin(\alpha) - w\cos(\alpha))\,\hat{i} + (r\cos(\theta_n) + H_{1_n})\,\hat{j} + (r\sin(\theta_n) + H_{2_n}\cos(\alpha) + w\sin(\alpha))\,\hat{k}$. Taking the cross product of this distance with equation (3.49) the net moment generated about the shaft reaction-point from the swash-plate reaction on the *n*th slipper is expressed

$$M_{sw_n} = \begin{cases} -\left(\begin{array}{l} F_{sw_n}\sin(\alpha)\,(r\cos(\theta_n) + H_{1_n}) + f_{s_n}\left(r\cos(\alpha)\cos^2(\theta_n) + r\sin^2(\theta_n)\right. \\ \left. + H_{1_n}\cos(\theta_n)\cos(\alpha) + H_{2_n}\sin(\theta_n)\cos(\alpha) + w\sin(\theta_n)\sin(\alpha)\right) \end{array}\right)\hat{i} \\ +\left(\begin{array}{l} F_{sw_n}(r\sin(\theta_n)\sec(\alpha) + H_{2_n}) + f_{s_n}\cos(\theta_n)\sin(\alpha)\left(r\sin(\theta_n)(\tan(\alpha) - 1)\right. \\ \left. + H_{2_n}(\sin(\alpha) - \cos(\alpha)) - w(\sin(\alpha) + \cos(\alpha))\right) \end{array}\right)\hat{j} \\ -\left(\begin{array}{l} F_{sw_n}\cos(\alpha)\,(r\cos(\theta_n) + H_{1_n}) - f_{s_n}\left(r\tan(\alpha)\,(\cos(\alpha)\cos^2(\theta_n) + \sin^2(\theta_n))\right. \\ \left. + H_{1_n}\cos(\theta_n)\sin(\alpha) + H_{2_n}\sin(\theta_n)\sin(\alpha) - w\sin(\theta_n)\cos(\alpha)\right) \end{array}\right)\hat{k} \quad . \end{cases} \tag{3.50}$$

3.4.5 Slipper-Balance Force

To provide hydrostatic lubrication to the slipper, it is customary to drill a small hole through the slipper and the piston to ensure that fluid from the piston bore is supplied to the slipper / swash-plate interface. (See Chapter 2.) A shallow relief is cut into the slipper face

and, for this analysis, it is assumed that the fluid occupying this shallow volume is pressurized to the same level as the piston bore, P_n. (If the leakage from the slipper is excessive this assumption may be invalid.) The pressure, P_n, acts on the effective pressurized-area of the slipper, A_s, to force the slipper *away* from the swash plate. Since it is not desirable for the slipper to actually lift from the swash plate, A_s must be designed properly so as to "balance" the forces that are trying to move the slipper *toward* the swash plate; thus, the resultant force is often called the "slipper-balance" force. This force may generally be expressed as

$$F_{bal_n} = A_s P_n \cos(\alpha)\,\hat{i} + 0\hat{j} - A_s P_n \sin(\alpha)\,\hat{k} \quad . \tag{3.51}$$

Again, the centroid of this force acts through the center of the slipper; therefore, the distance of this force away from the shaft reaction is $r\tan(\alpha)\sin(\theta_n)\,\hat{i} + r\cos(\theta_n)\hat{j} + r\sin(\theta_n)\,\hat{k}$. Taking the cross product of this distance with equation (3.51) shows that the net moment generated about the shaft reaction from the pressure-balance force acting on a single slipper is given by

$$M_{bal_n} = -A_s P_n r \sin(\alpha)\cos(\theta_n)\,\hat{i} + A_s P_n r \sec(\alpha)\sin(\theta_n)\hat{j} - A_s P_n \cos(\alpha)\, r\cos(\theta_n)\,\hat{k} \quad . \tag{3.52}$$

3.4.6 Summary

By substituting the results of equations (3.43), (3.45), (3.47), (3.49) and (3.51) into equation (3.41) the net force acting on the *n*th slipper may be rewritten as

$$
\begin{aligned}
M_s r \tan(\alpha)\, \omega^2 \sin(\theta_n)\, \hat{i} + M_s r\, \omega^2 \cos(\theta_n)\, \hat{j} + M_s r\, \omega^2 \sin(\theta_n)\, \hat{k} \;=\; & \\
& \left(F_{s_n}^x + f_{s_n} \sin(\alpha) \cos(\theta_n) - A_s P_n \cos(\alpha) + F_{hd} \cos(\alpha) - F_{sw_n} \cos(\alpha)\right) \hat{i} \\
& + \left(F_{s_n}^y - f_{s_n} \sin(\theta_n)\right) \hat{j} \\
& + \left(F_{s_n}^z + f_{s_n} \cos(\alpha) \cos(\theta_n) + A_s P_n \sin(\alpha) - F_{hd} \sin(\alpha) + F_{sw_n} \sin(\alpha)\right) \hat{k} \quad .
\end{aligned}
\tag{3.53}
$$

Similarly, by substituting equations (3.44), (3.46), (3.48), (3.50) and (3.52) into equation (3.42) it can be shown that the net moment about the shaft reaction-point, due to forces acting on a single slipper, is given by

$$
\begin{aligned}
\mathbf{0} = \Bigg\{ & \left(\begin{array}{l}
r \cos(\theta_n) F_{hd} \sin(\alpha) - r \cos(\theta_n) F_{s_n}^z + r \sin(\theta_n) F_{s_n}^y - r \cos(\theta_n) \sin(\alpha) A_s P_n \\
- F_{sw_n} \sin(\alpha) (r \cos(\theta_n) + H_{1_n}) - f_{s_n} \left(r \cos(\alpha) \cos^2(\theta_n) + r \sin^2(\theta_n) \right. \\
\left. + H_{1_n} \cos(\theta_n) \cos(\alpha) + H_{2_n} \sin(\theta_n) \cos(\alpha) + w \sin(\theta_n) \sin(\alpha) \right)
\end{array} \right) \hat{i} \\
& + \left(\begin{array}{l}
- r \sin(\theta_n) F_{hd} (\cos(\alpha) + \sin(\alpha)) - r \sin(\theta_n) F_{s_n}^x + r \sin(\theta_n) \tan(\alpha) F_{s_n}^z \\
+ F_{sw_n} (r \sin(\theta_n) \sec(\alpha) + H_{2_n}) + f_{s_n} \cos(\theta_n) \sin(\alpha) \left(r \sin(\theta_n) (\tan(\alpha) - 1) \right. \\
\left. + H_{2_n} (\sin(\alpha) - \cos(\alpha)) - w (\sin(\alpha) + \cos(\alpha)) \right) + r \sin(\theta_n) A_s P_n \sec(\alpha)
\end{array} \right) \hat{j} \\
& + \left(\begin{array}{l}
r \cos(\theta_n) F_{hd} \cos(\alpha) - r \sin(\theta_n) \tan(\alpha) F_{s_n}^y - r \cos(\theta_n) \cos(\alpha) A_s P_n \\
- F_{sw_n} \cos(\alpha) (r \cos(\theta_n) + H_{1_n}) + f_{s_n} \left(r \tan(\alpha) (\cos(\alpha) \cos^2(\theta_n) + \sin^2(\theta_n)) \right. \\
\left. + H_{1_n} \cos(\theta_n) \sin(\alpha) + H_{2_n} \sin(\theta_n) \sin(\alpha) - w \sin(\theta_n) \cos(\alpha) \right) + r \cos(\theta_n) F_{s_n}^x
\end{array} \right) \hat{k} \quad .
\end{aligned}
\tag{3.54}
$$

Equations (3.53) and (3.54) may now be used to complete the solutions for equations (3.23), (3.24), (3.39) and (3.40).

3.5 Summary

In this section, the results of this chapter are gathered to describe specific physical quantities within the pump. This part of the chapter begins by presenting several symmetry relationships that are used to simplify the results of this analysis. Finally, the analytical results are summarized using categories specific to the cylinder block, the pistons, and the slippers.

3.5.1 Symmetry Considerations

Because the pistons are positioned evenly in a circular array within the cylinder block, several simplifications arise due to symmetry. These symmetry relationships are not immediately obvious; they are, however, based upon the following series relationships:

$$\sum_{n=1}^{N} \sin\left(\frac{\xi \pi}{N} (n-1) \right) = 0 \tag{3.55}$$

and

$$\sum_{n=1}^{N} \cos\left(\frac{\xi \pi}{N} (n-1) \right) = 0 \quad . \tag{3.56}$$

Equations (3.55) and (3.56) are always valid for $N > 1$ and $\xi = 2, 4, 6, \ldots$.

If the angular position of each piston is referenced from piston one, the circular position of the nth piston may be expressed as $\theta_n = \theta_1 + 2\pi (n-1)/N$. Using this relationship and equation (3.55) with the identity $\sin(a+b) = \sin(a)\cos(b) + \cos(a)\sin(b)$, it can be shown that

$$\sum_{n=1}^{N} \sin(\theta_n) = 0 \tag{3.57}$$

for $N > 1$. Similarly, using the identity $\cos(a+b) = \cos(a)\cos(b) - \sin(a)\sin(b)$, and equation (3.56) it can be shown that

$$\sum_{n=1}^{N} \cos(\theta_n) = 0 \tag{3.58}$$

for $N > 1$. Using the symmetry relationships of equations (3.55) and (3.56) and the identities $\sin(a+b) = \sin(a)\cos(b) + \cos(a)\sin(b)$ and $\sin(a)\cos(b) = \sin(a+b)/2 + \sin(a-b)/2$, the following result is valid for $N > 1$:

$$\sum_{n=1}^{N} \sin(\theta_n)\cos(\theta_n) = 0 \quad . \tag{3.59}$$

Using equations (3.55) and (3.56) and the two identities $\sin^2(a) = 1/2 - \cos(2a)/2$ and $\cos(a+b) = \cos(a)\cos(b) - \sin(a)\sin(b)$ it can be shown that

$$\sum_{n=1}^{N} \sin^2(\theta_n) = \frac{N}{2} \tag{3.60}$$

for $N > 1$. Lastly, using the trigonometric identities $\cos(a+b) = \cos(a)\cos(b) - \sin(a)\sin(b)$ and $\cos^2(a) = 1/2 + \cos(2a)/2$ with equations (3.55) and (3.56), the result

$$\sum_{n=1}^{N} \cos^2(\theta_n) = \frac{N}{2} \tag{3.61}$$

is shown to be valid for $N > 1$.

3.5.2 Cylinder-Block Equations

Using the *i*th component of equation (3.24), each component of equation (3.39), the *j*th and *k*th components of equation (3.40), each component of equation (3.53), and the symmetry relationship of equation (3.59), the torque exerted on the cylinder block by the shaft in the positive x-direction is given by

$$T = \sum_{n=1}^{N} A_p P_n r \tan(\alpha) \cos(\theta_n) + \sum_{n=1}^{N} f_{p_n} r \tan(\alpha) \cos(\theta_n) + \sum_{n=1}^{N} f_{s_n} r \left(\sin^2(\theta_n) + \sec(\alpha) \cos^2(\theta_n)\right) + f_v \quad . \tag{3.62}$$

Equation (3.62) is presented as the primary equation of investigation for this work and will be examined and evaluated throughout this dissertation.

Further cylinder-block results are summarized by using the *j*th component of equation (3.23), the *i*th and *j*th components of equation (3.39), the *k*th component of equation (3.40), the *j*th component of equation (3.53), and the symmetry relationship of equation (3.58) to show that the force exerted by the shaft on the cylinder block in the y-direction is

$$F_{sh}^{y} = -\sum_{n=1}^{N} f_{s_n} \sin(\theta_n) \quad . \tag{3.63}$$

Similarly, using the *k*th component of equation (3.23), the *i*th and *k*th components of equation (3.39), the *j*th component of equation (3.40), the *i*th and *k*th components of equation (3.53), and the symmetry relationship of equation (3.57), the force exerted by the shaft on the cylinder block in the z-direction is given by

$$F_{sh}^{z} = \sum_{n=1}^{N} A_p P_n \tan(\alpha) + \sum_{n=1}^{N} f_{p_n} \tan(\alpha) + \sum_{n=1}^{N} f_{s_n} \sec(\alpha) \cos(\theta_n) \quad . \tag{3.64}$$

From the *i*th component of equation (3.23) it can be shown that the force exerted on the cylinder block by the valve plate is expressed

$$F_v = F_{sp} + \sum_{n=1}^{N} A_b P_n + \sum_{n=1}^{N} f_{p_n} \quad . \tag{3.65}$$

The geometric position of the force represented in equation (3.65) is shown in Figure 3-2 by the dimensions E_1 and E_2 . The dimension in the *y*-direction (E_1) can be found using the *i*th component of equation (3.23), the *k*th component of equation (3.24), the *i*th and *j*th components of equation (3.39), the *k*th component of equation (3.40), the *j*th component of equation (3.53), and the symmetry relationship of equation (3.59). This expression is written

$$E_1 = \frac{\sum_{n=1}^{N} A_b P_n r \cos(\theta_n) + \sum_{n=1}^{N} f_{p_n} r \cos(\theta_n) - \sum_{n=1}^{N} f_{s_n} r \tan(\alpha) \sin^2(\theta_n)}{F_{sp} + \sum_{n=1}^{N} A_b P_n + \sum_{n=1}^{N} f_{p_n}} \quad . \tag{3.66}$$

The dimension in the negative *z*-direction (E_2) can be found using the *i*th component of equation (3.23), the *j*th component of equation (3.24), the *i*th and *k*th components of equation (3.39), the *j*th component of equation (3.40), the *i*th and *k*th components of equation (3.53), and the symmetry relationship of equation (3.60). This expression is written as

$$E_2 = \frac{\left\{ \begin{array}{c} -\sum_{n=1}^{N} P_n (A_b + A_p \tan^2(\alpha))\, r \sin(\theta_n) - \sum_{n=1}^{N} f_{p_n} (1 + \tan^2(\alpha))\, r \sin(\theta_n) \\ -\sum_{n=1}^{N} f_{s_n} \tan(\alpha) \sec(\alpha)\, r \sin(\theta_n) \cos(\theta_n) + N/2\, (M_p + M_s)(\tan(\alpha) + \tan^3(\alpha))\, r^2\, \omega^2 \end{array} \right\}}{F_{sp} + \sum_{n=1}^{N} A_b P_n + \sum_{n=1}^{N} f_{p_n}} \quad . \tag{3.67}$$

3.5.3 Piston Equations

From the *i*th and *j*th components of equations (3.39), the *k*th component of equation (3.40) and the *j*th component of equation (3.53), the reaction in the *y*-direction of the *n*th piston against the inner edge of the bushing within the *n*th piston-bore may be expressed

$$F_{l_n}^{y} = -\left((M_p + M_s)\, r\, \omega^2 \cos(\theta_n) + f_{s_n} \sin(\theta_n)\right)\left(\frac{m_o - r \tan(\alpha) \sin(\theta_n)}{l_p}\right) - \frac{A_{p_n}^{y} P_n}{2} \quad , \tag{3.68}$$

where the ratio $(m_o - r \tan(\alpha) \sin(\theta_n))/l_p$ is commonly referred to as the instantaneous piston overhang-ratio. Similarly, by using the *i*th and *k*th components of equation (3.39), the *j*th component of equation (3.40), and the *i*th and *k*th components of equation (3.53), the reaction in the *z*-direction of the *n*th piston against the inner edge of the bushing within the *n*th piston-bore is shown to be

(3.69)

$$F_{l_n}^{z} = \left(\begin{array}{c} -(M_p + M_s)(1 + \tan^2(\alpha))\, r\, \omega^2 \sin(\theta_n) + A_p P_n \tan(\alpha) \\ + f_{p_n} \tan(\alpha) + f_{s_n} \sec(\alpha) \cos(\theta_n) \end{array} \right)\left(\frac{m_o - r \tan(\alpha) \sin(\theta_n)}{l_p}\right) - \frac{A_{p_n}^{z} P_n}{2} \quad .$$

Continuing in this same fashion for the reaction of the *n*th piston against the *outer* edge of the

bushing, using the *i*th and *j*th components of equation (3.39), the *k*th component of equation (3.40), and the *j*th component of equation (3.53) the reaction in the *y*-direction of the *n*th piston against the outer edge of the bushing within the *n*th piston-bore may be expressed

$$F_{o_n}^{y} = \left((M_p + M_s)\, r\, \omega^2 \cos(\theta_n) + f_{s_n} \sin(\theta_n)\right)\left(1 + \frac{m_o - r\tan(\alpha)\sin(\theta_n)}{l_p}\right) - \frac{A_{p_n}^{y} P_n}{2} \quad . \tag{3.70}$$

Again, using the *i*th and *k*th components of equation (3.39), the *j*th component of equation (3.40), and the *i*th and *k*th components of equation (3.53), the reaction in the *z*-direction of the *n*th piston against the outer edge of the bushing within the *n*th piston-bore is shown to be

(3.71)

$$F_{o_n}^{z} = \left(\begin{array}{c}(M_p + M_s)\,(1 + \tan^2(\alpha))\, r\, \omega^2 \sin(\theta_n) - A_p P_n \tan(\alpha) \\ - f_{p_n}\tan(\alpha) - f_{s_n}\sec(\alpha)\cos(\theta_n)\end{array}\right)\left(1 + \frac{m_o - r\tan(\alpha)\sin(\theta_n)}{l_p}\right) - \frac{A_{p_n}^{z} P_n}{2} \quad .$$

3.5.4 Slipper Equations

From the *i*th component of equation (3.39), it can be seen that the force in the *x*-direction from the *n*th slipper against the *n*th piston is simply given as

$$F_{s_n}^{x} = A_p P_n - M_p\, r \tan(\alpha)\, \omega^2 \sin(\theta_n) + f_{p_n} \quad . \tag{3.72}$$

Similarly, from the *j*th component of equation (3.53), the force in the *y*-direction from the *n*th slipper against the *n*th piston is expressed

$$F_{s_n}^{y} = M_s\, r\, \omega^2 \cos(\theta_n) + f_{s_n} \sin(\theta_n) \quad . \tag{3.73}$$

Using the *i*th component of equation (3.39) and the *i*th and *k*th components of equation (3.53), the force in the *z*-direction from the *n*th slipper against the *n*th piston may be written as

$$F_{s_n}^{z} = \left[(M_p + M_s)\tan^2(\alpha) + M_s\right] r\,\omega^2 \sin(\theta_n) - A_p P_n \tan(\alpha) - f_{p_n}\tan(\alpha) - f_{s_n}\sec(\alpha)\cos(\theta_n) \quad . \quad (3.74)$$

From the *i*th component of equation (3.39) and the *i*th component of equation (3.53), the swash-plate reaction against the *n*th slipper is given by

(3.75)

$$F_{sw_n} = P_n(A_p\sec(\alpha) - A_s) - (M_p + M_s)\tan(\alpha)\sec(\alpha)\, r\,\omega^2\sin(\theta_n) + F_{hd} + f_{p_n}\sec(\alpha) + f_{s_n}\tan(\alpha)\cos(\theta_n) \quad .$$

The geometric position of the force described by equation (3.75) is shown in Figure 3-4 by the dimensions H_{1_n} and H_{2_n}. These dimensions may be found using the *i*th, *j*th and *k*th components of equation (3.53), and the *i*th and *k*th components of equation (3.54). They are

$$H_{1_n} = \frac{-f_{s_n} w \sin(\theta_n)}{F_{sw_n}} \qquad (3.76)$$

and

$$H_{2_n} = \frac{f_{s_n} w \cos(\theta_n)}{F_{sw_n}} \quad , \qquad (3.77)$$

where F_{sw_n} is given in equation (3.75).

3.6 Conclusion

In this chapter, the equations that govern the behavior of the major components within an axial-piston hydrostatic pump have been derived. Specifically, the equations summarized in Section 3.5 of this chapter predict the behavior of the cylinder block, the pistons, and the slippers as they work under normal operating conditions within the pump. The results of this analysis will be used in subsequent chapters to model friction and to validate the expectations for the torque on the cylinder block of an axial-piston swash-plate type hydrostatic pump.

CHAPTER 4. PISTON PRESSURE

4.1 Introduction

Moving pressurized fluid is the means for transmitting power hydraulically; therefore, a fundamental component of this study is to analyze the pressure as it acts within the cylinder bore of each piston. This analysis begins by deriving the pressure-rise-rate equation using a control-volume approach that is common to previous research (Manring and Johnson 1994; Johnson and Manring 1994; Inoue and Nakazato 1993; Manring 1993; Zeiger and Akers 1986, 1985; Lin, Akers, and Zeiger 1985; Yamaguchi 1966). Once this equation and its basic components are derived, a numerical solution of the equation as it pertains to the geometry and operating conditions of a hydrostatic pump is presented. Finally, this chapter concludes with a simplified approximation of this pressure and a geometric interpretation of its profile. It is important for the reader to note that throughout this analysis the pressures within the intake and discharge ports of the pump are assumed to be constant values respectively.

4.2 Control-Volume Analysis

Figure 4-1 shows a piston as it operates within its bore where the volume of fluid within the bore is taken as the control volume of study. The pressure outside the piston bore, P_b, is shown to vary with time to simulate the fact that as the cylinder block rotates about the x-axis, this pressure repeatedly changes from a high discharge pressure, P_d, to a low intake

pressure, P_i. The discharge area of the piston bore, A_o, is also shown to vary with time to model the transition regions on the valve plate where the slots provide a variable opening into each port.

If one notes that the instantaneous mass within the piston bore is given by $M = \rho V$, where ρ is the instantaneous fluid mass-density and V is the instantaneous volume within the piston bore, one can show that the fluid mass time-rate-of-change is given by

$$\frac{dM}{dt} = \frac{d\rho}{dt} V + \rho \frac{dV}{dt} \quad . \tag{4.1}$$

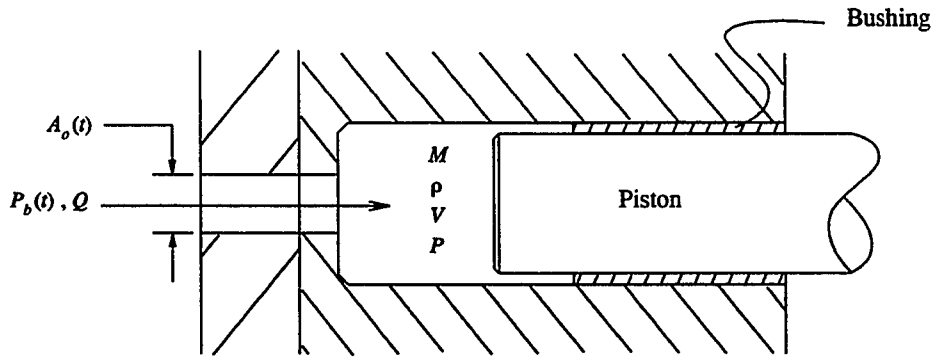

Figure 4-1. Schematic of a cylinder-bore control volume.

Furthermore, the conservation of mass within the piston bore requires that

$$\frac{dM}{dt} = \rho Q \quad , \tag{4.2}$$

where Q is the volumetric flow rate *into* the piston bore. From the definition of the fluid bulk-modulus, β, it is observed that

$$\frac{d\rho}{dt} = \frac{\rho}{\beta}\frac{dP}{dt} \quad , \tag{4.3}$$

where P is the instantaneous pressure within the piston bore. By substituting equations (4.2) and (4.3) into equation (4.1), and rearranging terms, the general equation describing the pressure time-rate-of-change within the nth piston bore may be written as

$$\frac{dP}{dt} = \frac{\beta}{V}\left(Q - \frac{dV}{dt}\right) \quad . \tag{4.4}$$

If it is assumed that the flow in and out of the piston bore occurs at a high velocity (and thus a high Reynolds-number), the flow rate Q may be modeled using the orifice equation that is commonly used in fluid-power modeling (Merritt 1967). This equation is given by

$$Q = \text{sign}(P_b - P)\, C_d A_o \sqrt{\frac{2|P_b - P|}{\rho}} \quad , \tag{4.5}$$

where the "sign" function takes on the value ± 1 depending upon the sign of its argument, C_d is the orifice discharge-coefficient, and P_b is the boundary pressure outside the control volume (either P_i or P_d). The instantaneous volume of the nth piston-bore may be determined using the ith component of equation (3.27) given in Chapter 3, the area on the face of a single piston, A_p, and the reference volume, V_o. This quantity is expressed

$$V = V_o - A_p r \tan(\alpha) \sin(\theta) \quad . \tag{4.6}$$

If the shaft of the pump is turning at a an angular speed, ω, then $\theta = \omega t$. Since ω is a

constant in this analysis, it is obvious that $dt = \frac{d\theta}{\omega}$. Using this result with equations (4.4), (4.5) and (4.6), the pressure-rise-rate within a single piston chamber may be rewritten as

$$\frac{dP_n}{d\theta_n} = \frac{\beta}{V_o - A_p r \tan(\alpha) \sin(\theta_n)} \left(\frac{\text{sign}(P_{b_n} - P_n) C_d A_o}{\omega} \sqrt{\frac{2|P_{b_n} - P_n|}{\rho}} + A_p r \tan(\alpha) \cos(\theta_n) \right) \quad , (4.7)$$

where the subscript n denotes that this equation applies to the nth piston-bore.

Equation (4.7) is a non-linear, first order, differential equation that does not have an analytical solution. In the following subsection, the behavior of this equation will be examined using numerical techniques.

4.3 Numerical Solutions

The solution to equation (4.7) was examined numerically using a Gear's Stiff integration routine within the ACSL program for numerical modeling. Run times were approximately three seconds for one revolution of the cylinder block using a 486-DX2 66-MHz personal-computer. Figure 4-2 shows a typical result of this study. Note: both pressure, P_n, and port area, A_o, are plotted in this figure.

As shown in Figure 4-2, the typical numerical solution to equation (4.7) demonstrates rather uninteresting behavior for the pressure, P_n. As the piston bore passes over either the intake port or the discharge port of the valve plate, the port area, A_o, remains at a maximum constant. Within these regions, the pressure within the nth piston-bore also appears to remain

fairly constant (i.e., $P_n \approx P_i$ or P_d). The two ports on the valve plate are bridged by transition regions where A_o goes from a maximum value to a minimum value, slowly grows within the transition slot, and then quickly returns to the original maximum value. As the *n*th piston-bore passes over the transition regions, the pressure changes almost linearly from one port

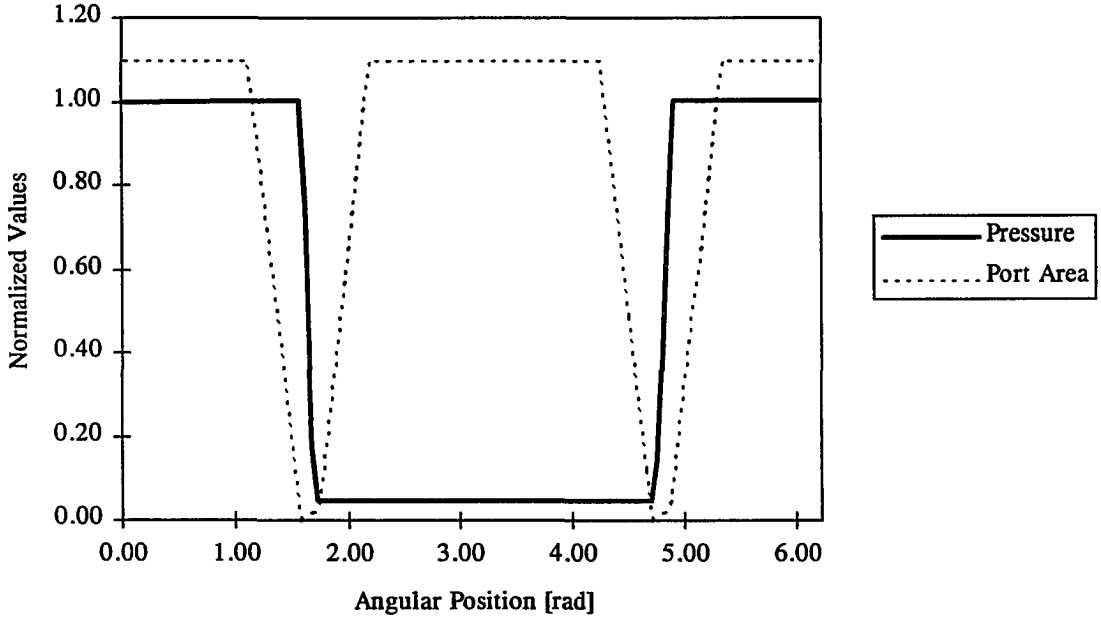

Figure 4-2. A numerical pressure-profile for the *n*th piston exhibiting essentially no overshoot or undershoot in the transition regions.

pressure to the other. Actual measured-data has shown these same basic trends (Bolinger 1982).

Figure 4-3 shows another result of this study where the pressure drop between ports has been reduced. Figure 4-3 represents a run using one sixth of the discharge pressure of

Figure 4-2. From Figure 4-3 it can be seen that a lower pressure drop between ports tends to create significant pressure spikes within the transition regions of the valve plate. The reason for this peculiarity has been discussed at length in previous work (Manring 1993, 20-23); however, it can be stated here that this phenomenon is strictly a result of the volumetric

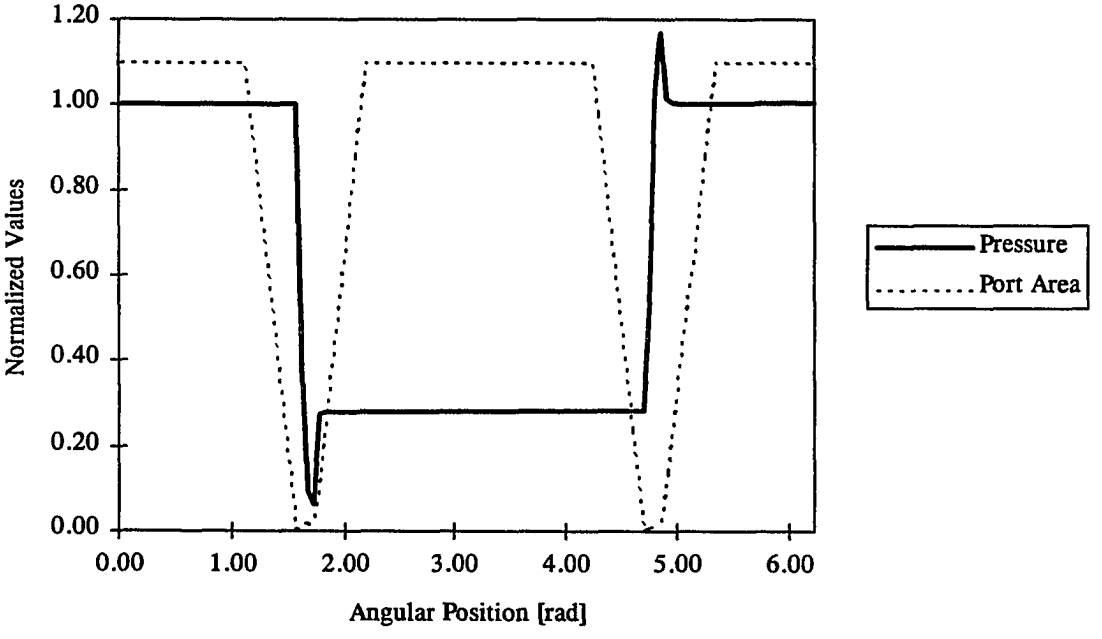

Figure 4-3. A numerical pressure-profile for the *n*th piston exhibiting overshoot and undershoot in the transition regions.

compression and expansion within the chamber. In the first case, the chamber volume decreases at a rate faster than the fluid can squeeze out through the port. If the boundary pressure is not sufficiently large compared to the starting pressure, volumetric compression of the fluid will cause the pressure within the piston bore to overshoot the approaching

boundary condition. In the second case, the chamber volume *increases* at a rate faster than the fluid can enter the piston bore. If the boundary pressure is not sufficiently small compared to the starting pressure, the pressure within the piston bore will undershoot the approaching boundary pressure. In either case, the pressure relaxes itself back to the appropriate boundary condition once sufficient flow is permitted by an increase in discharge or intake area.

4.4 Piston-Pressure Profile

Figures 4-2 and 4-3 show two different characteristics of the pressure within the piston bore. While both of these characteristics are real, it should be noted that the profile of Figure 4-3 is encountered much less often than that of Figure 4-2. In other words, the more uninteresting result is the more common. For this reason, it has become popular in industry to represent the pressure profile of the piston using the schematic of Figure 4-4. This schematic emphasizes the fact that the piston sees a constant pressure as it passes directly over either port and that it undergoes a transition in pressure as it passes over the slots on the valve plate. This transition occurs through some average angular-distance which is noted in Figure 4-4 as γ. The angular distance, γ, is commonly referred to as the pressure carry-over angle and has been illustrated and / or discussed in previous research dealing with related topics (Manring and Johnson 1994; Johnson and Manring 1994; Manring 1993; Lin, Akers, and Zeiger 1985; Yamaguchi 1966).

Since equation (4.7) is complicated to solve, it is sometimes convenient to express the

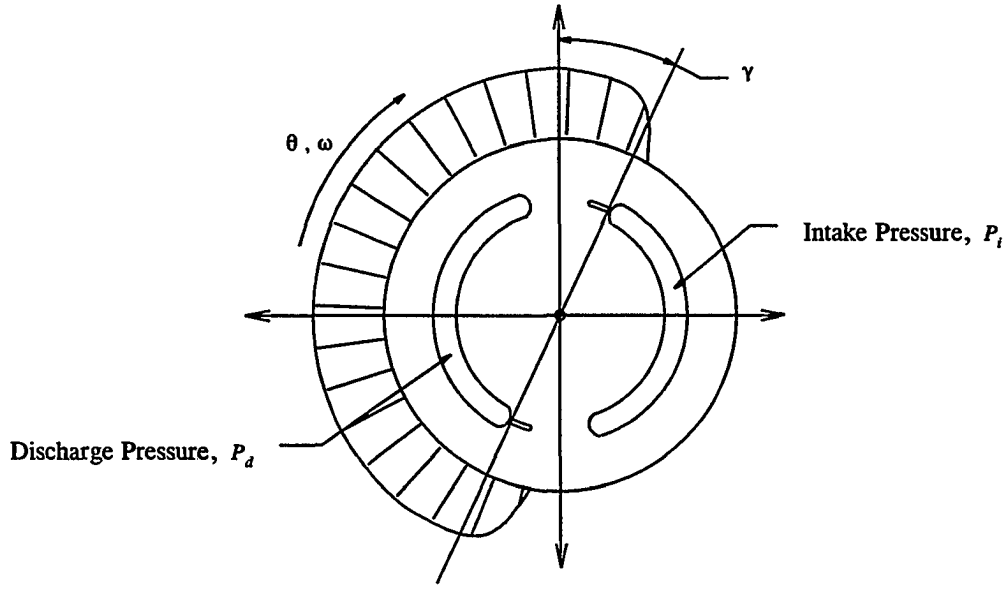

Figure 4-4. Approximate pressure-profile schematic. The magnitude of the discharge pressure is referenced from the magnitude of the intake pressure.

pressure within the *n*th piston bore using a discontinuous though much simpler expression. This expression assumes that the pressure remains constant as the piston passes over either the intake or discharge ports and that the pressure transition between ports occurs *linearly* over the range of the pressure carry-over angle, γ. This expression is written as

$$P_n = \begin{cases} P_d & 3\pi/2 + \gamma < \theta_n < \pi/2 \\ P_d - m(\theta_n - \pi/2) & \pi/2 < \theta_n < \pi/2 + \gamma \\ P_i & \pi/2 + \gamma < \theta_n < 3\pi/2 \\ P_i + m(\theta_n - 3\pi/2) & 3\pi/2 < \theta_n < 3\pi/2 + \gamma \end{cases}, \tag{4.8}$$

where $m = (P_d - P_i)/\gamma$.

4.5 Conclusion

The work of this chapter has shown that the pressure within the *n*th piston chamber does not typically exhibit unusual behavior. Furthermore, it has been proposed that in many cases it is sufficient to approximate this pressure using the discontinuous expression shown in equation (4.8). In this dissertation, both the numerical and the closed-form approximations for the pressure within the *n*th piston chamber will be used extensively.

CHAPTER 5. EFFECTIVE PRESSURIZED-AREAS

5.1 Introduction

The analysis of Chapter 3 has assumed that it is known how to quantify the parameters that describe the effective pressurized-areas throughout the pump. Specifically, these areas are the radially pressurized-area on each piston ($A_{p_n}^{y}$ and $A_{p_n}^{z}$), the balanced pressurized-area on each slipper (A_s), and the clamping pressurized-area within each piston bore of the cylinder block (A_b). In this chapter the one dimensional Reynolds-equation is used for calculating fluid pressures within the thin clearances that are associated with each part. By integrating these pressures within defined geometric boundaries, the results of each problem are equated to what has been defined in Chapter 3 as the effective pressurized-area of each component.

5.2 Effective Pressurized Piston-Area

In Chapter 3, Subsection 3.2.6, it was mentioned that the fluid pressure between the nth piston and its bushing drops along the bushing length from an existing bore-pressure, P_n, to some nominally low-pressure that is outside the cylinder block. (Typically all pressures within the pump are referenced from this nominally low-pressure and so its value is taken to be zero.) It was also mentioned in Chapter 3 that this pressure drop does not occur symmetrically about the centerline of the piston bore; rather, it varies in a slightly skewed fashion. This skewed transition results from the cocked orientation of the piston within its

bore. Figure 5-1 illustrates the piston's orientation and the skewed pressure-drop along the length of the bushing (i.e., in the x-direction). It must be mentioned that this orientation is not a uniquely-defined orientation of the piston within its bore. There is nothing to say that the piston cannot ride *completely* along one edge of the bore in a shifted position, or that the piston doesn't instantaneously center itself within the bore on occasions. The orientation of these positions could very well take place for some instantaneous conditions; however, as discussed in Subsection 3.2.7 of Chapter 3, the evidence supplied by the worn cylinder blocks

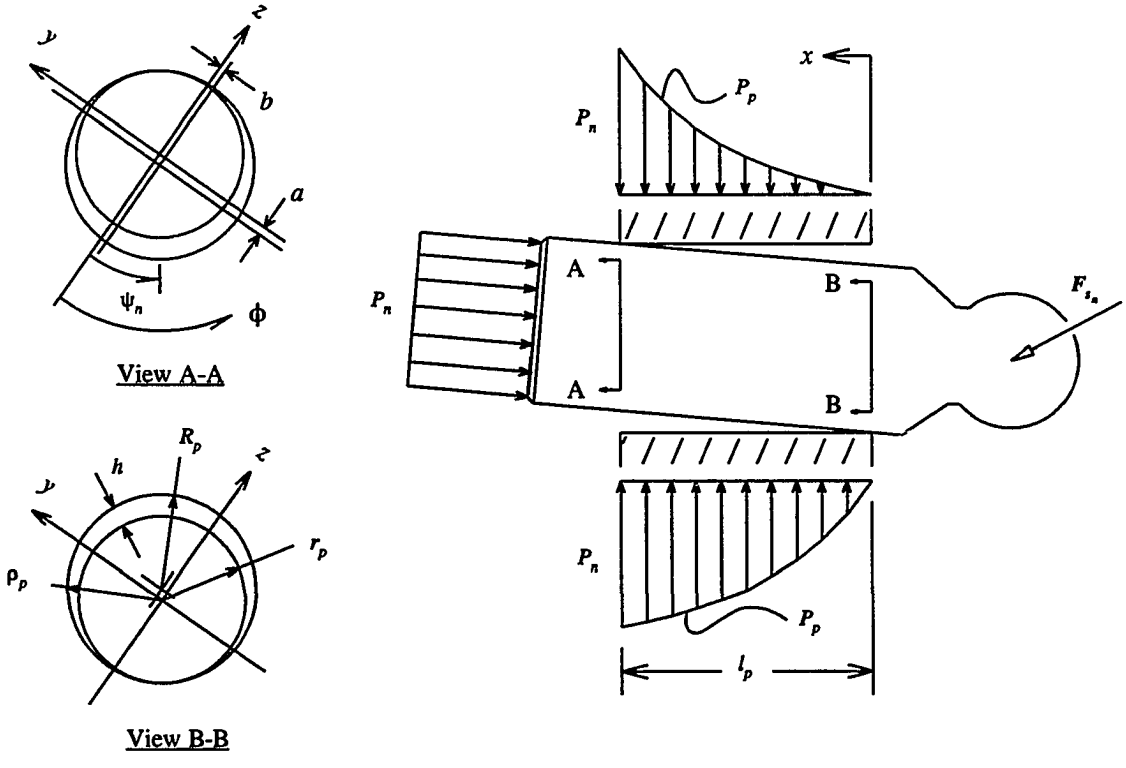

Figure 5-1. A schematic of the cocked orientation of a piston within its bore and the skewed pressure-profile resulting from this orientation.

suggests that the piston is predominately oriented in a *cocked* position within its bore. In an effort to gain insight into the dominant behavior of the hydrostatic pump, and to arrive at some closed-form approximation of the effective pressurized-area, it will be assumed throughout this analysis that the piston *always* orients itself within the bore as shown in Figure 5-1.

To determine the effective pressurized-area of the piston in the radial direction, one must begin by determining the pressure itself as it varies along the length of the bushing. To do this, it is assumed that the pressure behaves according to the one dimensional Reynolds-equation and that the translational velocity of the piston is zero (i.e., relative motion between the piston and bore is not considered). A well-presented derivation of the Reynolds equation is given by Shigley and Mitchell (1983, 524-29) and is rewritten here in its specialized form as follows:

$$\frac{d}{dx}\left\{h^3 \frac{dP_p}{dx}\right\} = 0 \quad . \tag{5.1}$$

In equation (5.1), h is the fluid-film thickness and P_p is the pressure along the length of the bushing. The one-dimensional Reynolds equation is based upon the following assumptions: 1) the flow and pressure gradient in the ϕ-direction is negligible, 2) the fluid is Newtonian, 3) the fluid inertia is small (i.e., the flow is characterized by a low Reynolds-number), 4) the fluid is incompressible, and 5) the pressure does not vary in the direction radially normal to the piston. While most of these assumptions are only *partially* true at best, and though the

degree of their truth may vary as operating conditions change, equation (5.1) is used as an estimation, and an estimation *only*, of the pressure P_p as it varies along the length of the bushing. Results based upon this analysis must be interpreted with this in mind.

Before solving equation (5.1), the geometric characteristics of the fluid film thickness, h, must be determined. From Figure 5-1 it can be seen that

$$h = \rho_p - r_p \quad , \tag{5.2}$$

where

$$\rho_p = \sqrt{(R_p \cos(\phi) - a)^2 + (R_p \sin(\phi) - b)^2} \quad . \tag{5.3}$$

Using these two results, and linearizing ρ_p for small values of a and b, the fluid-film thickness may be approximated as

$$h = (R_p - r_p) - \cos(\phi)\, a - \sin(\phi)\, b \quad . \tag{5.4}$$

From geometry, it can be seen that

$$a = (R_p - r_p^*)\left(1 - \frac{2x}{l_p}\right)\cos(\psi_n) \tag{5.5}$$

and

$$b = (R_p - r_p^*)\left(1 - \frac{2x}{l_p}\right)\sin(\psi_n) \quad , \tag{5.6}$$

where r_p^* is some value slightly greater than r_p. Using equations (5.4), (5.5) and (5.6), and letting $h_{max} = 2(R_p - r_p)$ and $h_{min} = r_p^* - r_p$, the fluid-film thickness between the piston and bushing may be expressed

$$h = \frac{h_{max}}{2} - \left(\frac{h_{max}}{2} - h_{min} \right) \left(1 - \frac{2x}{l_p} \right) \cos(\phi - \psi_n) \quad . \tag{5.7}$$

To solve for the pressure P_p, equation (5.7) is substituted into equation (5.1). Solving for the boundary conditions $P_p(x = l_p) = P_n$ and $P_p(x = 0) = 0$, it can be shown that

$$P_p = \frac{P_n x \left(h_{max} + \cos(\phi - \psi_n)(h_{max} - 2h_{min}) \right)^2 \left((x - l_p)\cos(\phi - \psi_n)(h_{max} - 2h_{min}) + l_p h_{max} \right)}{h_{max} \left((2x - l_p)\cos(\phi - \psi_n)(h_{max} - 2h_{min}) + l_p h_{max} \right)^2} \quad . \tag{5.8}$$

To solve for the effective pressured-area on the piston in the z-direction, the pressure force in this direction must be integrated over the entire area of the bushing. This integral is given by

$$\int_0^{2\pi} \int_0^{l_p} P_p(x, \phi) \cos(\phi)\, r_p\, dx\, d\phi = P_n l_p (2\pi r_p) \cos(\psi_n) K_p \quad , \tag{5.9}$$

where

$$K_p = \frac{1}{2} \left(\frac{1}{2} - \frac{h_{min}}{h_{max}} \right) \quad . \tag{5.10}$$

From the definition of the radial pressure-force on the cylinder block (see equation (3.13) of Chapter 3) it can be seen that equation (5.9) must equal $-A_{p_n}^{z} P_n$, where $A_{p_n}^{z}$ is the effective pressurized-area within the nth piston-bore in the z-direction. Therefore,

$$A_{p_n}^{z} = -l_p (2\pi r_p) \cos(\psi_n) K_p \quad . \tag{5.11}$$

Similarly, integrating the pressure-force on the piston in the y-direction yields

$$\int_0^{2\pi} \int_0^{l_p} P_p(x, \phi) \sin(\phi)\, r_p\, dx\, d\phi = P_n\, l_p (2\pi r_p) \sin(\psi_n) K_p \quad . \tag{5.12}$$

Setting this force equal to $-A_{p_n}^{y} P_n$, where $A_{p_n}^{y}$ is the effective pressurized-area within the nth piston-bore in the y-direction, it may be shown that

$$A_{p_n}^{y} = -l_p (2\pi r_p) \sin(\psi_n) K_p \quad . \tag{5.13}$$

Equations (5.11) and (5.13) appear to describe quantities of area that are negative; however, the negative signs are a result of choosing the wrong direction of force in equation (3.13) of Chapter 3 and should not be confused with such an absurd physical impossibility as a negative area might imply.

Equations (5.11) and (5.13) represent the effective pressurized-areas within the nth piston-bore. These equations depend upon two parameters that have not yet been discussed: the angle ψ_n (see Figure 5-1) and the fluid-film factor K_p. To approximate the angle ψ_n, the

angle of the slipper-reaction vector acting on the ball of the piston relative to the y and z-axis is evaluated and used. This result is given by

$$\psi_n = \tan^{-1}(F_{s_n}^y / F_{s_n}^z) \quad , \tag{5.14}$$

where $F_{s_n}^y$ and $F_{s_n}^z$ are given in equations (3.73) and (3.74) of Chapter 3. From equation (5.10), it can be seen that the value of K_p depends strictly upon the ratio of the minimum and maximum fluid film thicknesses. Since this actual ratio is definitely unknown, and considering that the previous analysis has only been used to yield *approximate* results, K_p will simply be regarded as a constant and a reasonable guess will be made to estimate its value. Clearly, reasonable values of K_p range from 0 to 1/4. For the specific pump-design analyzed in this dissertation, modeling has shown that $K_p \approx 0.12$.

5.3 Effective Pressurized Slipper-Area

In Subsection 3.4.5 of Chapter 3, the effective pressurized-area of the slipper was presented as it contributes to a force that lifts the slipper *away* from the swash plate. This effective area is made up of two parts: 1) the area within the shallow relief of the slipper, and 2) the effective pressurized-area on the outside land (or foot) of the slipper. Figure 5-2 illustrates both of these pressurized areas. The quantity describing the effective pressurized-area of a slipper has been discussed and published in literature (Kazama and Yamaguchi 1993; Pang, Wenjie, and Jingwu 1993; Koc, Hooke, and Li 1992; Hooke and Kakoullis 1981,

1978). In this section, the basis for some of this research is presented as it pertains specifically to the geometry of Figure 5-2.

To determine the effective pressurized-area of the slipper, one begins by examining the effective pressurized-area of the slipper's outside land. By assuming a constant flow across

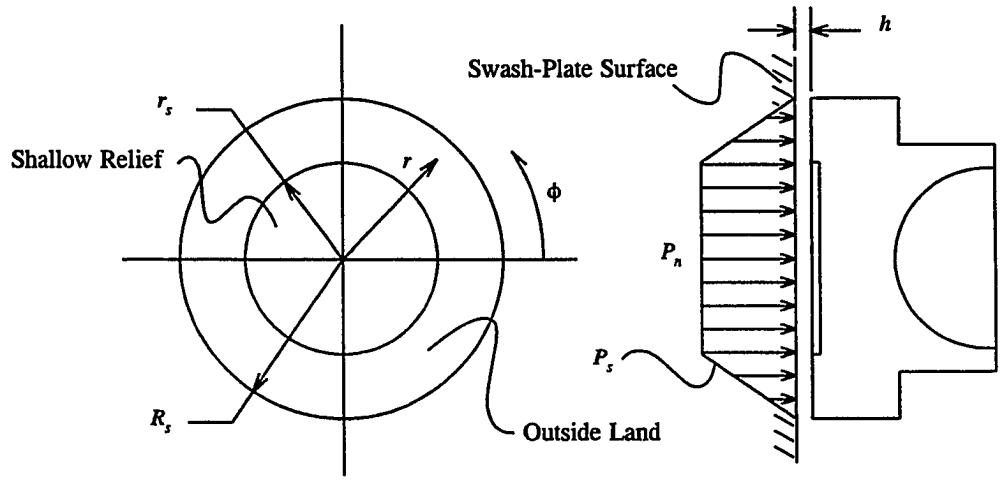

Figure 5-2. A schematic of the pressure profile beneath a slipper.

this land in the radial direction, the radial version of the one-dimensional Reynolds equation (assuming no relative motion between the slipper and the swash plate) is given as

$$\frac{d}{dr}\left\{h^3 r \frac{dP_s}{dr}\right\} = 0 \quad , \tag{5.15}$$

where h is the fluid-film thickness between the swash plate and the slipper, P_s is the pressure distribution across the outside land, and r is the independent variable measuring distances radially outward from the center of the slipper. If it is assumed that the fluid-film thickness h

is a constant, equation (5.15) may be solved using the boundary conditions illustrated in Figure 5-2. These boundary conditions are $P_s(r = r_s) = P_n$ and $P_s(r = R_s) = 0$ and the resulting solution of equation (5.15) is given by

$$P_s = P_n\left(1 - \frac{\ln(r/r_s)}{\ln(R_s/r_s)}\right) \quad . \tag{5.16}$$

If equation (5.16) is now integrated over the area of the outside land, and the force from the pressurized area of the slipper's shallow relief is added, the net pressure-force on the slipper may be expressed as

$$\int_0^{2\pi}\int_{r_s}^{R_s} P_s(r)\, r\, dr\, d\phi + P_n \pi r_s^2 = P_n \frac{\pi}{2} \frac{(R_s^2 - r_s^2)}{\ln(R_s/r_s)} \quad . \tag{5.17}$$

From the definition of the balanced pressure-force on the nth slipper (see equation (3.51) of Chapter 3) it can be shown that equation (5.17) must equal $A_s P_n$, where A_s is the effective pressurized-area of the slipper. Therefore

$$A_s = \frac{\pi}{2} \frac{(R_s^2 - r_s^2)}{\ln(R_s/r_s)} \quad . \tag{5.18}$$

Again, this same result has been derived in previous research.

5.4 Effective Pressurized Cylinder-Block Area

In Chapter 3, Subsection 3.2.5, an effective pressurized-area within a single piston-bore that tended to force the cylinder block toward the valve plate was discussed. This force was called the pressure-clamping force. In general, this force is a result of the pressurized area *inside* the piston bore minus the effective pressurized-area *outside* the piston bore. Figure 5-3 illustrates both of these pressurized areas. To calculate the effective pressurized-area outside the piston bore, one must consider three regions of the diametrical land on the cylinder

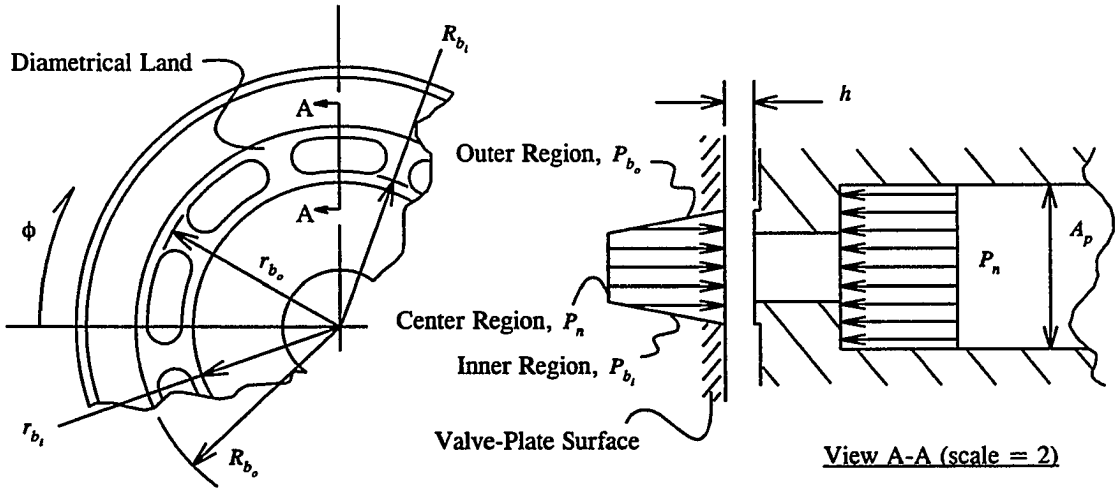

Figure 5-3. A schematic of the pressure-profile on the cylinder block near the valve plate.

block: an outer region, a center region, and an inner region. See Figure 5-3. The pressurized area inside the piston bore is simply the area of a single piston, A_p.

To determine the effective pressurized-area of a single piston-bore it is assumed, for calculation purposes, that all piston bores are pressurized to the same level, P_n. In this

analysis, the fluid-film thickness between the cylinder block and the valve plate is considered to be constant. Using the general form of equation (5.15), and the boundary conditions given by $P_{b_o}(r = r_{b_o}) = P_n$ and $P_{b_o}(r = R_{b_o}) = 0$, it can be shown that the pressure in the outer region of the diametrical land is given by

$$P_{b_o} = P_n \left(1 - \frac{\ln(r/r_{b_o})}{\ln(R_{b_o}/r_{b_o})} \right) \quad . \tag{5.19}$$

Similarly, using the general form of equation (5.15) and the boundary conditions given by $P_{b_i}(r = r_{b_i}) = 0$ and $P_{b_i}(r = R_{b_i}) = P_n$ the pressure within the *inside* region of the diametrical land on the cylinder block may be expressed

$$P_{b_i} = P_n \frac{\ln(r/r_{b_i})}{\ln(R_{b_i}/r_{b_i})} \quad . \tag{5.20}$$

By integrating equations (5.19) and (5.20) over the entire area of their respective boundaries, adding the pressurized force acting on the center region of the diametrical land, and subtracting the force of each pressurized piston-bore, the net pressure-force acting on the cylinder block is given by

$$\int_0^{2\pi} \int_{r_{b_o}}^{R_{b_o}} P_{b_o}(r)\, r\, dr\, d\phi + \int_0^{2\pi} \int_{r_{b_i}}^{R_{b_i}} P_{b_i}(r)\, r\, dr\, d\phi + P_n \pi (r_{b_o}^2 - R_{b_i}^2) - P_n N A_p = P_n \frac{\pi}{2} \frac{(R_{b_o}^2 - r_{b_o}^2)}{\ln(R_{b_o}/r_{b_o})} - P_n \frac{\pi}{2} \frac{(R_{b_i}^2 - r_{b_i}^2)}{\ln(R_{b_i}/r_{b_i})} - P_n N A_p \quad , \tag{5.21}$$

where N is the total number of piston bores within the cylinder block. From the original definition of the clamping force within each piston bore (see equation (3.11) of Chapter 3) it can be seen that equation (5.21) must equal $-NA_b P_n$, where A_b is the effective pressurized-area within a single piston-bore. This quantity may then be expressed

$$A_b = A_p - \frac{\pi}{2N}\left\{\frac{(R_{b_o}^2 - r_{b_o}^2)}{\ln(R_{b_o}/r_{b_o})} - \frac{(R_{b_i}^2 - r_{b_i}^2)}{\ln(R_{b_i}/r_{b_i})}\right\} . \tag{5.22}$$

5.5 Conclusion

In this chapter, approximate closed-form solutions for some very complicated behaviors within the pump have been derived and presented. Specifically, this analysis has developed expressions to describe the effective pressurized-areas on the pistons, the slippers, and the cylinder block using the one-dimensional Reynolds equation without considering any relative motion between parts. These results are used in subsequent chapters for modeling the friction for each of these components and for eventually modeling the net torque on the cylinder block of the axial-piston pump. The acceptability of these expressions will be determined based upon the correlation of the overall torque-model with actual test-data.

CHAPTER 6. TRIBOLOGY AND THE COEFFICIENT-OF-FRICTION

6.1 Introduction

Tribology is the science of rubbing surfaces. Since friction plays a very important role in the work of this dissertation, a discussion of tribology is inevitable. In this chapter the classical theories of tribology, as they pertain mainly to the application of journal bearings, are used to develop a general closed-form equation that describes the coefficient-of-friction within an axial-piston swash-plate type hydrostatic pump. This discussion begins with an overview of three different lubrication conditions that exist within the hydrostatic machine: boundary lubrication, mixed lubrication, and fully hydrodynamic-lubrication. Based upon these three types of lubrication, the coefficient-of-friction is modeled as a function of fluid viscosity, sliding speed, and normal loads.

6.2 Lubrication and the Stribeck Curve

Within an axial-piston hydrostatic pump, it is assumed that great opportunity exists for the lubrication of moving parts. Generally, the parts of a hydrostatic pump are bathed in moving fluid (usually of a petroleum base) and are therefore constantly being wiped and re-coated with lubricant. Needless to say, this lubricating process reduces the friction losses within the machine; however, it does not eliminate the friction altogether.

Traditionally, friction has been modeled by multiplying the normal load of contact

between two sliding surfaces with a coefficient-of-friction that is usually considered to be a constant. Generally, coefficients-of-friction are *not* constant, which is certainly the case within a hydrostatic pump. The coefficient-of-friction varies continuously throughout the machine and depends highly upon the relative speeds of the moving parts, the asperity heights

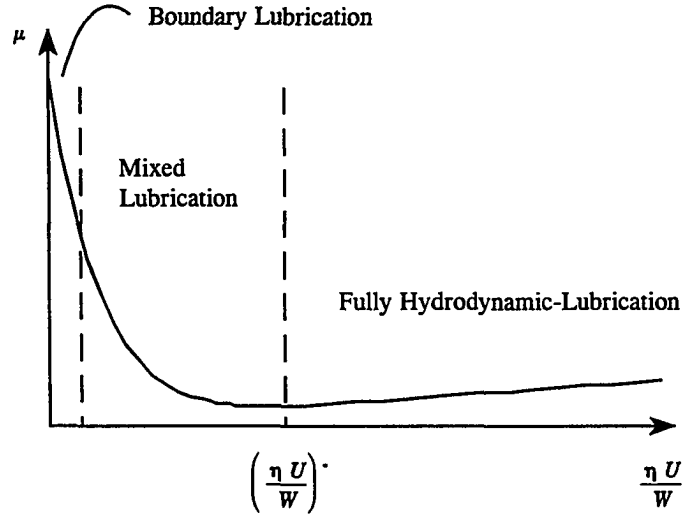

Figure 6-1. The Stribeck curve showing the variation of the coefficient-of-friction with the dimensionless ratio $\eta U/W$.

of each moving surface, the condition of the lubricating fluid, and the normal load of contact between each surface. The analysis of journal bearings, in particular, has shown that the coefficient-of-friction (for conditions similar to those in a hydrostatic pump) is a function of the non-dimensional ratio $\frac{\eta U}{W}$, where η is the viscosity of the fluid, U is the relative speed of the moving parts, and W is the normal load per unit width between the two surfaces

(Shigley and Mitchell 1983, 520-21). This analysis has proven itself valid for reasonably high values of the non-dimensional ratio $\frac{\eta U}{W}$; but, the analysis has not done a good job explaining the behavior of the coefficient-of-friction for conditions when this ratio is small. To describe the behavior for the coefficient-of-friction as it varies between high and low values of the ratio $\frac{\eta U}{W}$, it has been common to refer to a curve known as the Stribeck curve. See Figure 6-1. This curve illustrates the coefficient-of-friction as the lubrication conditions vary throughout the range of boundary, mixed, and hydrodynamic lubrication. The Stribeck curve is used in this dissertation as a basis for modeling the coefficient-of-friction within the hydrostatic pump.

6.2.1 Boundary Lubrication

Boundary lubrication is defined as a condition when fluid lubrication is nonexistent. In hydrostatic machines, this condition may occur locally as the fluid lubricant is squeezed or wiped away from the relative surface of contact. Under such conditions, the contact between two (metal) surfaces is often characterized as "metal-to-metal" contact (i.e., surface asperities are fully engaged). The result of such contact is usually high wear and high friction.

Figure 6-1 notes the boundary-lubrication zone near the vertical-axis of the Stribeck curve. Accordingly, the boundary-lubrication zone shows the highest coefficient-of-friction on the curve. This zone is characterized by very slow operating speeds, high loading of parts, and very thin oil (i.e., low fluid-viscosity). Because the theories that explain the coefficient-of-friction in this zone vary widely, this work will rely on empirical test-data to establish the

maximum boundary coefficient-of-friction realized during boundary-lubrication conditions. These values are published in various forms of literature (Avallone and Baumeister 1978, Hutchings 1992, Stachowiak and Batchelor 1993) and are readily available for a wide range of material pairs.

6.2.2 Mixed Lubrication

Mixed lubrication is defined as a lubrication condition that occurs between boundary-lubrication conditions and fully hydrodynamic-lubrication conditions. The lubrication is said to be mixed because the mating surfaces are separated by a thin film of fluid; and yet, the film is thin enough to allow for the interaction of larger surface asperities. This region of lubrication is shown on the Stribeck curve near the center-left. The coefficient-of-friction within this zone drops quickly from the boundary-lubrication zone and smoothly approaches the fully hydrodynamic-lubrication zone.

6.2.3 Fully Hydrodynamic-Lubrication

Lubrication that is characterized by a fully hydrodynamic-condition can be said to fully separate the mating surfaces in such a way as to allow for *no asperity interaction* between surfaces. This condition is friendly to analysis and corresponds to the validation of Petroff's analysis of the friction within journal bearings (Shigley and Mitchell 1983, 520-21). As shown in Figure 6-1, the fully hydrodynamic-lubrication zone is located to the center-right of

the Stribeck curve; therefore, it may be observed that fully hydrodynamic-lubrication occurs when relative speeds are high, normal contact-loads are low, and the fluid is thick (i.e., high fluid-viscosity).

6.2.4 Critical Fluid-Film Thickness

The critical parameter in determining the transition point between the mixed-lubrication zone and the fully hydrodynamic-lubrication zone is the fluid-film thickness. This critical fluid-film thickness is, of course, a function of the asperity heights on each surface. Tribologists have generally agreed that the critical fluid-film thickness defining the transition point between mixed lubrication and fully hydrodynamic-lubrication is given by

$$h^* = 3\sqrt{R_a^2 + R_b^2} \quad , \tag{6.1}$$

where R_a and R_b are the RMS surface roughnesses on surface "a" and surface "b" respectively (Stachowiak and Batchelor 1993, 384-90). For typical machined sliding-surfaces within the pump, $h^* \approx 1\,\mu\text{m}$.

6.3 Modeling the Coefficient-of-Friction

In the following analysis, the coefficient-of-friction within the pump, μ, will be modeled by simulating the Stribeck curve in Figure 6-1. (It should be noted that, unless specified otherwise, μ is always a function of the non-dimensional ratio $\frac{\eta U}{W}$. Throughout

this analysis, the symbol $\hat{\mu}$ will be used to refer to any *constant values* of the coefficient-of-friction.) In general, the coefficient-of-friction will be modeled by considering two basic parts of the Stribeck curve: the boundary / mixed lubrication part, and the fully hydrodynamic part. The modeled coefficient-of-friction then assumes the following form:

$$\mu = \mu_{mix} + \mu_{hyd} \quad . \tag{6.2}$$

6.3.1 Boundary and Mixed-Lubrication Conditions

As discussed earlier, the Stribeck curve of Figure 6-1 shows that the coefficient-of-friction drops off rapidly from the boundary-lubrication zone and smoothly approaches the fully hydrodynamic-lubrication zone. It is the author's choice to model the coefficient-of-friction in the boundary and mixed-lubrication zones using an exponential decay with respect to the non-dimensional ratio $\eta U / W$. Therefore, the coefficient-of-friction in this region will be modeled as

$$\mu_{mix} = \hat{\mu}\,\mathrm{Exp}\left(-A \frac{\eta U}{W} \right) \quad , \tag{6.3}$$

where $\hat{\mu}$ is the maximum boundary coefficient-of-friction as determined from experiments and A behaves as the "decay constant" regulating the rate of exponential decay. (Note: equation (6.3) is not based upon any experimental studies that show an exponential transition in the mixed lubrication zone. This result is simply a best guess as to how the coefficient-of-friction

may behave.) For modeling purposes, it is necessary that the parameter A be specified in such a way as to insure that 98% of the coefficient-of-friction associated with mixed lubrication dies away by the time that fully hydrodynamic-lubrication is achieved. The transition point from mixed lubrication to fully hydrodynamic-lubrication is shown in Figure 6-1 at the point when $\frac{\eta U}{W} = \left(\frac{\eta U}{W}\right)^{*}$, where the superscript asterisk denotes that a sufficient fluid-film thickness has been achieved to insure complete separation of surfaces. At this point, the coefficient-of-friction associated with mixed lubrication (μ_{mix}) should equal 0.02 $\hat{\mu}$. Therefore,

$$A = \frac{4}{(\eta U / W)^{*}} \quad . \tag{6.4}$$

6.3.2 Fully Hydrodynamic-Lubrication Conditions

As mentioned earlier, the coefficient-of-friction in the fully hydrodynamic-lubrication zone of the Stribeck curve is easy to analyze. Figure 6-2 shows a schematic of two surfaces separated by a thick film of fluid. Conventionally, the tangential force required to move the upper surface across the fluid medium is given by $W \mu_{hyd}$. Setting this force equal to the fluid shear-force acting at the surface $y = h_{min}$ (where h_{min} is the minimum fluid-film thickness), it can be seen that

$$W \mu_{hyd} = \int_{0}^{l} \tau \, dx \quad . \tag{6.5}$$

(Note: the units of W are force per unit width.) Assuming that the fluid is Newtonian, the fluid shear is defined as

$$\tau = \eta \frac{du}{dy} \quad , \tag{6.6}$$

where u is the one-dimensional fluid velocity-profile. Now, approximating u linearly with respect to y (i.e., $u = \frac{U}{h_{min}} y$), equation (6.5) may be integrated to yield

$$\mu_{hyd} = \frac{\eta U}{W} \frac{l}{h_{min}} \quad . \tag{6.7}$$

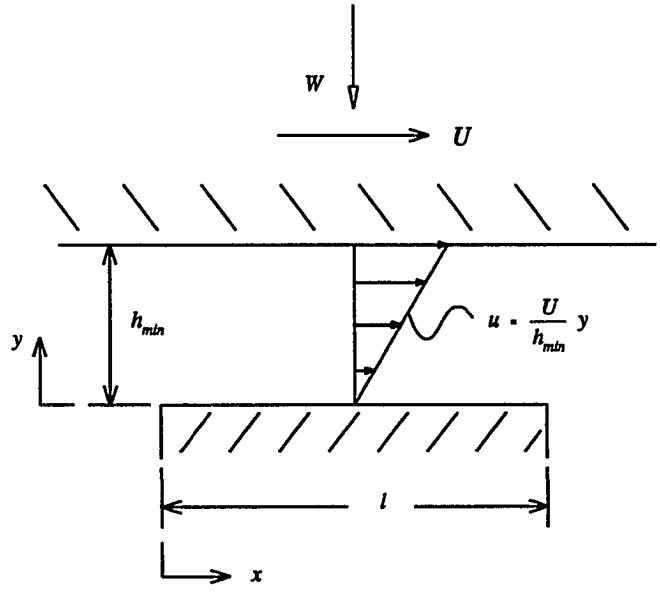

Figure 6-2. Fully hydrodynamic-lubrication illustrated using two surfaces moving relative to each other at a velocity U and separated by a fluid-film of thickness of h_{min}.

6.3.3 Minimum Fluid-Film Thickness

Equation (6.7) describes the coefficient-of-friction as a function of the minimum fluid-film thickness, h_{min}. In this subsection, the parameter h_{min} is modeled using the generic illustration of a tilted bearing-pad as shown in Figure 6-3. An important boundary-condition

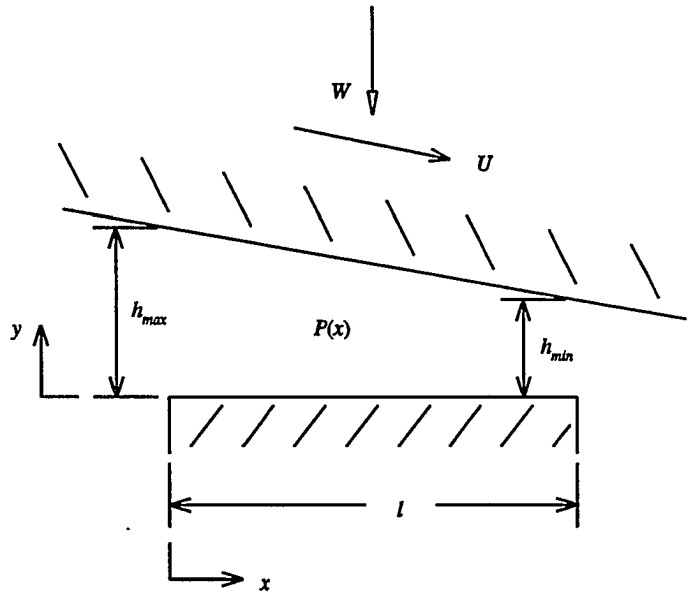

Figure 6-3. Geometry of a tilted bearing-pad, used to illustrate the calculation of the minimum fluid-film thickness h_{min}.

called the "no-slip" boundary condition requires that the fluid be adhered to the surfaces of both the bearing pad and the mating part. Because of the no-slip boundary condition (and the angular geometry of Figure 6-3) the flow of lubricant is forced through a diminishing gap (h_{min}) and creates a pressure, $P(x)$, between the bearing and its mating partner. By summing the forces of Figure 6-3 in the vertical-direction, it may be observed that

$$W = \int_0^l P(x)\, dx \quad . \tag{6.8}$$

To model the pressure between the bearing and the mating part, it is customary to use the classical Reynolds-equation for one-dimensional flow while considering the relative motion between surfaces (i.e., the velocity U). This expression is

$$\frac{d}{dx}\left\{\frac{h^3}{6\eta}\frac{dP}{dx}\right\} = \frac{d}{dx}\{U\, h\} \quad , \tag{6.9}$$

where the fluid-film thickness varies linearly and is given by

$$h = h_{max} - \frac{(h_{max} - h_{min})}{l}\, x \quad . \tag{6.10}$$

As mentioned in Chapter 5, the one-dimensional Reynolds equation is based upon the following assumptions: 1) there is no flow in the y and z-directions, 2) the fluid is Newtonian, 3) the fluid inertia is negligible, 4) the fluid is incompressible, and 5) the pressure does not vary in the y and z-directions.

If the boundary conditions $P(x = 0) = P(x = l) = 0$ are assumed, and the dimensionless parameter $\zeta = \frac{h_{max}}{h_{min}} + 1$ is defined, equation (6.9) may be solved to yield

$$P(x) = 6\eta\, U\, \frac{l\, x\, (l - x)\, (\zeta - 2)}{h_{min}^2\, \zeta\, (l\, (1 - \zeta) + x\, (\zeta - 2))^2} \quad . \tag{6.11}$$

It should be noted that the boundary conditions $P(x = 0) = P(x = l) = 0$, used to solve equation (6.9), *never* apply to any actual conditions within the hydrostatic pump. For instance, the

slipper is pressurized at the center of its bearing pad and therefore a discontinuous integration of equation (6.9) using different boundary-conditions would appear to be more appropriate for this case. A more difficult example of this same problem exhibits itself in the bearing conditions of the piston where it is clear that the pressure on at least *one* end of the piston bearing is *not* zero. Even the bearing conditions between the valve plate and the cylinder block are not characterized by boundary-conditions that are similar to $P(x = 0) = P(x = l) = 0$. So why are they used? The answer is this: When non-zero boundary conditions are considered, equation (6.11) simply becomes augmented with extra terms containing the boundary information. These terms are independent of speed and viscosity and are therefore not hydrodynamic in nature. They are *hydrostatic* in nature. Hydrostatic forces effectively reduce the applied load W and have already been considered in Chapter 5 by calculating the effective pressurized-areas within the axial-piston machine. To include these terms again in this analysis would be an error.

Substituting the result of equation (6.11) into equation (6.8), the bearing load (per unit width) may be solved for and written as

$$W = 6 \eta U \left(\frac{l}{h_{min}} \right)^2 K_{\mu} \quad , \tag{6.12}$$

where

$$K_{\mu} = \frac{2 (2 - \zeta) + \zeta \ln(\zeta - 1)}{\zeta (\zeta - 2)^2} \quad . \tag{6.13}$$

The parameter K_μ is a function of the fluid-film thickness ratio, $\frac{h_{max}}{h_{min}}$ (or ζ), only; and, since this actual ratio is clearly unknown, K_μ will be considered a constant and a reasonable guess will be made to estimate its value. Taking the limits of equation (6.13) as ζ varies between 2 and ∞ shows that the value of K_μ ranges from 0.27 to 0 (Hutchings 1992, 64). The modeling of this dissertation has shown that $K_\mu \approx 0.014$. Equation (6.12) may now be rearranged to yield the following result for the minimum fluid-film thickness:

$$h_{min} = l \sqrt{6 K_\mu \frac{\eta U}{W}} \quad . \tag{6.14}$$

6.3.4 Summary

Using the results of equations (6.3), (6.4), (6.7), and (6.14) to complete equation (6.2), it can be seen that the Stribeck curve is modeled using the analytical equation

$$\mu = \hat{\mu}\, \mathrm{Exp}\left(- \left(\frac{2 l \sqrt{6 K_\mu}}{h^\cdot} \right)^2 \frac{\eta U}{W} \right) + \frac{1}{\sqrt{6 K_\mu}} \sqrt{\frac{\eta U}{W}} \quad , \tag{6.15}$$

where it has been recognized from equation (6.14) that

$$\left(\frac{\eta U}{W} \right)^\cdot = \left(\frac{h^\cdot}{l \sqrt{6 K_\mu}} \right)^2 \tag{6.16}$$

and the value of $h^\cdot$ is determined using equation (6.1). Equation (6.15) will be used generally in this dissertation for modeling the coefficient-of-friction throughout the axial-piston swash-

plate type hydrostatic pump.

6.4 Conclusion

In this chapter the Stribeck curve has been analytically modeled and presented in equation (6.15). Though the Stribeck curve has been historically used to describe the coefficient-of-friction within journal bearings, the model of this curve will be used in this dissertation to represent the varying coefficient-of-friction throughout the entire axial-piston pump. Equation (6.15) will be employed in the following chapter to derive models for the friction between the pistons and the cylinder block, the slippers and the swash plate, and the cylinder block and the valve plate.

CHAPTER 7. FRICTION MODELS

7.1 Introduction

In this chapter, the individual components of friction within an axial-piston hydrostatic pump are modeled using the normal loads derived in Chapter 3 and the general form of the coefficient-of-friction derived in Chapter 6. In the following sections, the friction between the *n*th piston and the cylinder block (f_{p_n}), the friction between the *n*th slipper and the swash plate (f_{s_n}), and the friction between the cylinder block and the valve plate (f_v) will be modeled.

7.2 Piston Friction

Unlike any other frictional behavior within the pump, piston friction is bidirectional. That is, the *n*th piston's friction force assumes its direction based upon the direction of the *n*th piston's travel at any given instant in time and this direction is noted to change as a result of the reciprocating motion of the piston. The bidirectional nature of the friction within the piston bore creates a discontinuity in the expression for piston friction; furthermore, the magnitude of friction in one direction is actually less than in the other. This last statement is not supposed to be obvious and will be explained later; suffice it to say, based upon the previous statement, that the equation describing friction for an advancing piston (motion in the positive x-direction) must be *different* than the equation describing the friction for a retreating piston (motion in the negative x-direction).

Figure 7-1 shows the configuration of a piston in an advancing mode *and* in a retreating mode. This figure also illustrates a difference in the location of fluid-film thicknesses, h, between the two modes. This phenomenon will be explained in Subsection 7.2.2; however, for both an advancing mode and a retreating mode the friction on the nth piston is conventionally expressed

$$f_{p_n} = \text{sign}(U_{p_n}) \left(\sqrt{F_{l_n}^{y\,2} + F_{l_n}^{z\,2}}\ \mu_{l_n} + \sqrt{F_{o_n}^{y\,2} + F_{o_n}^{z\,2}}\ \mu_{o_n} \right) \quad , \tag{7.1}$$

where $\sqrt{F_{l_n}^{y\,2} + F_{l_n}^{z\,2}}$ and $\sqrt{F_{o_n}^{y\,2} + F_{o_n}^{z\,2}}$ are the magnitudes of the normal loads at the inner and outer edges of the nth bushing, μ_{l_n} and μ_{o_n} are the appropriate coefficients-of-friction, and U_{p_n} is the instantaneous velocity of the nth piston in the x-direction. In the following subsections these forces and coefficients-of-friction will be examined in closer detail.

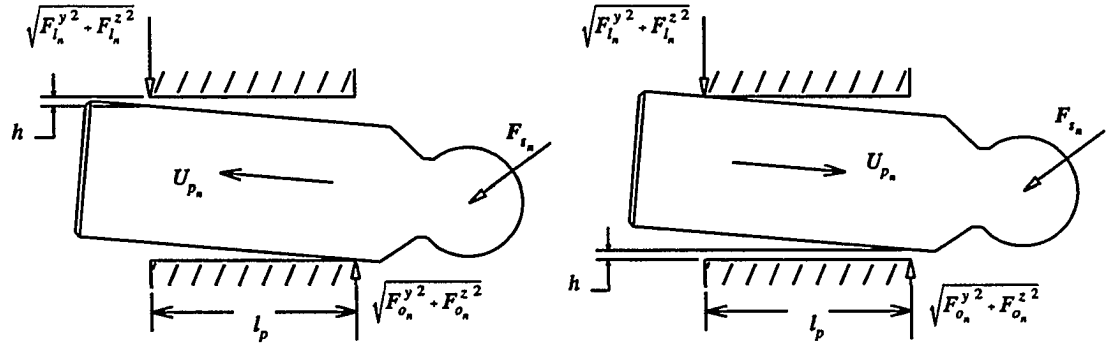

Figure 7-1. A schematic of normal loads and fluid-film thicknesses for an advancing piston and a retreating piston.

7.2.1 Normal Loads

As mentioned before, the normal loads on the piston are located at the inner and outer edges of the bushing within the *n*th piston-bore of the cylinder block. See Figure 7-1. The magnitudes of each force are given respectively as $\sqrt{F_{l_n}^{y\,2} + F_{l_n}^{z\,2}}$ and $\sqrt{F_{o_n}^{y\,2} + F_{o_n}^{z\,2}}$, where the components of these forces, $F_{l_n}^{y}$, $F_{l_n}^{z}$, $F_{o_n}^{y}$, and $F_{o_n}^{z}$, have been derived in Chapter 3. The results from Chapter 3 are rewritten here for convenience:

(7.2)

$$F_{l_n}^{y} = -\left((M_p + M_s)\, r\, \omega^2 \cos(\theta_n) + f_{s_n} \sin(\theta_n)\right)\left(\frac{m_o - r\tan(\alpha)\sin(\theta_n)}{l_p}\right) - \frac{A_{p_n}^{y} P_n}{2} \quad ,$$

$$F_{l_n}^{z} = \left(\begin{array}{c} -(M_p + M_s)\,(1 + \tan^2(\alpha))\, r\, \omega^2 \sin(\theta_n) + A_p P_n \tan(\alpha) \\ + f_{p_n} \tan(\alpha) + f_{s_n} \sec(\alpha) \cos(\theta_n) \end{array}\right)\left(\frac{m_o - r\tan(\alpha)\sin(\theta_n)}{l_p}\right) - \frac{A_{p_n}^{z} P_n}{2} \quad ,$$

$$F_{o_n}^{y} = \left(M_p + M_s\right) r\, \omega^2 \cos(\theta_n) + f_{s_n} \sin(\theta_n)\left(1 + \frac{m_o - r\tan(\alpha)\sin(\theta_n)}{l_p}\right) - \frac{A_{p_n}^{y} P_n}{2} \quad ,$$

$$F_{o_n}^{z} = \left(\begin{array}{c} (M_p + M_s)\,(1 + \tan^2(\alpha))\, r\, \omega^2 \sin(\theta_n) - A_p P_n \tan(\alpha) \\ - f_{p_n} \tan(\alpha) - f_{s_n} \sec(\alpha) \cos(\theta_n) \end{array}\right)\left(1 + \frac{m_o - r\tan(\alpha)\sin(\theta_n)}{l_p}\right) - \frac{A_{p_n}^{z} P_n}{2} \quad .$$

7.2.2 Coefficients-of-Friction

Figure 7-1 shows a schematic of normal loads for both an advancing piston and a retreating piston. This schematic also illustrates the locations of hydrodynamic lubrication signified by the locations of the fluid-film thickness, h. As shown in Figure 7-1 for an

advancing piston, hydrodynamic lubrication *only* occurs at the contact point of the load $\sqrt{F_{l_n}^{y\,2} + F_{l_n}^{z\,2}}$ (i.e., the inner edge of the bushing). At the contact point of load $\sqrt{F_{o_n}^{y\,2} + F_{o_n}^{z\,2}}$ the localized geometry of an advancing piston actually dissuades hydrodynamic behavior and is even suspect for pulling a vacuum in this region. For a retreating piston, as shown in Figure 7-1, the previous scenario becomes inverted and the hydrodynamic and the non-hydrodynamic locations switch places. This description of hydrodynamic behavior is not necessarily intuitive and therefore the following explanation is offered in its defense:

At the contact point of the load $\sqrt{F_{l_n}^{y\,2} + F_{l_n}^{z\,2}}$, the advancing piston forces the fluid attached to the surface of the piston through the diminishing gap, h. This behavior creates a pressure rise within this region which is indicative of a growing fluid film-thickness and the presence of hydrodynamic lubrication. On the other hand, at the contact point of the load $\sqrt{F_{o_n}^{y\,2} + F_{o_n}^{z\,2}}$, the advancing piston draws fluid *away* from the point of contact creating a pressure drop in this region and dissuading any hydrodynamic behavior whatsoever. For the retreating piston, the argument is similar.

Equation (6.15) of Chapter 6, describes the varying coefficient-of-friction throughout the pump based upon an assumption of varying lubricating conditions (i.e., transitions between boundary lubrication, mixed lubrication, and fully hydrodynamic lubrication). In the case of an *advancing* piston, the contact point of the load $\sqrt{F_{o_n}^{y\,2} + F_{o_n}^{z\,2}}$ does not undergo any lubricating transition whatsoever — it is *always* characterized by boundary lubrication since no fluid-film thickness is present. This is the similar situation for a *retreating* piston at the contact point

of the load $\sqrt{F_{l_n}^{y\,2} + F_{l_n}^{z\,2}}$. In other words, the coefficient-of-friction at these two points (operating in their respective modes) is characterized by a maximum constant-value, $\hat{\mu}_p$. Operating in these same modes, the coefficients-of-friction at the opposite points of contact are *indeed* characterized by hydrodynamic transitions and are therefore modeled using the general form of equation (6.15). If the loads per unit width at the inner and outer edges of the bushing are written respectively as

$$W_{l_n} = \sqrt{F_{l_n}^{y\,2} + F_{l_n}^{z\,2}} / D_p \tag{7.3}$$

and

$$W_{o_n} = \sqrt{F_{o_n}^{y\,2} + F_{o_n}^{z\,2}} / D_p \quad , \tag{7.4}$$

where D_p is the diameter of the piston, using equation (6.15) of Chapter 6, the appropriate coefficients-of-friction for the nth piston may be discontinuously expressed as

(7.5)

$$\mu_{l_n} = \begin{cases} \hat{\mu}_p \, \mathrm{Exp}\left(-\left(\dfrac{2 l_p \sqrt{6 K_\mu}}{h^*} \right)^2 \dfrac{\eta U_{p_n}}{\sqrt{F_{l_n}^{y\,2} + F_{l_n}^{z\,2}} / D_p} \right) + \dfrac{1}{\sqrt{6 K_\mu}} \sqrt{\dfrac{\eta U_{p_n}}{\sqrt{F_{l_n}^{y\,2} + F_{l_n}^{z\,2}} / D_p}} & U_{p_n} > 0 \\ \hat{\mu}_p & U_{p_n} < 0 \quad , \end{cases}$$

$$\mu_{o_n} = \begin{cases} \hat{\mu}_p & U_{p_n} > 0 \\ \hat{\mu}_p \, \mathrm{Exp}\left(\left(\dfrac{2 l_p \sqrt{6 K_\mu}}{h^*} \right)^2 \dfrac{\eta U_{p_n}}{\sqrt{F_{o_n}^{y\,2} + F_{o_n}^{z\,2}} / D_p} \right) + \dfrac{1}{\sqrt{6 K_\mu}} \sqrt{\dfrac{-\eta U_{p_n}}{\sqrt{F_{o_n}^{y\,2} + F_{o_n}^{z\,2}} / D_p}} & U_{p_n} < 0 \quad , \end{cases}$$

where equation (3.28) of Chapter 3 shows that $U_{p_n} = r\,\omega\tan(\alpha)\cos(\theta_n)$. For further explanations of equation (7.5) the reader is referred to Chapter 6.

7.2.3 Summary

By substituting equation (7.5) into equation (7.1) the final expression for the friction between the *n*th piston and the cylinder block is written as

$$f_{p_n} = \begin{cases} \sqrt{F_{l_n}^{y\,2} + F_{l_n}^{z\,2}}\,\hat{\mu}_p\ \mathrm{Exp}\left(-\left(\dfrac{2\,l_p\sqrt{6\,K_\mu}}{h^*} \right)^2 \dfrac{\eta\,U_{p_n}}{\sqrt{F_{l_n}^{y\,2} + F_{l_n}^{z\,2}}\,/\,D_p} \right) \\ \quad + \dfrac{\sqrt{F_{l_n}^{y\,2} + F_{l_n}^{z\,2}}}{\sqrt{6\,K_\mu}} \sqrt{\dfrac{\eta\,U_{p_n}}{\sqrt{F_{l_n}^{y\,2} + F_{l_n}^{z\,2}}\,/\,D_p} + \sqrt{F_{o_n}^{y\,2} + F_{o_n}^{z\,2}}\,\hat{\mu}_p} \end{cases} \quad U_{p_n} > 0 \\ \\ \begin{cases} \sqrt{F_{o_n}^{y\,2} + F_{o_n}^{z\,2}}\,\hat{\mu}_p\ \mathrm{Exp}\left(\left(\dfrac{2\,l_p\sqrt{6\,K_\mu}}{h^*} \right)^2 \dfrac{\eta\,U_{p_n}}{\sqrt{F_{o_n}^{y\,2} + F_{o_n}^{z\,2}}\,/\,D_p} \right) \\ \quad + \dfrac{\sqrt{F_{o_n}^{y\,2} + F_{o_n}^{z\,2}}}{\sqrt{6\,K_\mu}} \sqrt{\dfrac{-\eta\,U_{p_n}}{\sqrt{F_{o_n}^{y\,2} + F_{o_n}^{z\,2}}\,/\,D_p} + \sqrt{F_{l_n}^{y\,2} + F_{l_n}^{z\,2}}\,\hat{\mu}_p} \end{cases} \quad U_{p_n} < 0\ , \end{cases} \tag{7.6}$$

where the components of the normal loads are given in equation (7.2). Note the important differences between the friction of an advancing piston and the friction of a retreating piston; i.e., $\sqrt{F_{l_n}^{y\,2} + F_{l_n}^{z\,2}}$ and $\sqrt{F_{o_n}^{y\,2} + F_{o_n}^{z\,2}}$ have traded locations within the equation.

7.2.4 Experiments

In an effort to verify the basic result of equation (7.6), the test-device shown in Figure 7-2 was built to measure friction within a single piston bore. As shown in Figure 7-2, the piston bore was simulated by using a long tube with bushings pressed in place similar to the design of an actual piston-bore within a hydrostatic pump. The tube was hardened and polished, mounted within a precision frictionless-linear-bearing, and pressurized from the opposite end by an external pressure-source. Once the tube was placed within the bearing,

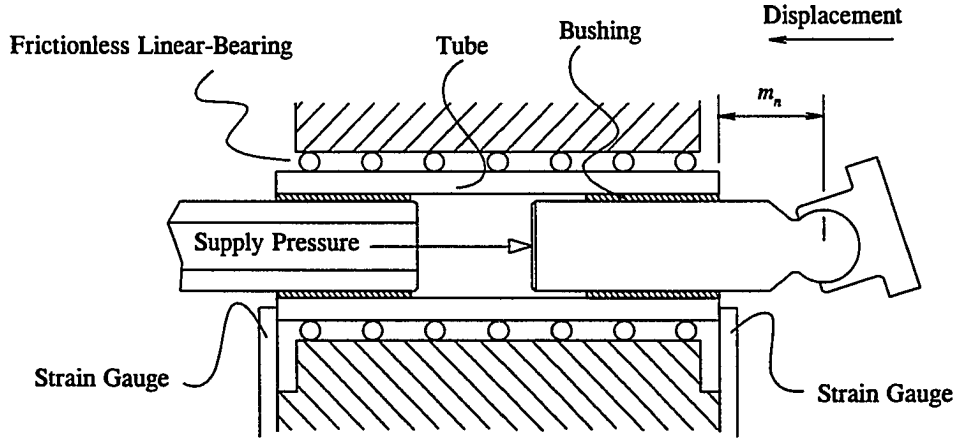

Figure 7-2. A schematic of the basic single-piston test-device.

two strain-gauged members were attached to the outside of the bearing housing (i.e., one on each end). These strain-gauged members were used to hold the tube within the bearing itself and to measure any forces that might try to push the tube out of the bearing (i.e., piston friction). A conventional piston / slipper assembly was placed within the tube and a driving mechanism was used to push the piston back and forth within the simulated piston-bore. (The

driving mechanism is not shown in Figure 7-2.) The driving mechanism simulated a swash-plate component utilizing an angled wedge and was linearly displaced back and forth by an electronic linear-actuator. This device generated no relative motion between the slipper and the swash-plate component and thereby eliminated all slipper friction (f_{s_n}) from the measurements. For this test device, the maximum pressure within the piston bore was 100 bar and the average velocity of the piston was 0.4 mm/s.

7.2.4.1 Mathematical Model of the Test

In general, a mathematical model of the piston friction must follow the basic form of equation (7.1); however, since slipper friction has been eliminated and since testing was done at very slow speeds, the piston loads in the *y*-direction may be ignored (i.e., $F_{l_n}^y \approx F_{o_n}^y \approx 0$). See equation (7.2). Furthermore, for low operating speeds of the piston one may assume that $\mu_{l_n} \approx \mu_{o_n} \approx \hat{\mu}_p$ where $\hat{\mu}_p$ is a constant. Substituting these results into equation (7.1), and rearranging terms, it may be shown that during the tested operating-conditions of the single-piston test device an approximate model for the piston friction may be written

$$f_{p_n} \approx \frac{A_p P_n}{\dfrac{l_p}{\text{sign}(U_{p_n})\,(l_p + 2\,m_n)\,\hat{\mu}_p \tan(\alpha)} - 1}\,, \tag{7.7}$$

where the overhang length m_n is illustrated in Figure 7-2. Note: all forcing terms associated with speed have been neglected in equation (7.7). Recognizing that the coefficient-of-friction

within the bore, $\hat{\mu}_p$, is typically small, equation (7.7) may be approximated as

$$f_{p_n} \approx A_p P_n \left(\frac{(l_p + 2\, m_n) \tan(\alpha)\, \hat{\mu}_p}{l_p} \right) \left(\text{sign}(U_{p_n}) + \frac{(l_p + 2\, m_n) \tan^2(\alpha)\, \hat{\mu}_p}{l_p} \right) \quad . \tag{7.8}$$

The first thing to notice from equation (7.8) is the effect of the "sign function" on the behavior of piston friction. This sign function conventionally produces a positive-valued friction force for an advancing piston (i.e., $U_{p_n} > 0$) and a negative-valued friction force for a retreating piston (i.e., $U_{p_n} < 0$). More than this, however, the sign function actually reduces the *magnitude* of friction for a retreating piston compared to an advancing piston. This is somewhat unexpected, however, it may be explained in the following way:

For an advancing piston, friction effectively contributes (adds) to the driving load of the piston, $A_p P_n$. This added load is realized (through the swash-plate angle) by the side load of the piston and therefore *increases* the piston friction. On the other hand, the friction for a retreating piston tends to detract (subtracts itself) from the driving load of the piston and thereby reduces the expected side-load on the piston. This reduction in side load tends to *reduce* the magnitude of piston friction.

From equation (7.8) it can be seen that a fully extended piston (i.e., a maximum value for m_n) is expected to generate more friction than a piston that is pushed far into the cylinder block (i.e., a small value for m_n). This phenomenon is strictly a result of mechanics and may be likened to the effect of gaining leverage (higher forcing capability) when one uses a longer

moment-arm for any given application. This increased leverage amounts to an increased side-load on the piston creating higher piston friction.

7.2.4.2 Experimental Results

Experiments were conducted for a range of pressures between 20 and 100 bar. Figure 7-3 shows the results of a typical run compared to the theoretical expectations of equation (7.8). Note: the correlation between test data and equation (7.8) is quite good. Figure 7-3 shows that the magnitude of friction for an advancing piston is indeed greater than the magnitude of friction for a retreating piston and that equation (7.8) predicts this behavior quite

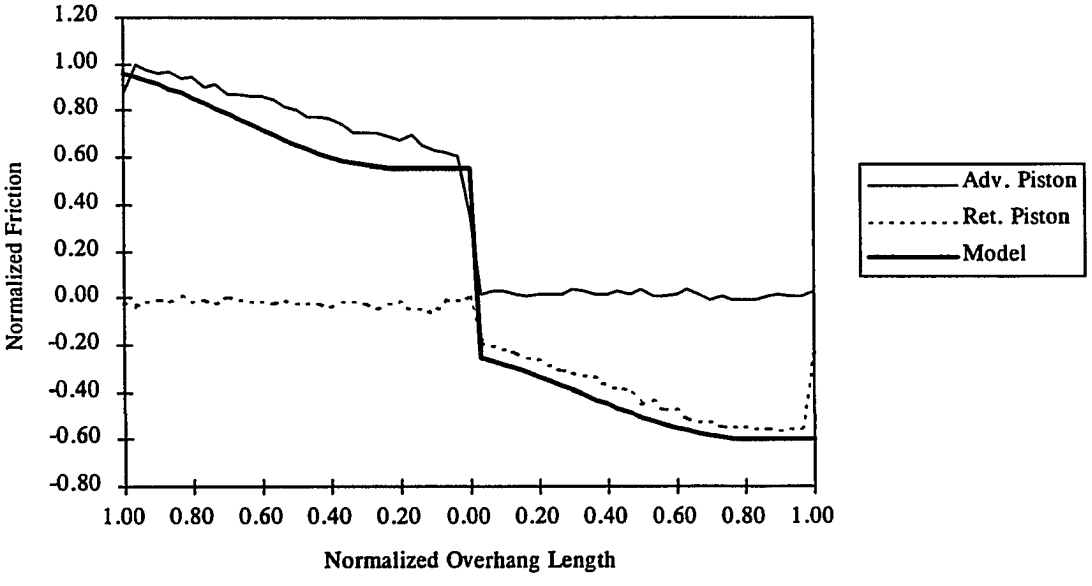

Figure 7-3. A typical comparison of test data with the results of equation (7.8).

well. Furthermore, Figure 7-3 shows that a fully-extended piston creates the highest piston friction for both an advancing piston and a retreating piston. This behavior was also predicted by equation (7.8).

7.2.4.3 Literature

Experimental studies of the type previously described have been conducted and published in the literature (Tanaka, Nakahara, and Kyogoku, 1993; Ezato and Ikeya, 1986); however, in this published work, the reciprocating motion of the piston was generated by a rotating angled-plate that created friction at the slipper. For the experiments of this dissertation, it has been desirable to separate the slipper friction from the piston friction and therefore a different driving mechanism was used. Furthermore, the previously published research does not contain results that are explained analytically. For instance, Tanaka, Nakahara, and Kyogoku do not even *attempt* to explain their results and it is not at all apparent to the reader why their results look the way they do. Ezato and Ikeya do a much better job discussing their work and many of their conclusions are supported by the research of this dissertation; however, Ezato and Ikeya were not trying to validate a theoretical model and therefore they do not offer a comparison of test data with theoretical expectations.

7.2.4.4 Conclusions

The range of examination within this study shows very good correlation with theoretical models. Though due to the limited scope of these experiments it can not be said conclusively that equation (7.6) has been verified, it can still be said that this study has bolstered the analysis of this dissertation in a positive way. Remaining concerns of the model pertain to the fact that the high-speed and high-pressure conditions of the piston have not been tested and discussed in this subsection. This aspect of the model must be verified at a more macroscopic level during the testing of an entirely-assembled hydrostatic pump.

7.3 Slipper Friction

Figure 7-4 shows a two-dimensional view of a slipper as it slides relative to the swash plate. This figure illustrates the loads acting on the slipper from the swash plate and the fluid-film thickness, h, between the swash plate and the slipper. In this section, the friction between the nth slipper and the swash plate is modeled using the conventional relationship

$$f_{s_n} = F_{sw_n} \mu_{s_n} \quad , \tag{7.9}$$

where F_{sw_n} is the normal load of contact between the nth slipper and the swash plate and μ_{s_n} is the instantaneous coefficient-of-friction between the two surfaces. The reader should note that the distance $w\,\mu_{s_n}$ shown in Figure 7-4 is easily inferred using equation (7.9) and equations (3.76) and (3.77) of Chapter 3.

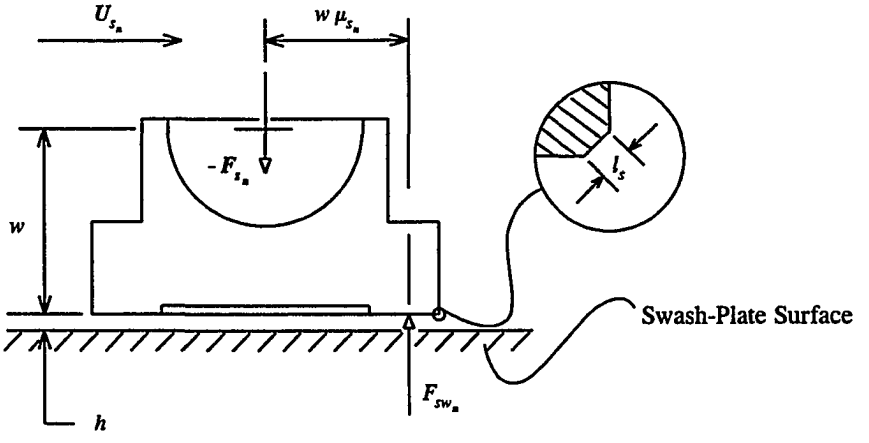

Figure 7-4. A two-dimensional view of a slipper sliding relative to the swash plate.

7.3.1 Normal Load

The normal load between the slipper and the swash plate, F_{sw_n}, has already been derived in equation (3.75) of Chapter 3 and is rewritten here for convenience:

(7.10)

$$F_{sw_n} = P_n(A_p \sec(\alpha) - A_s) - (M_p + M_s)\tan(\alpha)\sec(\alpha)\, r\, \omega^2 \sin(\theta_n) + F_{hd} + f_{p_n}\sec(\alpha) + f_{s_n}\tan(\alpha)\cos(\theta_n) \ .$$

7.3.2 Coefficient-of-Friction

Figure 7-4 shows the basic loading of a slipper. By examining this figure, it is easy to see that slippers do not load themselves in a way that is conducive to hydrodynamic sliding since the centroid of the slipper load, F_{sw_n}, is carried by the leading "foot" of the slipper. This

scenario can be likened to a person trying to water-ski by standing on the leading edge of a sheet of plywood. Intuitively, this does not work. Extensive use of slippers, however, has shown that they *do* work, and the only explanation for this lies in the fact that slippers tend to wear themselves into a configuration (during the initial "break-in" period of the machine) that *is* hydrodynamically conducive. Perhaps Koc, Hooke, and Li (1992, 767) have summarized the research of this phenomenon best:

> ...A comprehensive analysis by Fisher (1962) of overclamped, perfectly flat slippers operating under isoviscous conditions showed conclusively that slippers could not work ... Fisher then suggested that either viscosity changes from front to rear of the slipper or some nonflatness of the running face must be present and that these might be responsible for successful slipper operation...
>
> ...Hooke and Kakoullis (1978) were able to show that viscosity changes, alone, could not account for slipper lubrication and that the only possible explanation lay in some profiling of the slipper running surface either accidentally, during manufacture, or as a result of running-in... Detailed investigation (Hooke and Kakoullis, 1983; Hooke and Li, 1989) showed that... [the successful operation of the slipper] was remarkably insensitive to the actual profile [of nonflatness] and that nonflatnesses ranging in height from less than 0.1 μm to over 10 μm could generate adequate lubrication films. Almost any surface geometry was found to be acceptable, provided... the surface was generally convex.
>
> The design of overclamped slippers is, then, unlike that of conventional bearings in that [successful] operation depends on a parameter that is never specified or controlled during manufacture [i.e., surface flatness].

The fact that slippers of new hydrostatic pumps plastically deform during break-in is so well known by the designers of these machines that they give this phenomenon its own name. It is called "slipper roll". This name describes the plastic deformation that appears on the outside edge of the slipper running-face and is shown in Figure 7-4 using the dimension, l_s. It is this deformation that allows the slipper to slide along the swash-plate surface in a hydrodynamic fashion. The deformation is small; however, as researchers have noted, it is sufficient.

The general expression for the varying coefficient-of-friction (including hydrodynamic behavior) has been derived in equation (6.15) of Chapter 6. If the load per unit width between the swash plate and the *n*th slipper is expressed as

$$W_{s_n} = F_{sw_n} / D_s \quad , \tag{7.11}$$

where D_s is the outside diameter of the slipper land, the general form of equation (6.15) and the geometry of Figure 7-4 may be used to express the coefficient-of-friction for the *n*th slipper as

$$\mu_{s_n} = \hat{\mu}_s \, \mathrm{Exp}\left(-\left(\frac{2 l_s \sqrt{6 K_\mu}}{h^*} \right)^2 \frac{\eta \, U_{s_n}}{(F_{sw_n} / D_s)} \right) + \frac{1}{\sqrt{6 K_\mu}} \sqrt{\frac{\eta \, U_{s_n}}{(F_{sw_n} / D_s)}} \quad , \tag{7.12}$$

where U_{s_n} is easily shown to be $r \omega$.

7.3.3 Summary

The model of friction as it acts on the *n*th slipper is summarized by substituting equation (7.12) into equation (7.9) to yield

$$f_{s_n} = F_{sw_n}\hat{\mu}_s \,\mathrm{Exp}\left(-\left(\frac{2\,l_s\sqrt{6\,K_\mu}}{h^*} \right)^2 \frac{\eta\, U_{s_n}}{(F_{sw_n}/D_s)} \right) + \frac{F_{sw_n}}{\sqrt{6\,K_\mu}} \sqrt{\frac{\eta\, U_{s_n}}{(F_{sw_n}/D_s)}} \quad , \tag{7.13}$$

where the normal load F_{sw_n} is given in equation (7.10).

7.3.4 Experiments

As part of modeling the friction between the *n*th slipper and the swash plate, the author of this dissertation did not have the luxury to conduct an experimental verification of equation (7.13); however, previous slipper-research has involved significant experimentation. For example, the work of Koc, Hooke, and Li (1992) and Hooke and Kakoullis (1981, 1978) has emphasized the direct measurement of fluid-film thicknesses between the slipper and the swash plate during the actual operation of an *entirely-assembled* hydrostatic pump. This research does not attempt to explain the resulting friction-forces between the slipper and the swash plate. Another study done by Pang, Wenjie, and Jingwu (1993) focuses on the *hydrostatic* lubrication of the slipper but does not concern itself directly with the verification of a model similar to equation (7.13). The validity of equation (7.13) must be determined based upon the tests of an entirely-assembled pump.

7.4 Valve-Plate Friction

In equation (3.10) of Chapter 3, the friction at the valve plate was considered, not as a force, but as a moment about the x-axis. Since the cylinder block is designed in such a way as to maintain tight contact with the valve plate in the neighborhood of the piston pitch-radius, r, it makes good sense to use this dimension as an effective moment-arm for the frictional

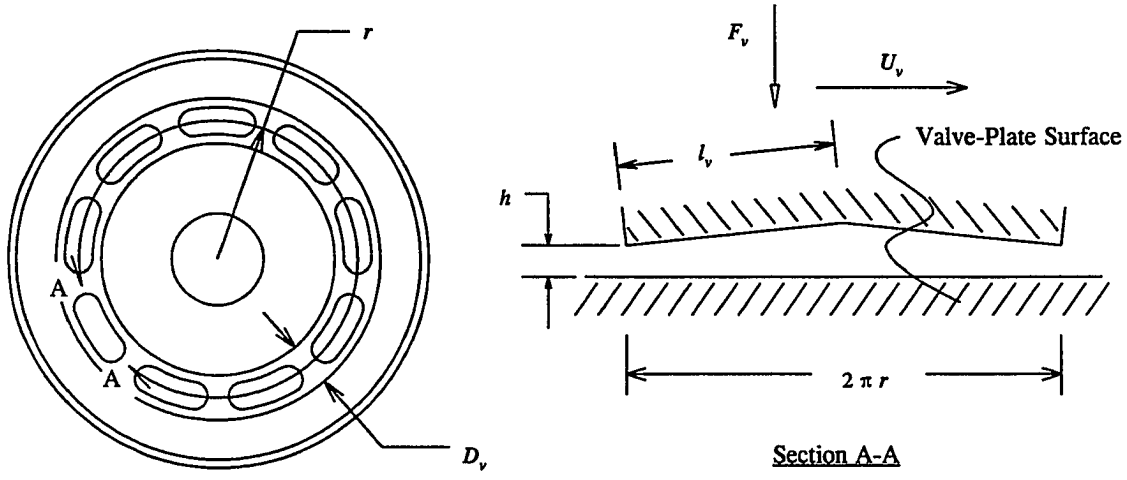

Figure 7-5. A two-dimensional view of the nonparallel sliding-conditions between the valve plate and the cylinder block.

moment generated about the x-axis. Figure 7-5 shows a view of the cylinder block sectioned through the piston pitch-radius. This figure illustrates the loads acting on the valve plate through the cylinder block and the thickness of the fluid-film, h, that exists between the cylinder block and the valve plate. The reader should note that the sectioned view of Figure 7-5 generally shows the cylinder block in a position that is not perfectly parallel with the valve

plate. This aspect of Figure 7-5 will be discussed later. The dimension D_v in Figure 7-5 is the width of the diametrical land on the cylinder block. The frictional moment about the x-axis due to friction at the valve plate is modeled as

$$f_v = F_v r \mu_v \quad , \tag{7.14}$$

where F_v is the normal load of contact between the cylinder block and the valve plate, and μ_v is the associated coefficient-of-friction.

7.4.1 Normal Load

The normal load between the cylinder block and the valve plate has been derived and presented in equation (3.65) of Chapter 3. This result is rewritten here for convenience:

$$F_v = F_{sp} + \sum_{n=1}^{N} A_b P_n + \sum_{n=1}^{N} f_{p_n} \quad . \tag{7.15}$$

7.4.2 Coefficient-of-Friction

In general, the likelihood that the cylinder block lays perfectly flat against the valve plate is slim to none. See Figure 7-5. The reason for this is the fact that the machined parts (and the assembly of the pump itself) have certain tolerances within an acceptable range that stack up to produce an assembled nonparallel-relationship between the valve-plate surface and the cylinder block. Furthermore, a quick glance at Figure 3-1 of Chapter 3 shows that the

reaction force between the cylinder block and the valve plate, F_v, is not *centrally* located on the x-axis and that this load is offset toward one quadrant of the valve plate. This offset condition of loading serves to enhance the possibility of a slightly tipped cylinder-block with respect to the valve plate. This non-parallelism between the valve plate and the cylinder block provides a geometry for half of the cylinder block that is conducive to hydrodynamic sliding. This half is signified by the dimension, l_v.

Assuming that the two-dimensional geometry of Figure 7-5 is correct, and noting that the load per unit width between the swash plate and the valve plate is given by

$$W_v = F_v / D_v \quad , \tag{7.16}$$

the coefficient-of-friction between the valve plate and the cylinder block is modeled according to the general form of equation (6.15) in Chapter 6. This result is given by

$$\mu_v = \hat{\mu}_v \, \mathrm{Exp}\left(-\left(\frac{2 l_v \sqrt{6 K_\mu}}{h^*} \right)^2 \frac{\eta U_v}{(F_v / D_v)} \right) + \frac{1}{\sqrt{6 K_\mu}} \sqrt{\frac{\eta U_v}{(F_v / D_v)}} \quad , \tag{7.17}$$

where U_v is given by $r \omega$.

7.4.3 Summary

The model of friction between the valve plate and the cylinder block is summarized by substituting equation (7.17) into equation (7.14). This result is given by

$$f_v = F_v r \hat{\mu}_v \operatorname{Exp}\left(-\left(\frac{2 l_v \sqrt{6 K_\mu}}{h^\cdot} \right)^2 \frac{\eta U_v}{(F_v / D_v)} \right) + \frac{F_v r}{\sqrt{6 K_\mu}} \sqrt{\frac{\eta U_v}{(F_v / D_v)}} \quad , \tag{7.18}$$

where the normal load, F_v, is given in equation (7.15).

7.4.4 Experiments

In this subsection a simple experiment that has been used to determine the frictional effects resulting from the load applied to the valve plate by the cylinder-block spring is presented. The intention of this test has been to quantify the differences in measured torque on the cylinder block while using different assembled block-spring loads during low speed operation.

From equations (7.14) and (7.15) it can be seen that the effect of increasing the spring load, F_{sp}, is to increase the friction between the cylinder block and the valve plate. For experimentation, two cylinder-block spring loads, F_{sp_1} and F_{sp_2}, with a 94% difference in magnitude were tested while turning the cylinder block at a speed of 1 RPM. The torque on the cylinder block was measured while the pressure on the discharge side of the pump was increased from 50 to 350 bar. Differences in the measured torque between the two spring

tests, ΔT_m, were calculated at each pressure.

7.4.4.1 Mathematical Model of the Test

Assuming all other parameters were equal, equation (3.62) of Chapter 3 and equations (7.14) and (7.15) were used to calculate the theoretical torque-difference that should be expected when the block-spring load is reduced. This result is given by

$$\Delta T_t = (F_{sp_1} - F_{sp_2})\, r\, \mu_v \quad . \tag{7.19}$$

Note: at the speed of 1 RPM $\mu_v \approx \hat{\mu}_v$ where $\hat{\mu}_v$ is a constant.

7.4.4.2 Experimental Results

The test results given by ΔT_m were compared to equation (7.19) to evaluate the experimental versus theoretical influence of the cylinder-block spring load on valve-plate friction. Figure 7-6 shows a graph of this comparison. The percent difference between the value of the theoretical torque-difference, ΔT_t, and the values of the measured torque-difference, ΔT_m, were calculated and shown to be less than 7%.

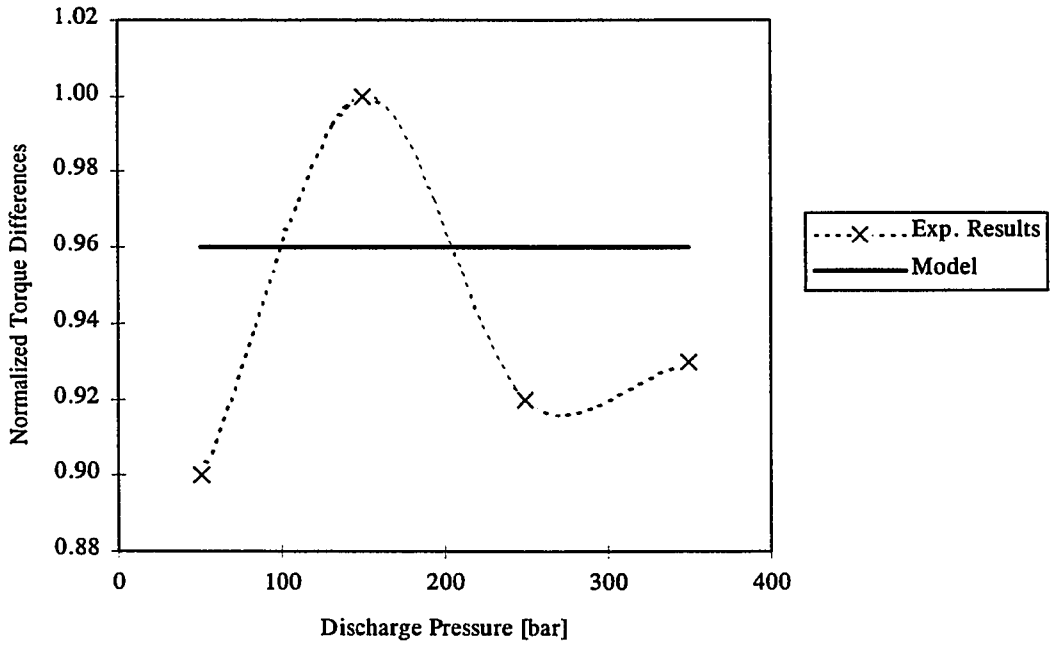

Figure 7-6. Experimental results compared to the result of equation (7.19).

7.4.4.3 Conclusions

The simple experiment described in this subsection has served to validate equation (7.19) which describes only a small portion of equation (7.18). The primary benefit of this investigation has shown that the moment arm, r, used to model the frictional moment on the cylinder block, is an acceptable choice for this parameter. Since these tests have neglected to measure the high-speed conditions between the valve plate and the cylinder block, further validation of equation (7.18) must be conducted on a more macroscopic scale during the tests of a fully-assembled pump.

7.5 Conclusion

This chapter has been used to develop the basic models of friction within the axial-piston hydrostatic pump. Specifically, these models pertain to the friction between the piston and the cylinder block (see equation (7.6)), the friction between the slipper and the swash plate (see equation (7.13)), and the friction between the cylinder block and the valve plate (see equation (7.18)). The remaining work of this dissertation investigates the interaction of these frictional components within an entirely-assembled machine.

CHAPTER 8. TORQUE ON THE CYLINDER BLOCK

8.1 Introduction

The general equation describing the torque on the cylinder block of an axial-piston swash-plate type hydrostatic-pump has been presented in equation (3.62) of Chapter 3. In this chapter, the models for each component of equation (3.62) are assembled and the final model describing the net torque on the cylinder block is examined. For convenience, equation (3.62) is rewritten here:

$$T = \sum_{n=1}^{N} A_p P_n r \tan(\alpha) \cos(\theta_n) + \sum_{n=1}^{N} f_{p_n} r \tan(\alpha) \cos(\theta_n) + \sum_{n=1}^{N} f_{s_n} r \left(\sin^2(\theta_n) + \sec(\alpha) \cos^2(\theta_n)\right) + f_v \quad . \tag{8.1}$$

Two divisions of equation (8.1) are considered in this chapter: 1) the *idealized torque* on the cylinder block and 2) the torque that is lost due to friction. This second aspect of equation (8.1) is commonly referred to as "torque loss".

8.2 Idealized Torque

The idealized torque on the cylinder block of an axial-piston hydrostatic pump is given by the equation

$$T_I = \sum_{n=1}^{N} A_p P_n r \tan(\alpha) \cos(\theta_n) \quad , \tag{8.2}$$

which is the first part of equation (8.1). Equation (8.2) represent the *instantaneous* idealized-torque exerted on the cylinder block. To determine the *average* idealized torque on the cylinder block, the summation sign of equation (8.2) is replaced with $\frac{N}{2\pi}\int_0^{2\pi}$ and the equation is integrated with respect to θ_n. This expression is given by

$$\bar{T}_I = \frac{N}{2\pi}\int_0^{2\pi} A_p P_n r \tan(\alpha)\cos(\theta_n)\, d\theta_n \quad . \tag{8.3}$$

Using the quantity for P_n given in equation (4.8) of Chapter 4, the evaluated form of equation (8.3) is

$$\bar{T}_I = \frac{N A_p (P_d - P_l) r \tan(\alpha)}{\pi} \frac{\sin(\gamma)}{\gamma} \quad , \tag{8.4}$$

where the reader is reminded that γ describes the pressure carry-over angle on the valve plate. (See Figure 4-4 of Chapter 4.) Recognizing that γ is typically small, equation (8.4) may be approximated as

$$\bar{T}_I = \frac{N A_p (P_d - P_l) r \tan(\alpha)}{\pi}\left(1 - \frac{\gamma^2}{6}\right) \quad . \tag{8.5}$$

8.2.1 Theoretical Torque

Traditionally, literature and technical manuals (Pourmovahed 1992; McCandlish and Dorey 1984; Zarotti and Nervegna 1981; Browns, Rolfe, and Chapple 1978; Turnbull 1978;

Hanna 1967; Peterson 1966) have presented the theoretical torque on the cylinder block of an axial-piston pump as

$$T_{TH} = \frac{\Delta P \, V_d}{2\pi} \quad , \tag{8.6}$$

where ΔP is the pressure drop across the discharge and intake ports of the valve plate, and V_d is the volumetric displacement of the pump given in units of volume per revolution. A careful comparison shows that this representation of the theoretical torque on the cylinder block corresponds to the first term of equation (8.5) where $V_d = 2 N A_p r \tan(\alpha)$; therefore, a more explicit representation of the theoretical torque on the cylinder block is given by

$$T_{TH} = \frac{N A_p (P_d - P_i) r \tan(\alpha)}{\pi} \quad . \tag{8.7}$$

8.2.2 The Pressure Carry-Over Effect

In the past, equation (8.7) has been considered to be the *idealized* torque on the cylinder block of an axial-piston pump; however, a comparison of equation (8.7) with equation (8.5) shows that this has generally been a mistake. The difference between these two expressions is a result of the pressure carry-over on the valve plate and may be expressed as

$$T_\gamma = - \frac{N A_p (P_d - P_i) r \tan(\alpha)}{\pi} \frac{\gamma^2}{6} \quad . \tag{8.8}$$

From equation (8.8) it can be seen that the pressure carry-over effect serves to *reduce* the

idealized torque on the cylinder block of the pump. The reason that the pressure carry-over effect has gone unnoticed in the past is that the value of γ is usually small; and, as shown in equation (8.8), when this small number is squared the effect of gamma can be negligible. Only when γ becomes larger does the pressure carry-over effect become noticeable. The author of this dissertation has numerically observed values of γ that approach 24° (0.42 rad). A simple substitution of this magnitude into equation (8.5) shows that the pressure carry-over effect can reduce the idealized torque on the cylinder block by up to 3%.

8.2.3 Discrete Considerations

For a physical interpretation of equation (8.5), it is helpful to look back at the discrete representation of the idealized torque exerted on the cylinder block (i.e., equation (8.2)). It is also helpful to use Figure 8-1 which shows a schematic of the valve plate with a shadowed layer of the pistons as they pass over each port. An idealized representation of the *force* exerted on the cylinder block by the *n*th piston, F_n, is shown in Figure 8-1 as well. Using Figure 8-1 and equation (8.2), it can be seen that

$$F_n = A_p P_n \tan(\alpha) \tag{8.9}$$

and that the distance of this force away from the z-axis is given by

$$d_n = r\cos(\theta_n) \quad . \tag{8.10}$$

The torque exerted on the cylinder block by the *n*th piston is then

$$T_n = F_n d_n \quad , \tag{8.11}$$

where equation (8.2) is simply the summation of these individual torques.

From geometry, it can be seen that the pistons on the high-pressure side of the valve plate exert a torque that *adds* to the overall torque on the cylinder block, while the pistons on the low pressure side of the valve plate exert a torque that *subtracts* from the overall torque on the cylinder block. Since the forces on the high-pressure side of the valve plate are much

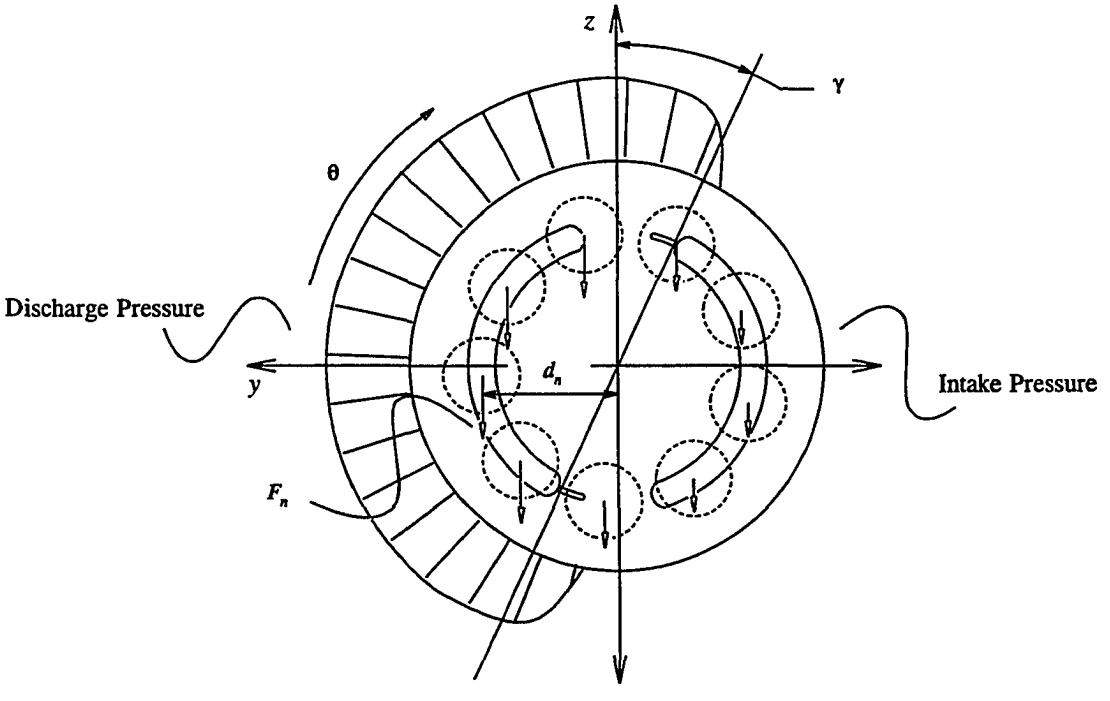

Figure 8-1. A schematic illustrating the forces and moments that create the idealized torque on the cylinder block.

greater than the forces on the low-pressure side of the valve plate, the net torque exerted on the cylinder block is a positive quantity that linearly varies with the pressure drop between the high and low-pressure ports of the valve plate. See equation (8.5).

The effect of the pressure carry-over angle, γ, on the idealized cylinder-block torque is illustrated in Figure 8-1. As the pistons pass through each transition slot on the valve plate, their pressures are neither discharge pressure, P_d, nor intake pressure, P_i. They are something in between. Strictly speaking, the theoretical calculation of torque on the cylinder block (see equation (8.7)) assumes that these transition states do not exist. In reality, the effect of these transitions is to enhance a subtractive torque at top-dead-center by increasing the theoretical expectations of F_n through the low-pressure slot, and to diminish an additive torque at bottom-dead-center by reducing the theoretical expectations of F_n through the high-pressure slot. As previously mentioned, the net effect of this behavior is to *reduce* the idealized torque on the cylinder block. See equation (8.8). It should be mentioned that the torque-reducing effect of gamma cannot be considered a "torque loss". You cannot lose a torque that you don't put in. In actuality, the "gamma effect" simply reduces the effective displacement and makes the pump appear smaller than it really is from both an input and an output perspective.

8.3 Torque Loss

The second and, perhaps, more interesting aspect of the torque on the cylinder block of an axial-piston pump is the aspect of torque loss. Torque loss is defined as the amount of torque that is used to overcome friction within the pump. Obviously, friction is transmitted into heat and heat is naturally dissipated *away* from the machine; therefore, this torque is rightfully called a loss. From equation (8.1) it can be seen that the instantaneous torque-loss for an axial-piston pump is given by

$$T_L = \sum_{n=1}^{N} f_{p_n} r \tan(\alpha) \cos(\theta_n) + \sum_{n=1}^{N} f_{s_n} r \left(\sin^2(\theta_n) + \sec(\alpha) \cos^2(\theta_n)\right) + f_v \quad , \tag{8.12}$$

where f_p, f_s, and f_v are the frictional components relative to the pistons, the slippers, and the valve plate respectively.

In this dissertation, Chapter 7 has been devoted to modeling the frictional components of equation (8.12). The summarized models for the friction at the pistons, at the slippers, and at the valve plate are given in equations (7.6), (7.13), and (7.18) respectively. It should be noted that the equations modeling piston friction and slipper friction (equations (7.6) and (7.13)) are intrinsically dependent upon each other. Furthermore, there is no explicit solution for these equations as their right and left-hand-sides are interconnected through transcendental functions. The equation that models valve-plate friction (equation (7.18)) does not exhibit this difficulty; however, it is highly dependent upon the results of equations (7.6) and (7.13). Clearly, any hope of solving equation (8.12) must be carried out numerically.

8.3.1 Numerical Simulation

To evaluate equation (8.12), the ACSL program for numerical modeling is employed. The advantage of using this program is the fact that ACSL contains several intrinsic functions that reduce the laborious task of writing numerical code. For example, the Gear's Stiff integration routine within ACSL was used in Chapter 4 to evaluate piston pressures and is extended to the work of this chapter for the very same purpose. Perhaps a more significant contribution of the ACSL program for this chapter is its IMPL function which is used to solve the implicit relationships between the piston friction and the slipper friction. This function provides a Newton-Raphson iteration method that quickly converges on a solution. Run times for this program are approximately 1 minute for 40° of pump rotation using a 486-DX2 66-MHz personal computer. A simple flow-chart for the numerical program is presented in Figure 8-2. This program is capable of calculating all relevant quantities presented in this dissertation, including the instantaneous *overall* torque on the cylinder block.

The desired-output of this program is both the *average* torque-loss value for the pump as a whole and the *average* torque-loss value for each frictional component of equation (8.12). By simulating the average torque-loss for the pump as a whole, torque-loss values generated by the model will be compared with actual test-data. By simulating the average values of torque-loss for the individual components of friction within the pump, it will be possible to distinguish between the more significant and less significant frictional-contributors. Note:

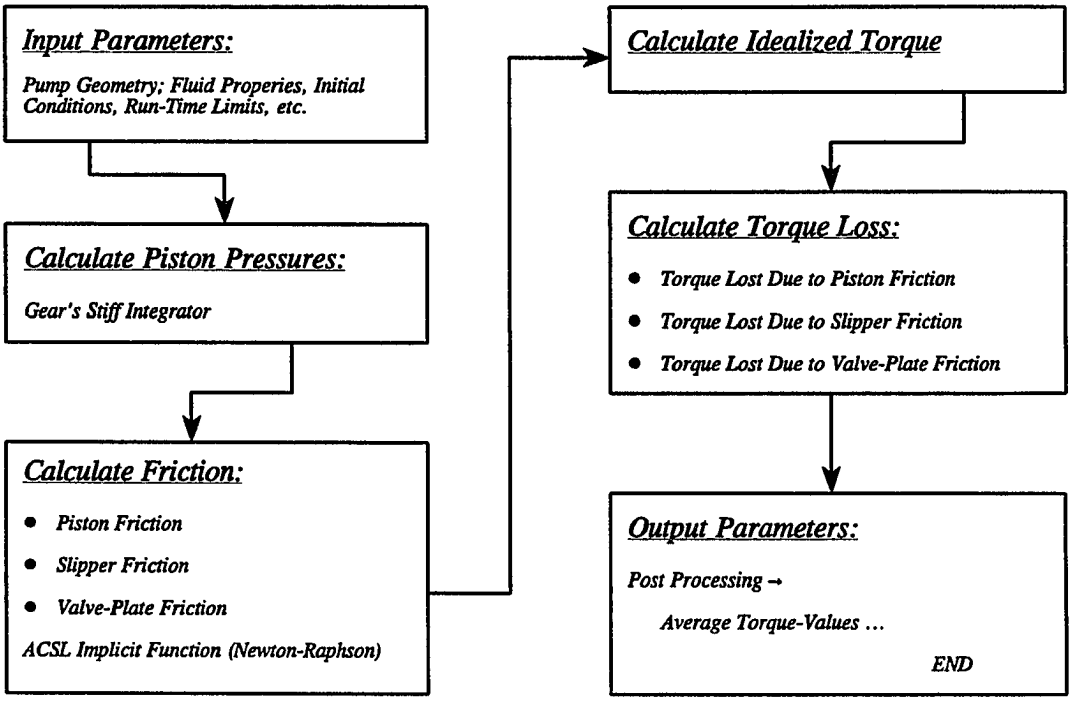

Figure 8-2. A flow chart of the numerical program used to calculate the torque on the cylinder block of an axial-piston swash-plate type hydrostatic pump.

an actual copy of this program is included in the Appendix.

8.3.2 Experiments

To support the research of this dissertation, experimental hardware of an axial-piston swash-plate type hydrostatic-pump was provided by the Sauer-Sundstrand, Co. of Ames, Iowa. The design features of this pump were similar to the pump described in Chapter 2. The experimental procedures were as follows:

The pump was mounted to a high-horsepower prime mover with the capability of

adjusting and setting a constant input-speed for the pump shaft. Downstream of the pump a load valve was used to restrict the output flow of the pump and thereby created high pressure in the discharge port of the valve plate. By adjusting the restriction in the load valve, a constant value for the discharge pressure was established. The intake port of the valve plate was pressurized by an *external* pump-source that controlled the intake pressure at a constant value of 20 bar for all tests. The temperature of the circulating fluid was maintained at 50 degrees Celsius within the discharge port of the valve plate. A strain-gauged torque shaft was placed between the pump and the prime mover and it was assumed that the torque measurement on the shaft was equivalent to the torque on the cylinder block. (As mentioned in Chapter 2, the shaft itself was supported at both ends by a heavy-duty *frictionless* bearing.) Special arrangements were made to drain any excess fluid away from the outside of the cylinder block to avoid any viscous losses that might result from the presence of this fluid.

As the input shaft of the pump was turned at a constant speed, and the discharge pressure was held constant, torque measurements were taken from the torque shaft at a sample rate of 1 Hz for a time duration of 100 seconds. This data was then numerically averaged to arrive at an average measured-torque, $\bar{T}$, on the cylinder block of the axial-piston pump. These measurements were taken for constant input-speeds ranging between 500 and 3800 RPM, and for constant discharge pressures ranging between 50 and 385 bar. Since the pressure carry-over effect discussed in Subsection 8.2.2 was impossible to measure empirically, the average torque-loss of the pump was calculated using

$$\bar{T}_L = \bar{T} - T_{TH} \quad , \tag{8.13}$$

where the theoretical torque, T_{TH}, is given in equation (8.7).

8.3.3 Data Correlation

To validate the model for torque loss presented in equation (8.12), and to thereby validate the previous modeling done for individual friction-components within the pump, the numerical solutions of equation (8.12) were compared to the actual measured test-data using the general form of equation (8.13). These results are presented in Figure 8-3. As shown in

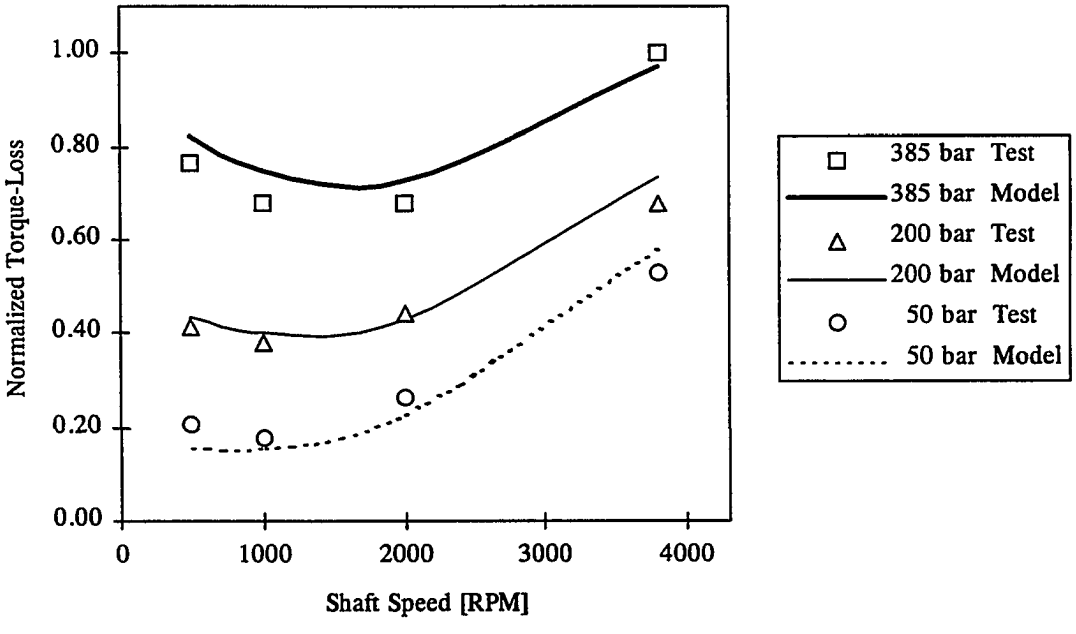

Figure 8-3. A comparison of the numerical results of equation (8.12) with actual test-data.

Figure 8-3, the model of equation (8.12) does a very good job of predicting the average torque-loss of an entirely-assembled pump. From this correlation of empirical test-data with the theoretical expectations, it is concluded that the analysis and modeling of Chapters 3 through 7 are valid.

8.3.4 Torque-Loss Separation

An important aspect of this study has been to determine the percent of the total torque-loss that each frictional component generates within the pump. Without the numerical model, this information is not obvious. Figure 8-4 shows the numerical separation of these torque

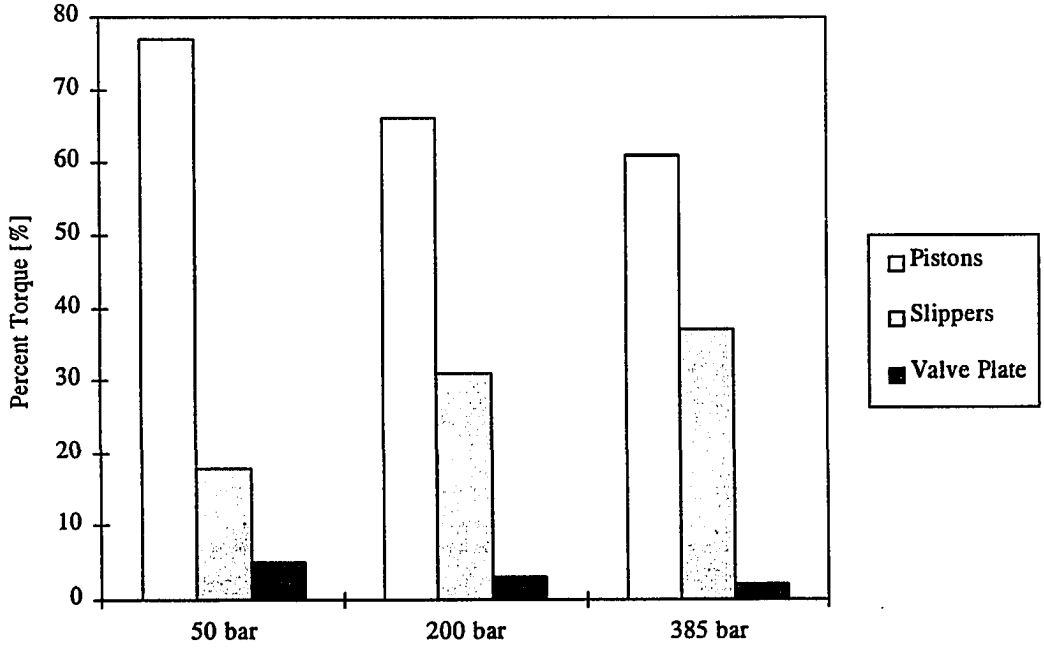

Figure 8-4. A bar chart showing the individual percent torque-losses within the pump.

losses by the percent of total torque that is lost within the pump. The results of Figure 8-4 were similar for each shaft speed examined in this study.

Figure 8-4 shows that the pistons consistently generate more than 60% of the torque loss within the pump. The primary explanation for this is the fact that the pistons undergo some of the highest normal-loading in the pump and that they see the greatest occurrence of boundary lubrication compared to either the slippers or the valve plate. From Figure 8-4 it can also be seen that the slipper generates only 18 to 37% of the total torque-loss within the pump. The reason that this percentage is not greater is due to the large effective pressurized-area on the slipper that tends to separate the slipper from the swash plate. Furthermore, the slipper tends to undergo a more constant hydrodynamic-lubrication than the pistons. The valve plate itself is shown to contribute very little to the overall torque-loss within the pump. The reason for this is the fact that the load between the valve plate and the cylinder block is not significantly large compared to the load between the swash plate and the slipper or between the cylinder block and the piston. Furthermore, the valve plate exhibits a very low coefficient-of-friction as it undergoes almost no boundary lubrication whatsoever.

8.4 Conclusion

In this chapter, the idealized torque on the cylinder block and the torque loss that results from friction have been numerically modeled and discussed. In particular, an improved model for the idealized torque on the cylinder block has been suggested to include the pressure

carry-over effect on the valve plate. This improved model is given in equation (8.5). Furthermore, in this chapter, the numerical evaluation of equation (8.1) has been compared with actual test-data and has shown that the analysis and modeling done in this dissertation has been valid. The numerical results of this chapter were also used to determine the relative amounts of torque that is lost at the pistons, the slippers and the valve plate. As Figure 8-4 shows, the pistons contribute to more than 60% of the torque loss within the pump while the slippers and valve plate contribute less than 37% and 5% respectively.

CHAPTER 9. VARIATION OF PARAMETERS

9.1 Introduction

Chapter 8 has been used to discuss the overall torque on the cylinder block of an axial-piston swash-plate type hydrostatic pump. It has also been used to show, by way of a direct comparison with test results, the validity of the previous analysis and modeling done in Chapters 3 through 7. In this chapter several parameters of the hydrostatic-pump design are numerically varied to examine the influence of small perturbations about nominal design values on the overall torque-loss. For this dissertation the effective pressurized slipper-area, A_s, the swash-plate angle, α, the maximum boundary coefficients-of-friction, $\hat{\mu}_p$, $\hat{\mu}_s$, and $\hat{\mu}_v$, the piston overhang-length, m_o, and the mass of the piston / slipper assembly, M_p and M_s, have been the parameters chosen for numerical perturbation.

Figure 9-1 shows a plot of torque loss versus the value of an arbitrary design-parameter, λ. The value λ_o is the nominal value of this parameter for which the numerical model presented in Chapter 8 is validated. To determine the influence of small variations in the value of λ_o on the overall torque-loss. λ is perturbed by 1% on either side of λ_o and the values of these perturbations are shown in Figure 9-1 as λ_a and λ_b. The values T_a and T_b in Figure 9-1 are the new values of torque loss that are produced by these perturbations respectively. The nominal value of torque is given by, T_o. As shown in Figure 9-1, a linear least-squares fit of these points produces the equation

$$T = \frac{T_o + 151T_a - 149T_b}{3} + \frac{50(T_b - T_a)}{\lambda_o}\lambda \quad . \tag{9.1}$$

Note: equation (9.1) is valid only for a $\pm 1\%$ variation in λ_o. This small percent-variation is chosen so as to produce a reasonable degree of linearity in the numerical perturbation.

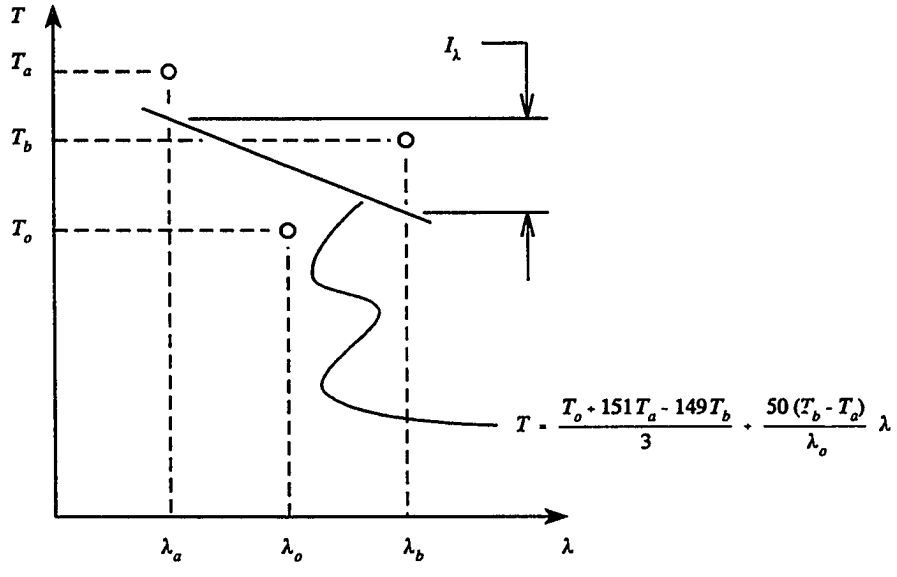

Figure 9-1. A schematic illustrating the definition of "influence" , I_λ, on the overall torque-loss for a $\pm 1\%$ variation in the design parameter λ about the nominal operating point λ_o.

In this chapter, the question to be answered is this: "Which parameter creates the largest change in torque loss when it is varied $\pm 1\%$ from its nominal value?" The parameter variation that creates the greatest change in torque loss is then considered to be the most "influential" parameter on the overall torque-loss within the pump. Using Figure 9-1, one can

show that the influence of a particular parameter variation on the overall torque-loss within the pump is given by

$$I_\lambda = |T_b - T_a| \quad . \tag{9.2}$$

Equation (9.2) will be used to discuss and compare the influence of varying *any* design parameter on the overall torque-loss within the pump.

9.2 Effective Pressurized Slipper-Area

Equation (9.2) is used for determining the influence of small variations in the effective pressurized slipper-area, A_s, on the overall torque-loss within the pump for the verified design of Chapter 8. From this study, it is concluded that the torque loss is more influenced by variations in the parameter, A_s, than any other parameter examined in this study. This influence is described in Figure 9-2 as it changes for different operating speeds and pressures. Because "influence" is defined using an absolute value of torque difference, it should be mentioned that increased values for the parameter, A_s, produce a *decrease* in torque loss while decreased values for this parameter produce an *increase* in torque loss.

Figure 9-2 shows that the influence of small changes in the effective pressurized slipper-area on the overall torque-loss within the pump is highly sensitive to the operating pressure. This is illustrated by the wide spread between iso-pressure lines in Figure 9-2. Equation (7.8) of Chapter 7 describes the normal loading between the swash plate and the

slipper. As shown in this equation, the effective pressurized-area of the *n*th slipper produces a normal load that is directly proportional to the pressure within the *n*th piston bore. As the effective pressurized-area increases, the normal load decreases. As the effective pressurized-area decreases, the normal load increases. This behavior corresponds respectively to a decrease and an increase in frictional torque-loss at the *slipper*. It was observed in this study that perturbations of the parameter, A_s, have negligible effect on torque loss at either the pistons or the valve plate.

Figure 9-2 shows that the influence of small variations of the pressurized slipper-area

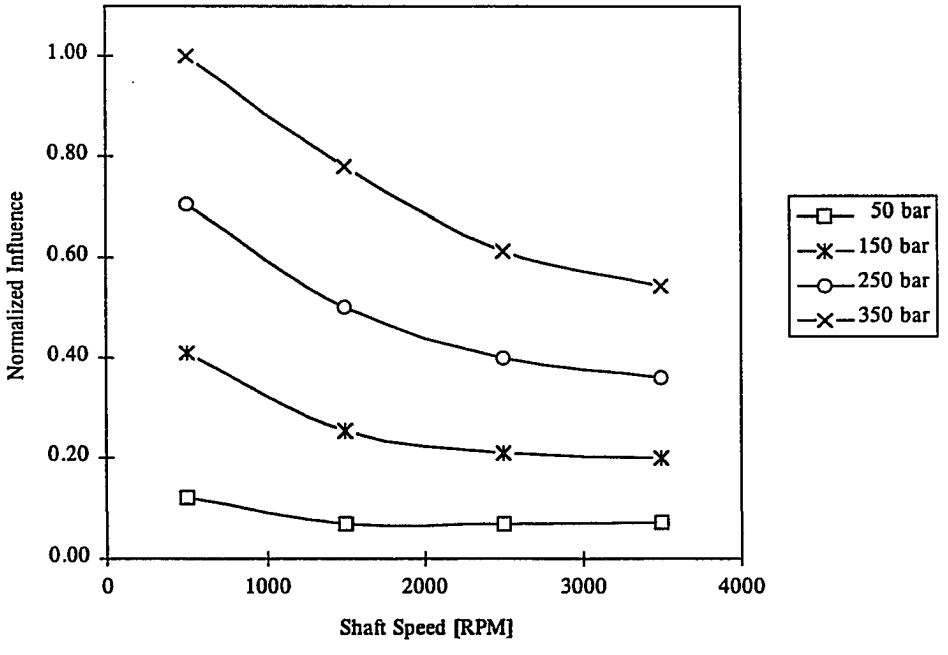

Figure 9-2. A plot illustrating the influence of a $\pm 1\%$ variation of the effective pressurized slipper-area, A_s, on the overall torque loss within the pump.

on torque loss exhibits a mild dependence on the operating speed of the pump. This dependence on speed can be simply explained by hydrodynamic sliding. As the speed increases, hydrodynamic lubrication increases and the coefficient-of-friction between the swash plate and slipper drops. This coefficient-of-friction is given in equation (7.12) of Chapter 7 and though it also may be shown to depend upon the operating pressure of the pump, clearly, for high speeds it is more dominated by speed than pressure.

9.3 Swash-Plate Angle

The torque on the cylinder block is influenced by the swash-plate angle, α, in two ways: 1) the *torque loss* on the cylinder block is influenced by the swash-plate angle, and 2) the *idealized torque* on the cylinder block is influenced by the swash-plate angle. These two different influences will be discussed in their respective order.

Figure 9-3 shows the influence of small variations of the swash-plate angle, α, on the *torque loss* within the pump. As can be seen, this figure exhibits dependencies on pressure and speed similar to that of Figure 9-2. This means that the physical explanations for the results of Figure 9-3 are similar to the physical explanations for the results of Figure 9-2 (i.e., the tradeoffs of high normal-loading within the pump and hydrodynamic sliding between moving surfaces must be considered). Note: the dependency of Figure 9-3 on speed is not as consistent as it was for Figure 9-2 in that the sensitivity always *decreases* with speed in Figure 9-2 as where it sometimes *increases* with speed in Figure 9-3. This will be discussed

later.

By increasing the swash-plate angle, the side load of the piston against the inside wall of the piston bore is also increased. See equation (7.2) of Chapter 7. This increased side load produces increased piston friction which in turn creates an increase in torque loss. Another

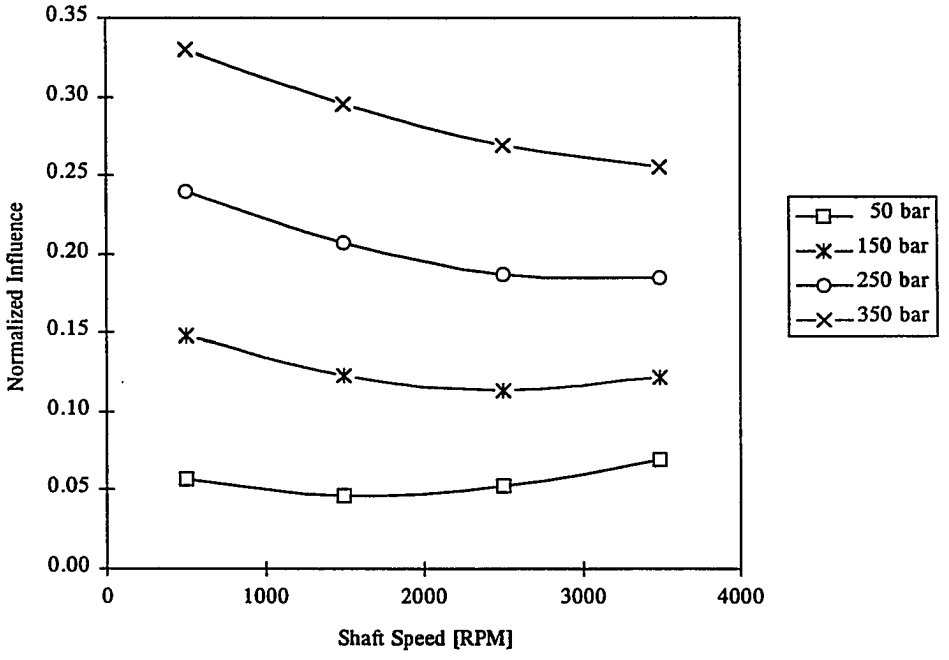

Figure 9-3. A plot illustrating the influence of a $\pm 1\%$ variation of the swash-plate angle, α, on the overall torque-loss within the pump.

effect of increased piston friction is an added clamping force on the slipper when the piston operates on the discharge side of the valve plate. See equation (7.10). This added clamping force serves to increase the frictional losses at the slipper and thereby increases the torque loss on the cylinder block. The results of this study have shown that increased swash-plate angles

have significant impacts on frictional losses at the piston and slippers while having negligible effects at the valve plate.

In general, Figure 9-3 shows that the influence of small variations in swash-plate angle on torque loss tends to decrease as speeds increase. Although this is the *general* trend, it does not always seem to be the case, especially at low pressures and high speeds. Under these conditions, it may be observed that the influence of small variations in swash-plate angle on torque loss actually *increases* as speeds increase. The reason for this is not obvious; however, it is integrally tied to the fact that the coefficient-of-friction throughout the pump depends on *both* normal loading and speed. See equation (6.15) of Chapter 6 for the tradeoffs effecting this parameter.

It must be remember that increased swash-plated angles tend to increase the *idealized torque* on the cylinder block as well. See equation (8.5) of Chapter 8. The reason that this is important is because of the fact that the idealized torque on the cylinder block is actually *more* influenced by small variations of the swash-plate angle than the torque loss is. (The ratio of this influence is approximately 4:1.) This can be determined by applying equation (8.5) of Chapter 8 to the definition of "influence" in equation (9.2). This means that while increased swash-plate angles tend to increase the torque loss, they also tend to increase the *idealized torque* at even a faster rate. In other words, by increasing the swash-plate angle, the *efficiency* of the pump is actually improved while still generating more wasted energy. This example serves to show how deceptive an efficiency calculation can be.

9.4 Maximum Boundary Coefficient-of-Friction

Figure 9-4 shows the influence on torque loss of making small variations to the maximum boundary coefficient-of-friction between the moving parts of the pump. These parameters are symbolized by $\hat{\mu}_p$, $\hat{\mu}_s$, and $\hat{\mu}_v$. Again, Figure 9-4 shows a strong dependence on pressure and now even a stronger dependence on speed than before. As previously argued, the inconsistent behavior of this influence with respect to speed is tied to the implicit relationship between normal loading and speed.

A surprising result of this study is the fact that maximum boundary coefficients-of-

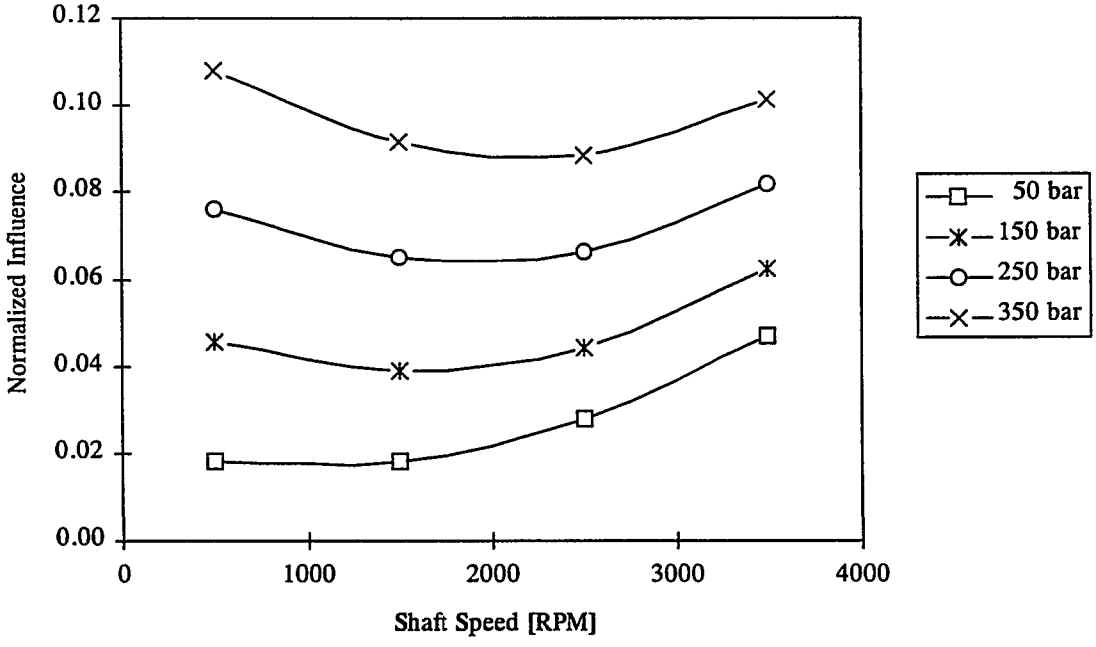

Figure 9-4. A plot illustrating the influence of a $\pm 1\%$ variation of the maximum boundary coefficients-of-friction, $\hat{\mu}_p$, $\hat{\mu}_s$, and $\hat{\mu}_v$, on the overall torque-loss within the pump.

friction do not have the greatest impact on torque loss. The torque loss on the cylinder block is influenced by these coefficients-of-friction only next to the effective pressurized-area of the slipper, A_s, and the swash-plate angle, α. The upshot of this statement is the fact that torque losses within the pump are driven more by pressurized loads (geometric design) then they are by material properties. The primary reason for this is the fact that most sliding within the pump is characterized by hydrodynamic behavior and that boundary lubrication only occurs occasionally. It should be noted, however, that small variations in maximum boundary coefficients-of-friction have an impact on both piston friction and slipper friction while the friction at the valve plate remains basically unaltered.

9.5 Nominal Piston Overhang-Length

The nominal piston overhang-length is symbolized by the variable, m_o, and is graphically shown in Figure 3-3 of Chapter 3. As discussed in Chapter 7, the overhang length serves to amplify the reaction forces of the *n*th piston within the *n*th piston bore of the cylinder block. These amplified reaction forces, in turn, amplify the friction within the piston bores and therefore are expected to increase the overall torque-loss of the pump. This expectation has been confirmed numerically by perturbing the value of m_o for the verified design of Chapter 8.

Figure 9-5 shows the influence of small variations in the overhang length of the piston on the overall torque-loss within the pump. Clearly, this influence is of the type previously

discussed in Sections 9.2, 9.3, and 9.4 (i.e., there is a heavy dependence on pressure and a mild dependence on speed). The heavy dependence on pressure is a result of the pressure driven side-loads on the pistons that are amplified by the overhang length, m_o. The inconsistent dependence on speed is a result of the implicit relationship of the coefficient-of-friction between speed and normal loading. It should be noted that variations of this parameter have significant impacts on both piston and slipper friction and that, once again, valve-plate friction remains basically unaltered.

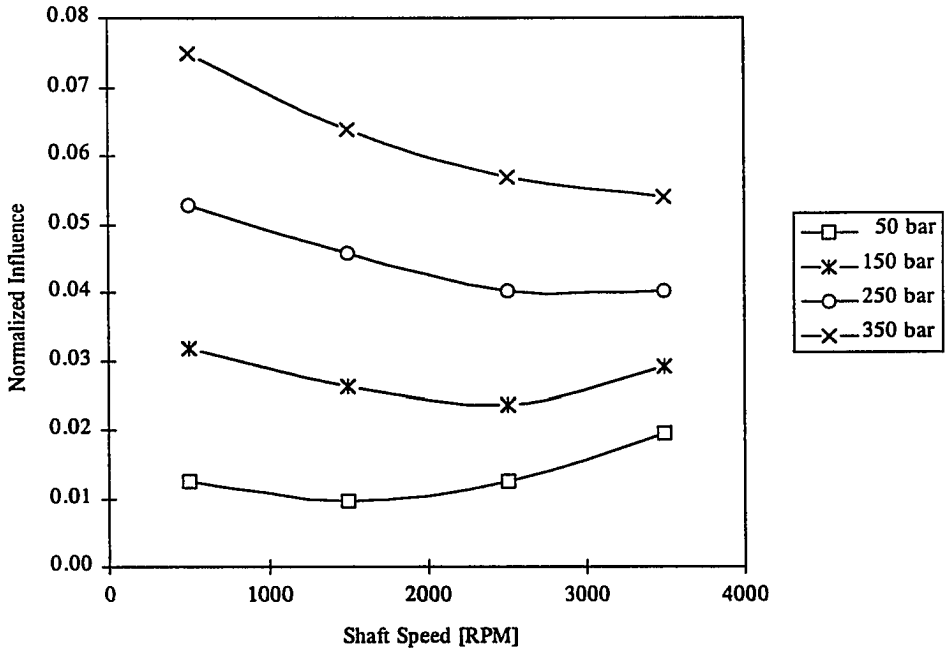

Figure 9-5. A plot illustrating the influence of a $\pm 1\%$ variation of the piston overhang-length, m_o, on the overall torque-loss within the pump.

9.6 Piston / Slipper Mass

The last parameter varied for this study is the mass of the piston / slipper assembly, M_p and M_s. The influence of small variations in the mass of the piston / slipper assembly on torque loss is shown in Figure 9-6. This figure illustrates an influence that is very dependent

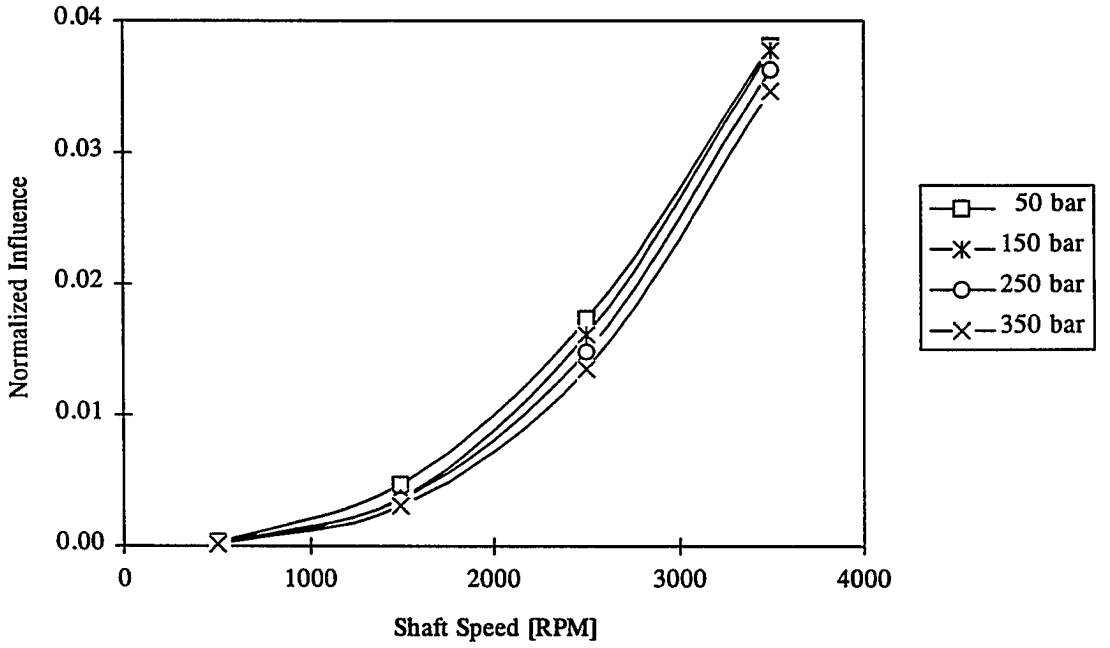

Figure 9-6 A plot illustrating the influence of a $\pm 1\%$ variation of the mass of the piston / slipper assembly, M_p and M_s, on the overall torque-loss within the pump.

on speed and only mildly dependent on pressure; however, it should be observed that the influence of small variations of the mass of the piston / slipper assembly on torque loss is extremely small compared to, say, the effective pressurized slipper-area (A_s).

The mass of the piston / slipper assembly is part of the inertial loading of reciprocating

and rotating motion. Primarily, the slipper absorbs the reciprocating inertia while the piston absorbs the rotating (centrifugal) inertia. To get this inertia, the mass is multiplied by an acceleration term that is proportional to the square of the shaft speed. See equation (3.29) of Chapter 3. Accordingly, the sensitivity of torque loss to small variations of the mass of the piston / slipper assembly is shown in Figure 9-6 as it increases parabolically with speed. The physical interpretation of this is the fact that increased speeds create increased inertia loads that, in turn, create increased friction at both the slipper and the piston. (As usual, valve-plate friction remains unaffected.) The net result is that small variations of the mass of the piston / slipper assembly create increased torque losses at high speeds.

The fact that the torque-loss sensitivity to small variations of the mass of the piston / slipper assembly is only mildly influenced by operating pressures is no surprise. The forces induced by increased masses are not pressure-induced forces — they are speed induced as previously discussed. Any influence of pressure as shown in Figure 9-6 is strictly a result of the implicit relationship between loading and speed and can be attributed to small changes in the calculation of the coefficient-of-friction throughout the machine.

9.7 Conclusion

In this chapter, the influence of the variation of several parameters on the torque-loss within the pump has been examined. Table 9.1 lists the varied parameters and their associated maximum influence as defined in Figure 9-1 and equation (9.2). From this table, it is clear

that the parameter variation with the *greatest* influence on the overall torque-loss within the pump is the effective pressurized-area of the slipper, A_s, while the parameter variation exerting the *least* influence on the overall torque-loss is the piston / slipper mass, M_p and M_s.

As previously discussed, it was found in this study that the torque loss from slipper friction was effected by the variation of each parameter. Furthermore, it was noted that the torque loss from piston friction was influenced by the variation of each parameter *except* the

Table 9.1 Perturbation characteristics of this study.

Perturbed Variables ($\pm 1\%$)	Maximum Normalized Influence, I_λ, on the Overall Torque-Loss within the Pump
A_s	1.00
α	0.33
$\hat{\mu}_p$, $\hat{\mu}_s$, and $\hat{\mu}_v$	0.11
m_o	0.07
M_p and M_s	0.04

effective pressurized-area of the slipper. In essence, this shows that piston friction is only mildly affected by slipper friction while the converse is strictly untrue. The torque loss from the friction at the valve plate was noted to be insensitive to each parameter variation within this study. The explanation for this insensitivity lies in the fact that valve-plate friction is dominated by the coefficient-of-friction between the valve-plate and the cylinder block which

is predominately characterized by hydrodynamic lubrication and therefore exhibits a very low value.

In this chapter it was noted that perturbations of the swash-plate angle, α, result in changes of the idealized torque as well as the torque loss. In general it was noted that the increases in the idealized torque are approximately four times greater than the increases in torque loss for a 1% increase of this parameter. The net result of increasing the swash-plate angle is to increase the efficiency of the pump while also increasing the amount of energy that is wasted. This scenario is a bit puzzling and illustrates the deceptiveness of an efficiency calculation.

Another surprising result of this study has been the fact that the maximum boundary coefficients-of-friction do not have the greatest impact on torque loss. The reason for this result is given by the fact that the sliding characteristics within the machine are dominated by hydrodynamic lubrication rather than boundary lubrication (metal-to-metal contact). The upshot of this statement is to illustrate the fact that the torque losses within the pump are driven more by pressurized loads (geometric design) and fluid viscosity than they are by material properties. In other words, efforts to change the torque characteristics of the pump are more profitably rewarded when one emphasizes the geometric design and fluid quality rather than the metallurgy of the sliding pairs.

CHAPTER 10. CONCLUSION

10.1 Summary

The effort of this dissertation has been to model the torque on the cylinder block of an axial-piston swash-plate type hydrostatic pump. The objectives of this dissertation have been outlined as follows:

1. To evaluate the theoretical torque on the cylinder block and to suggest an improved model for the well-known mathematical expression describing this quantity.

2. To develop a comprehensive model for the actual torque on the cylinder block and to verify this model using acquired test-data.

3. To determine the percent of the overall torque-loss within the pump that is generated by the pistons, the slippers, and the valve plate respectively.

4. To identify the design parameters of the pump that have the most significant impact on the overall torque-loss when they are perturbed a small amount from nominal conditions.

The mechanical analysis done in Chapter 3 has been the foundation for this work. This analysis has been used to derive the general model for the torque on the cylinder block which is given in equation (3.62). Other needed quantities have also been derived in Chapter 3; specifically, the load between the cylinder block and the valve plate is given in equation

(3.65), the loading between the *n*th piston and the cylinder block is given in equations (3.68) through (3.71), and the loading between the *n*th slipper and the swash plate is given in equation (3.75). These expressions are used to calculate the friction throughout the machine.

In Chapter 4, the pressure within the *n*th piston-bore is analyzed numerically. This fluid pressure is important because it is the fundamental means for transmitting power hydraulically. It is noted in Figure 4-2 that the pressure within the *n*th piston-bore typically exhibits very simple behavior and it is proposed that the discontinuous form of equation (4.8) may be used to generally approximate this pressure in closed-form. Both the numerical and the closed-form approximation have been used extensively in this dissertation.

Chapter 5 is used to derive several closed-form expressions that describe the effective pressurized-areas throughout the pump. These areas describe the effective pressurized-area between the piston and the cylinder block, the effective pressurized-area between the slipper and the swash plate, and the effective pressurized-area between the cylinder block and the valve plate. These quantities are presented in equations (5.11) and (5.13), (5.18), and (5.22) respectively.

Chapter 6 is used to derive a general model for the coefficient-of-friction as it varies throughout the machine. This model is based upon classical journal-bearing theories and utilizes the basic trends of the Stribeck curve presented in Figure 6-1. This curve is modeled in equation (6.15) and is generally applied to all sliding conditions that are susceptible to hydrodynamic behavior.

Utilizing the results of Chapter 3 and Chapter 6, Chapter 7 presents the models of friction as they pertain to the piston within the *n*th piston-bore, the *n*th slipper as it slides along the swash plate, and the cylinder block as it rotates against the surface of the valve plate. These quantities are given respectively in equations (7.6), (7.13), and (7.18).

Chapter 8 is used to assemble the work of Chapters 3 through 7 into a comprehensive model of torque on the cylinder block of an axial-piston swash-plate type hydrostatic pump. In this chapter, both the idealized torque and the torque loss are examined. A closed-form approach is used for discussing the idealized torque on the cylinder bock and generates the expression given in equation (8.5). The traditional form of this quantity is often referred to as the *theoretical* torque on the cylinder block and would appear identical to equation (8.5) if the compressibility effects in the valve plate transition-regions were not considered. In presenting equation (8.5), an improved model for the idealized torque on the cylinder block has been proposed and the first objective of this dissertation has been accomplished.

In Chapter 8, a numerical program has also been presented to numerically calculate the net torque on the cylinder block which includes both the idealized torque and the torque loss. The flow-chart for this program is shown in Figure 8-2 and a copy of the code is presented in the Appendix. A comparison of the torque loss as predicted by the program and measured on a physical test-stand is presented in Figure 8-3. The correlation shown in this figure is quite good and based upon this result the modeling done throughout this dissertation is considered to be valid. Figure 8-3 summarizes the second objective of this dissertation;

namely, to develop a comprehensive model of torque on the cylinder block and to verify this model with empirical test data. This model is now believed to be the most comprehensive and detailed model for the torque on the cylinder block of an axial-piston pump that has been validated and is available in the literature today.

A third objective of this dissertation has been to determine the percent of the overall torque loss that is generated by each component within the pump. Using the numerical program of Chapter 8, the torque losses associated with piston friction, slipper friction, and valve-plate friction have been numerically separated to determine which losses are most significant. This separation is illustrated in Figure 8-4 of Chapter 8. As shown in this figure, the pistons create more than 60% of the total friction-loss within the pump, the slippers contribute between 18 and 37% of this loss, and the valve plate generates less than 5% of the frictional loss. This information cannot be determined without the use of an accurate numerical-program and is fundamental for understanding the general characteristics of torque loss within the pump.

Finally, in Chapter 9, the numerical model of Chapter 8 is used to examine the effects of changing certain design characteristics by small amounts. Design characteristics that were examined in Chapter 9 are the effective pressurized area on the slipper, A_s, the swashplate angle, α, the maximum boundary coefficients-of-friction, $\hat{\mu}_p$, $\hat{\mu}_s$, and $\hat{\mu}_v$, the piston overhang-length, m_o, and the mass of the piston / slipper assembly, M_p and M_s. The results of perturbing these parameters by 1% of their nominal values are discussed at length in the

Chapter 9; however, a summary of the magnitude of influence is given in Table 9.1. From Table 9.1 it can be seen that the greatest changes in torque loss can be achieved by adjusting the effective pressurized area of the slipper, A_s. This table is presented as a summary that satisfies the fourth and final objective of this dissertation; namely, to identify the design parameters of the pump that have the most significant impact on the overall torque loss when they are perturbed a small amount from nominal conditions.

In Chapter 9 it was noted that perturbations of the swash-plate angle, α, resulted in changes of the *idealized torque* as well as the *torque loss* and that the increases in the idealized torque were approximately four times greater than the increases in torque loss for a 1% increase in α. This scenario results in an increased *efficiency* of the pump while also increasing the amount of energy that is lost due to friction (i.e., torque loss). The combination of these two effects is puzzling and illustrates the inherent deceptiveness of efficiency calculations in general.

Another surprising result of Chapter 9 is the minor influence that the maximum boundary coefficients-of-friction have on torque loss. This is surprising since a first glance at friction losses would suggest that the coefficient-of-friction plays a dominant roll in influencing the friction itself. For an axial piston pump, this is not the case. The reason for this result is given by the fact that the sliding characteristics within axial-piston pumps are dominated by hydrodynamic lubrication rather than boundary lubrication (metal-to-metal contact). The upshot of this statement is to illustrate the fact that the torque losses within the

pump are driven more by pressurized loads (geometric design) and fluid viscosity than they are by material properties. In other words, efforts to change the torque characteristics of the pump are more profitably rewarded when one emphasizes the geometric design and fluid quality rather than the metallurgy of the sliding pairs.

10.2 Future Work

The efforts of this study have emphasized the operation of axial-piston pumps. In practice, axial-piston pumps are frequently used in parallel with axial-piston motors to achieve the rotational output of a hydrostatic transmission. In industry, axial-piston pumps and axial-piston motors are viewed as identical machines running in opposite modes. The pump operates in a forward mode to deliver energy while the motor operates in a reverse mode to receive energy. It has not been explicitly mentioned until now, however, the analysis of this dissertation is very applicable to the analysis of both axial-piston pumps and axial-piston motors though the output of the modeling would not be the same for both machines. The reason for expected differences in the output may be considered in light of the differences noted between advancing pistons and retreating pistons in Chapter 7. In general, the highly-loaded piston of a pump operates in an advancing mode while the highly-loaded piston of a motor operates in a retreating mode. The frictional characteristics for these two modes are significantly different. Another difference may occur when one considers the assumption made in this dissertation that the pressure acting on the face of the nth slipper is the same as

the pressure within the *n*th piston-bore. For a pump, this may be true, since the piston friction on the high-pressure side acts to clamp the slipper against the swash-plate surface and thereby seals off any leakage that may cause a pressure difference between the piston bore and the slipper face. For a motor, however, the piston friction on the high-pressure side tends to pull the slipper away from the swash plate and may actually cause a pressure difference to occur. A more detailed investigation of this phenomenon would be required for the analysis of a motor. In any event, it is suggested that future work on the subject of torque loss be directed toward axial-piston motors using a similar approach as outlined in this dissertation.

Another aspect of energy loss within the axial-piston pump pertains to volumetric losses that occur when high-pressure fluid leaks away from the path of power transmission. The leakage of fluid within a pump (or motor) is a direct function of clearances and can sometimes be increased or diminished based upon the magnitude of loading between parts. Chapter 3 provides the analysis for most of this loading and would prove to be foundational, once again, for the analysis of volumetric losses. Further work along this line would require a fresh analysis of fluid flow and judicial choices would be required to simplify the model to a level that would be useful. In other words, it would be impractical to try solving a full set of Naiver-Stokes equations for any one leakage condition within the pump and an approach similar to Chapters 5 and 6 of this dissertation would be suggested (i.e., using one and two dimensional analysis that is linear rather than a nonlinear analysis that could be three dimensional in general). Of course, empirical validation of this analysis would be needed.

REFERENCES

Avallone, E. A., and T. Baumeister III, eds. 1978. *Marks' Standard Handbook for Mechanical Engineers*. 9th ed. New York: McGraw-Hill Book Company.

Bennet, T. P. 1961. "The Resistance to Tilt of Hydrostatic Slipper Pads." *British Hydromechanics Research Association Report* 713. December, (np).

Boinghoff, O. 1975. "The Friction Characteristic of the Pistons and of the Slipper Shoes in the Swash Plate Axial Piston Machine." Braunsweig Technical University.

Bolinger, J. W. 1982. "Considerations for Hydrostatic System Noise Control." Society of Automotive Engineers International Off-Highway Meeting and Exposition, Milwaukee, Wisconsin.

Browns, D. E., A. C. Rolfe, and P. J. Chapple. 1978. "A Discussion of the Factors which Affect Hydraulic Motor Torque under Starting Conditions." 5th International Fluid Power Symposium, University of Durham, England.

Crook, A., and M. J. Fisher. 1969. "An Investigation into the Dynamic Behavior of Hydrostatic Slipper Bearings." *British Hydromechanics Research Association Report* 1023. October, (np).

Cunningham, S. V., and D. McGillivaray. 1966. "The Design and Operation of Hydrostatic Slipper-Pad Bearings in Hydrostatic Motors." *Marine Applications of Fluid Power. I. Mech. E.*, (np).

Darling, J. 1985. Piston-cylinder dynamics in oil hydraulic axial piston pumps. Ph.D. thesis, School of Mechanical Engineering, University of Bath, England.

Edge, K. A., and J. Darling. 1989. The pumping dynamics of swash plate piston pumps. *Journal of Dynamic Systems, Measurement, and Control* 111:307-12.

Ezato, M., and M. Ikeya. 1986. "Sliding Friction Characteristics between a Piston and a Cylinder for Starting and Low-Speed Conditions in the Swashplate-Type Axial Piston Motor." 7th International Fluid Power Symposium, Bath, England.

Fisher, M. J. 1962. "A Theoretical Determination of Some Characteristics of a Tilted Hydrostatic Slipper Bearing." *British Hydromechanics Research Association Report* 728. April, (np).

Hanna, T. L. 1967. Hydrostatic pump efficiency tests with statistical analysis. Master's thesis, University of Illinois at Urbana-Champaign.

Hibi, A., and T. Ichikawa. 1975. "Torque Performance of Hydraulic Motor and its Mathematical Model." 4th International Fluid Power Symposium, Sheffield, UK.

Hibi, A. 1974. Starting torque of swash plate type axial piston motor. *Bulletin of the Japanese Society of Mechanical Engineers* 17, no. 106, (np).

Hooke, C. J., and Y. P. Kakoullis. 1983. The effect of non-flatness on the performance of slippers in axial piston pumps. *Proceedings of the Institution of Mechanical Engineers* 197C, (np).

Hooke, C. J., and Y. P. Kakoullis. 1981. "The Effects of Centrifugal Load and Ball Friction on the Lubrication of Slippers in Axial Piston Pumps." 6th International Fluid Power Symposium, St. John's College, Cambridge, England.

Hooke, C. J., and Y. P. Kakoullis. 1978. "The Lubrication of Slippers in Axial Piston Pumps." 5th International Fluid Power Symposium, University of Durham, England.

Howarth, R. B., and M. J. Newton. 1971. "Investigation of the Effects of Tilt and Sliding on the Performance of Hydrostatic Thrust Bearings." Conference on Externally Pressurized Bearings. I. Mech. E., April.

Hutchings, I. M. 1992. *Tribology: Friction and Wear of Engineering Materials*. London: CRC Press.

Iboshi, N., and A. Yamaguchi. 1986. Characteristics of a slipper bearing for swash plate type axial piston pumps and motors (4th report, effects of surface roughness). *Bulletin of the Japanese Society of Mechanical Engineers* 29, no. 254:2539-46.

Inoue, K., and M. Nakazato. 1993. "A New Prediction Method of Operating Moment and Cylinder Pressure of a Swash Plate Type Axial Piston Pump." *Fluid Power*, (np).

Johnson, R. E., and N. D. Manring. 1994. "Modeling a Variable Displacement Pump." American Society of Mechanical Engineering Fluid Machinery Forum, FED, Tahoe, Nevada.

Kakoullis, Y. P. 1977. Slipper lubrication in axial piston pumps. Master's thesis, University of Birmingham.

Kazama, T., and A. Yamaguchi. 1993. Application of a mixed lubrication model for hydrostatic thrust bearings of hydraulic equipment. *Journal of Tribology* 115:686-91.

Kim, S. D., H. S. Cho, and C. O. Lee. 1987. A parameter sensitivity analysis for the dynamic model of a variable displacement axial piston pump. *Proceedings of the Institution of Mechanical Engineers* 201, no. C4:235-43.

Kobayashi, S., M. Hirose, J. Hatsuse, and M. Ikeya. 1988. "Friction Characteristics of a Ball Joint in the Swashplate Type Axial Piston Motor." Proceedings of the 8th International Symposium on Fluid Power, Birmingham.

Koc, E., C. J. Hooke, and K. Y. Li. 1992. Slipper balance in axial piston pumps and motors. *Journal of Tribology* 114:766-72.

Kosodo, H. 1973. Studies on the intermittent lubrication system of axial piston pumps and motors. *Bulletin of the Japanese Society of Mechanical Engineers* 16, no. 92:301.

Lambeth, D. E., and J. W. Everett. 1964. "Hydrostatic Slipper Pads." *The Engineer*, (np).

Lin, S. J., A. Akers, and G. Zeiger. 1985. The effect of oil entrapment in an axial piston pump. *Journal of Dynamic Systems, Measurement, and Control* 107:246-51.

Manring, N. D., and R. E. Johnson. 1994. "Swivel Torque within a Variable-Displacement Pump." 46th National Conference on Fluid Power, Anaheim, California.

Manring, N. D. 1993. Modeling a variable-displacement pump. Master's thesis, University of Illinois at Urbana-Champaign.

Martin, L. S. 1969. "The Development of a Computer Program for Analyzing the Performance of Hydrostatic and Hydromechanical Transmissions." SAE National Farm, Construction and Industrial Machinery Meeting, Milwaukee, Wisconsin.

McCandlish, D., and R. E. Dorey. 1981. "Steady State Losses in Hydrostatic Pumps and Motors." 6th International Fluid Power Symposium, St. Johns's College, Cambridge, England.

McCandlish, D., and R. E. Dorey. 1984. The mathematical modelling of hydrostatic pumps and motors. *Proceedings of the Institution of Mechanical Engineers* 198, no. 10B:165-74.

Merrit, H. E. 1967. *Hydraulic Control Systems*. New York: John Wiley & Sons, Inc.

Nation, H. J. 1961. Presentation of the performance of hydraulic pumps and motors. *Journal of Agricultural Engineering Research* 6, no. 4, (np).

Nonnemacher, G. 1975. "Starting Characteristics of Hydraulic Motors. A Discussion of the Measurement Procedures and their Interpretation." 1st European Fluid Power Conference.

Olson, J. R. 1970. "Speed Varying Loads Effect the Stability of Hydrostatic Transmissions." 26th National Conference on Fluid Power, Chicago, Illinois.

Pang, Z., Z. Wenjie, and S. Jingwu. 1993. The study of hydrostatic lubrication of the slipper in a high-pressure plunger pump. *Tribology Transactions* 36:316-20.

Peterson, W. A. 1966. Efficiency comparison of axial piston hydrostatic pumps. Master's thesis, University of Illinois at Urbana-Champaign.

Pippenger, J. J. 1992. *Fluid Power — The Hidden Giant*. Jenks, Oklahoma: Amalgam Publishing Company.

Puormovahed, A. 1992. "Uncertainty in the Efficiencies of a Hydrostatic Pump / Motor." Winter Annual Meeting of the American Society of Mechanical Engineers, Anaheim, California.

Rolfe, A. C. 1976. Dynamic characteristics of a low speed hydraulic motor. Ph.D. thesis, University of Bath, England.

Royle, J. K., and R. S. Raizada. 1966. Numerical analysis of effects of tilt, sliding and squeeze action on externally pressurized oil film bearings. *Proceedings of the Institution of Mechanical Engineers* 180, (np).

Schlosser, W. M. J. 1969. "The Overall Efficiency of Positive Displacement Pumps." 1st British Hydromechanics Research Association Fluid Power Symposium, Cranfield, UK.

Schlosser, W. M. J. 1961. "Mathematical Model for Displacement Pumps and Motors." *Hydraulic Power Transmission.* April, (np).

Schoenau, G. J., R. T. Burton, and G. P. Kavanagh. 1990. Dynamic analysis of a variable displacement pump. *Journal of Dynamic Systems, Measurement, and Control* 112:122-32.

Shigley, J. E., and L. D. Mitchell. 1983. *Mechanical Engineering Design.* 4th ed. New York: McGraw-Hill Book Company.

Shute, N. A., and D. E. Turnbull. 1962. "The Losses of Hydrostatic Slipper Bearings under Various Operating Conditions." *British Hydromechanics Research Association Report* 743. October, (np).

Shute, N. A., and D. E. Turnbull. 1962. "The Minimum Power Loss of Hydrostatic Slipper Bearings." *British Hydromechanics Research Association Report* 721. April, (np).

Shute, N. A., and D. E. Turnbull. 1960. "An Experimental Study of the Lift of a Simple Hydrostatic Bearing." *British Hydromechanics Research Association Report* 659. April, (np).

Stachowiak, G. W., and A. W. Batchelor. 1993. *Engineering Tribology.* Amsterdam: Elsevier Science Publishers.

Tanaka, K., T. Nakahara, and K. Kyogoku. 1993. Piston rotation and frictional forces between piston and cylinder of piston and motor. *Transactions of the Japan Society of Mechanical Engineers* C, vol. 59, no. 560:1192-97.

Taylor, P. A. 1958. Measuring the performance of hydrostatic transmissions. *Journal of Agricultural Engineering Research* 3, no. 1, (np).

Thoma, J. U. 1979. *Hydrostatic Power Transmission.* Surrey, England: Trade & Technical Press.

Thoma, J. 1969. "Mathematical Model and Effective Performance of Hydrostatic Machines and Transmissions." *Hydraulic Pneumatic Power.* November, (np).

Toet, G., and T. Roorda. 1978. "Behavior of Hydraulic Motor Starting Torque." Proceedings of the 29th National Conference on Fluid Power.

Turnbull, D. E. 1978. "The Theoretical Efficiency of a Hydrostatic Transmission." 5th International Fluid Power Symposium, University of Durham, England.

Wilson, W. E., and C. D. Lemme. 1968. "The Hydromechanical Transmission - Ideal and Real." Society of Automotive Engineers Paper 680605.

Wilson, W. E. 1963. "Optimizing Hydrostatic Transmissions." *Machine Design*. January, (np).

Wilson, W. E. 1948. "Performance Criteria for Positive Displacement Pumps and Fluid Motors." American Society of Mechanical Engineers Semi-Annual Meeting.

Yamaguchi, A., and Y. Tanioka. 1976. Motion of pistons in piston-type hydraulic machines. *Bulletin of the Japanese Society of Mechanical Engineers* 19, no. 130:402-19.

Yamaguchi, A. 1966. Studies on the characteristics of axial plunger pumps and motors. *Bulletin of the Japanese Society of Mechanical Engineers* 9, no. 34:305-13.

Zarotti, G. L., and N. Nervegna. 1981. "Pump Efficiencies Approximation and Modelling." 6th International Fluid Power Symposium, St. John's College, Cambridge, England.

Zeiger, G., and A. Akers. 1986. Dynamic analysis of an axial piston pump swashplate control. *Proceedings of the Institution of Mechanical Engineers* 200, no. C1:49-58.

Zeiger, G., and A. Akers. 1985. Torque on the swashplate of an axial piston pump. *Journal of Dynamic Systems, Measurement, and Control* 107:220-26.

APPENDIX

The following numerical program was written using ACSL. This program calculates the instantaneous and average torque on the cylinder block of an axial-piston swash-plate type hydrostatic-pump. For the results of this program, see Chapters 8 and 9.

```
PROGRAM  Cylinder-Block Torque

INITIAL

! ---- Operating Constants

!              Discharge Pressure:

       CONSTANT  Pd          =     40E+06          ! [Pa]

!              Intake Pressure:

       CONSTANT  Pi          =     2E+06           ! [Pa]

!              Shaft Speed:

       CONSTANT  w           =     200.000         ! [rad/s]

!              Swashplate Angle:

       CONSTANT  alpha       =     α               ! [rad]

! ---- Fluid Properties

!              Fluid Bulk-Modulus:

       CONSTANT  beta        =     15E+08          ! [Pa]
```

```
!           Fluid Viscosity:
      CONSTANT  eta          =     2E-02          ! [Pa s]
!           Fluid-Film Constant:
      CONSTANT  Kmu          =     0.014          ! [no units]
!           Critical Fluid-Film Thickness:
      CONSTANT  hstar        =     1E-06          ! [m]
! ---- Cylinder-Block Parameters
!           Piston Pitch-Radius:
      CONSTANT  r            =     r              ! [m]
!           Balanced Area for a Single Piston-Bore:
      CONSTANT  Ab           =     A_b            ! [m^2]
!           Block-Spring Load:
      CONSTANT  Fsp          =     F_sp           ! [N]
! ---- Valve-Plate Parameters
!           Maximum Flow-Area:
      CONSTANT  Amax         =     148.25E-06     ! [m^2]
!           Maximum Slot-Area:
      CONSTANT  Asmax        =     3.2E-06        ! [m^2]
!           Valve-Plate Index:
      CONSTANT  del          =     -0.0325        ! [rad]
```

```
!           Valve-Plate Slot Angle 1:

                T1          =   1.8049 + del        ! [rad]

!           Valve-Plate Slot Angle 2:

                T2          =   4.9465 + del        ! [rad]

!           Piston Sweep-Angle:

      CONSTANT  phi         =   0.4682              ! [rad]

!           Diametrical-Land Width:

      CONSTANT  Dv          =   Dv                  ! [m]

!           Max Coefficient-of-Friction:

      CONSTANT  muvhat      =   0.14                ! [no units]

! ---- Piston-Bore Parameters

!           Piston Volume @ Zero Displacement:

      CONSTANT  Vo          =   Vo                  ! [m^3]

!           Piston Diameter:

      CONSTANT  Dp          =   Dp                  ! [m]

!           Piston Area:

      CONSTANT  Ap          =   Ap                  ! [m^2]

!           Bushing Length:

      CONSTANT  lp          =   lp                  ! [m]

!           Nominal Overhang-Length:
```

```
      CONSTANT mo          =    m_o              ! [m]
!           Piston Mass:
      CONSTANT Mp          =    M_p              ! [kg]
!           Effective Pressurized-Area Constant:
      CONSTANT Kp          =    0.12             ! [no units]
!           Max Coefficient-of-Friction:
      CONSTANT muphat      =    0.14             ! [no units]
! ---- Slipper Parameters
!           Slipper Mass:
      CONSTANT Ms          =    M_s              ! [kg]
!           Balanced Area for a Single Slipper:
      CONSTANT As          =    A_s              ! [m^2]
!           Slipper Hold-Down Force:
      CONSTANT Fhd         =    F_hd             ! [N]
!           Outside Slipper-Diameter:
      CONSTANT Ds          =    D_s              ! [m]
!           Slipper-Roll Length:
      CONSTANT ls          =    0.5E-03          ! [m]
!           Max Coefficient-of-Friction:
      CONSTANT mushat      =    0.14             ! [no units]
```

```
! ---- Calculate Theoretical Torque

      Tortheoretical      =     9*(Pd-Pi)*Ap*r*TAN(alpha)/3.14159

! ---- Set Dimensions

      DIMENSION Pic(9), Ao(9), Pb(9), V(9), dVdt(9), P(9), Th(9), dPdt(9), Q(9), &
                Tori(9), fp(9), Fo(9), Foy(9), Foz(9), Fl(9), Fly(9), Flz(9), muo(9), &
                mul(9), fs(9), Torp(9), Tor(9), Torv(9), Fv(9), mus(9), Fsw(9), &
                Tors(9), Apy(9), Apz(9), Fsy(9), Fsz(9), Up(9), psi(9)

! ---- Set Initial Conditions

      DO 1 n = 1, 9

            IF ((n.GE.8).OR.(n.LE.3)) THEN

                  Pic(n)      =     Pd

            ELSE

                  Pic(n)      =     Pi

            ENDIF

      1..CONTINUE

      count       =     0

      Torsum      =     0

      Torpsum     =     0

      Torssum     =     0

      Torvsum     =     0

END  ! of INITIAL

DYNAMIC
```

```
! ---- Integration Algorithm and Step Size
      ALGORITHM ialg          =     2                    ! Gear's Stiff Integration
      MAXTERVAL maxt          =     0.0044
      NSTEPS nstp             =     1000
DERIVATIVE
! ---- Set Circular Positions
DO 2 n = 1, 9
            Th(n)  =      T + 0.6981*(n-1)
      IF (Th(n).GT.6.283) THEN
            Th(n)  =      Th(n) - 6.283
      ELSE
            Th(n)  =      Th(n)
      ENDIF
! ---- Define Valve-Plate Porting Changes
      IF ((Th(n).GT.T2+phi/2).OR.(Th(n).LE.1.57+del-phi)) THEN
            Ao(n)  =      Amax
            Pb(n)  =      Pd
      ELSEIF (Th(n).LE.1.57+del) THEN
            Ao(n)  =      Amax-Amax*(Th(n)-1.57-del+phi)/phi
            Pb(n)  =      Pd
```

```
      ELSEIF (Th(n).LE.T1-phi/2) THEN
            Ao(n) =     Asmax*(Th(n)-1.57)/(T1-1.57-del-phi/2)
            Pb(n) =     Pi
      ELSEIF (Th(n).LE.T1+phi/2) THEN
            Ao(n) =     MAX(Asmax,Amax*(Th(n)-T1+phi/2)/phi)
            Pb(n) =     Pi
      ELSEIF (Th(n).LE.4.71-phi+del) THEN
            Ao(n) =     Amax
            Pb(n) =     Pi
      ELSEIF (Th(n).LE.4.71+del) THEN
            Ao(n) =     Amax-Amax*(Th(n)-4.71+phi-del)/phi
            Pb(n) =     Pi
      ELSEIF (Th(n).LE.T2-phi/2) THEN
            Ao(n) =     Asmax*(Th(n)-4.71)/(T2-4.71-del-phi/2)
            Pb(n) =     Pd
      ELSE
            Ao(n) =     MAX(Asmax, Amax*(Th(n)-T2+phi/2)/phi)
            Pb(n) =     Pd
      ENDIF
2..CONTINUE
```

```
! ---- Integrate Piston-Bore Pressure

      V     =    Vo-Ap*r*TAN(alpha)*SIN(Th)

      dVdt  =    -Ap*r*TAN(alpha)*COS(Th)*w

      Q     =    Ao*0.0296*SQRT(ABS(Pb-P))*SIGN(1,(Pb-P))

      dPdt  =    beta/V*(Q-dVdt)/w

      P     =    INTVC(dPdt,Pic)

DO 3 m = 1, 9

! ---- Calculate Piston-Bore Friction

      Apz(m) =   - lp*Dp*3.14*Kp*COS(psi(m))

      Apy(m) =   - lp*Dp*3.14*Kp*SIN(psi(m))

      psi(m) =   ATAN(Fsy(m)/Fsz(m))

      Fsy(m) =   Ms*r*w**2*COS(Th(m))+fs(m)*SIN(Th(m))

      Fsz(m) =   ((Mp+Ms)*TAN(alpha)**2+Ms)*r*w**2*SIN(Th(m))-Ap*P(m)* &
                 TAN(alpha)-fp(m)*TAN(alpha)-fs(m)*COS(Th(m)) /COS(alpha)

      Foy(m) =   ((Mp+Ms)*r*w**2*COS(Th(m))+fs(m)*SIN(Th(m)))*(1+(mo-r* &
                 TAN(alpha)*SIN(Th(m)))/lp) - Apy(m)*P(m)/2

      Foz(m) =   ((Mp+Ms)*(1 + TAN(alpha)**2)*r*w**2*SIN(Th(m)) - Ap*P(m)* &
                 TAN(alpha) - fp(m)*TAN(alpha) - fs(m)*COS(Th(m))/COS(alpha))* &
                 (1+(mo-r*TAN(alpha)*SIN(Th(m)))/lp) - Apz(m)*P(m)/2

      Fly(m) =   - ((Mp+Ms)*r*w**2*COS(Th(m)) + fs(m)*SIN(Th(m)))*(mo - r* &
                 TAN(alpha)*SIN(Th(m)))/lp - Apy(m)*P(m)/2

      Flz(m) =   - ((Mp+Ms)*(1+TAN(alpha)**2)*r*w**2*SIN(Th(m))-Ap*P(m)* &
                 TAN(alpha) - fp(m)*TAN(alpha) - fs(m)*COS(Th(m))/COS(alpha))* &
                 (mo-r*TAN(alpha)*SIN(Th(m)))/lp - Apz(m)*P(m)/2
```

```
Fo(m) =     SQRT(Foy(m)**2+Foz(m)**2)

Fl(m) =     SQRT(Fly(m)**2+Flz(m)**2)

Up(m) =     r*w*TAN(alpha)*COS(Th(m))

IF (Up(m).GT.0) THEN

        muo(m) =    muphat

        mul(m) =    muphat*EXP( - (2*lp*SQRT(6*Kmu)/hstar)**2*eta*Up(m)/ &
                    (Fl(m)/Dp))+1/SQRT(6*Kmu)*SQRT(eta*Up(m)/(Fl(m)/Dp))

ELSE

        muo(m) =    muphat*EXP((2*lp*SQRT(6*Kmu)/hstar)**2*eta*Up(m)/&
                    (Fl(m)/Dp))+1/SQRT(6*Kmu)*SQRT(-eta*Up(m)/(Fl(m)/Dp))

        mul(m) =    muphat

ENDIF

fp(m) =     IMPL(0,0.001,10,OOPSp,SIGN(1,Up(m))*(Fo(m)*muo(m)+Fl(m)*&
            mul(m)),0.0001)

! ---- Calculate Slipper Friction

Fsw(m) =    (Ap/COS(alpha)-As)*P(m)-(Mp+Ms)*TAN(alpha)/COS(alpha)*r* &
            w**2*SIN(Th(m))+Fhd+fp(m)/COS(alpha)+fs(m)*TAN(alpha)* &
            COS(Th(m))

IF (Fsw(m).LE.0) THEN

        mus(m) =    0

ELSE

        mus(m) =    mushat*EXP(-(2*ls*SQRT(6*Kmu)/hstar)**2*eta*r*w/&
                    (Fsw(m)/Ds))+1/SQRT(6*Kmu)*SQRT(eta*r*w/(Fsw(m)/Ds))
```

```
      ENDIF

      fs(m) =     IMPL(0,0.001,10,OOPSs,Fsw(m)*mus(m),0.0001)

! ---- Calculate Valve-Plate Reaction to each Piston

      Fv(m) =     Fsp/9+Ab*P(m)+fp(m)

3..CONTINUE

! ---- Calculate Valve-Plate Coefficient-of-Friction

      Fvtotal =   Fv(1)+Fv(2)+Fv(3)+Fv(4)+Fv(5)+Fv(6)+Fv(7)+Fv(8)+Fv(9)

      muv     =   muvhat*EXP(-(2*(2*3.1416*r)*SQRT(6*Kmu)/hstar)**2*eta*r*w/ &
                  (Fvtotal/Dv))+1/SQRT(6*Kmu)*SQRT(eta*r*w/(Fvtotal/Dv))

! ---- Calculate Ideal Torque

      Tori    =   Ap*P*r*TAN(alpha)*COS(Th)

      Toritotal = Tori(1)+Tori(2)+Tori(3)+Tori(4)+Tori(5)+Tori(6)+Tori(7)+&
                  Tori(8)+Tori(9)

! ---- Calculate Torque Loss from Pistons

      Torp    =   fp*r*TAN(alpha)*COS(Th)

      Torptotal = Torp(1)+Torp(2)+Torp(3)+Torp(4)+Torp(5)+Torp(6)+Torp(7)+&
                  Torp(8)+Torp(9)

! ---- Calculate Torque Loss from Slippers

      Tors    =   fs*r*(SIN(Th)**2+1/COS(alpha)*COS(Th)**2)

      Torstotal = Tors(1)+Tors(2)+Tors(3)+Tors(4)+Tors(5)+Tors(6)+Tors(7)+&
                  Tors(8)+Tors(9)

! ---- Calculate Torque Loss from Valve Plate
```

```
      Torv    =     Fv*muv*r

      Torvtotal =   Fvtotal*muv*r

! ---- Calculate Net Torque on the Cylinder Block

      Tor     =     Tori+Torp+Torv+Tors

      Tortotal =    Tor(1)+Tor(2)+Tor(3)+Tor(4)+Tor(5)+Tor(6)+Tor(7)+Tor(8)+&
                    Tor(9)

END   ! of DERIVATIVE

! ---- Calculate the Average Torque on the Cylinder Block

      count         =     count + 1

      Torsum        =     Torsum + Tortotal

      Torave        =     Torsum/count

! ---- Calcualte the Average Torque-Loss from the Pistons

      Torpsum       =     Torpsum + Torptotal

      Torpave       =     Torpsum/count

! ---- Calcualte the Average Torque-Loss from the Slippers

      Torssum       =     Torssum + Torstotal

      Torsave       =     Torssum/count

! ---- Calcualte the Average Torque-Loss from the Valve Plate

      Torvsum       =     Torvsum + Torvtotal

      Torvave       =     Torvsum/count

! ---- Calculate the Average Torque-Loss on the Cylinder Block
```

```
      Torloss      =     Torave - Tortheoretical          ! Neglecting Gamma Effect
!     Torloss      =     Torpave + Torsave + Torvave      ! Including Gamma Effect
! ---- Output Conditons
      CINTERVAL cint          =     0.0175
      CONSTANT tstop          =     0.6981
      TERMT (T.GE.tstop,'FINISHED')
END   ! of DYNAMIC
END   ! of PROGRAM
```